

**THEORETICAL STUDY OF STRUCTURAL,
THERMOPHYSICAL AND MECHANICAL
PROPERTIES OF SOME INTERMETALLIC
COMPOUNDS**

Thesis submitted for the award of the degree of

DOCTOR OF PHILOSOPHY

in

Physics

By

Nitika

Registration Number: 41900808

Supervised by

Dr. Vipul Srivastava (23642)

Department of Physics (Professor)

Lovely Professional University



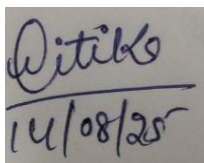
**L OVELY
P ROFESSIONAL
U NIVERSITY**

Transforming Education Transforming India

**LOVELY PROFESSIONAL UNIVERSITY, PUNJAB
2025**

DECLARATION

I hereby declared that the presented work in the thesis entitled “**Theoretical study of structural, thermophysical and mechanical properties of some intermetallic compounds**” in fulfillment of the degree of **Doctor of Philosophy (Ph. D)** is an outcome of research work carried out by me under the supervision of Dr. Vipul Srivastava, working as Professor in the School of Chemical Engineering and Physical Sciences of Lovely Professional University, Punjab, India. In keeping with the general practice of reporting scientific observations, due acknowledgments have been made whenever the work described here has been based on the findings of other investigators. This work has not been submitted in part or full to any other University or Institute for the award of any degree.



(Signature of Scholar)

Nitika

Registration No.: 41900808

Department/school: Physics

Lovely Professional University,

Punjab, India

CERTIFICATE

This is to certify that the work reported in the Ph. D. thesis entitled “**Theoretical study of structural, thermophysical and mechanical properties of some intermetallic compound**” submitted in fulfillment of the requirement for the award of degree of **Doctor of Philosophy (Ph.D.)** in the School of Chemical Engineering and Physical Sciences of Lovely Professional University, Punjab, India, is a research work carried out by Nitika, 41900808, is bonafide record of her original work carried out under my supervision and that no part of thesis has been submitted for any other degree, diploma or equivalent course.

Date: 14/08/2025



Signature of Supervisor

Dr. Vipul Srivastava

Professor

Department of Physics

School of Chemical Engineering and Physical Sciences

Lovely Professional University

Phagwara, Punjab

ABSTRACT

Nowadays, the majority of technologies are employed to create the New World. Owing to the progress of various fields, we have examined a variety of materials, which we are accustomed to accelerating and producing a multitude of concepts in novel domains. We study parameters, thermodynamic characteristics, mechanical properties, and other aspects of distinct binary systems using a variety of scientific disciplines. These factors provide us with a variety of information, such as the compound's molecular structure and stability. We base our research efforts on the materials commonly referred to as intermetallic compounds. The majority of intermetallic compounds are hard and brittle by nature, and it's important enough to sacrifice some toughness and ease of processing. Most intermetallic compounds are grouped with a transition metal group and by alloying the elements of group-II have extraordinary physical properties. These intermetallic compounds are typically composed of metallic alloy that forms an ordered solid-state geometry. They have a very high melting point and are typically brittle at room temperature. Properties of these intermetallic compounds, such as Debye temperature, specific heat at constant volume, and thermal expansion coefficients, are extremely high temperatures. Due to their numerous mechanical and physical characteristics, binary intermetallic compounds are interesting and have a wide range of uses. They have a variety of uses in aviation and spacecraft because of the compound's mechanical stability, high tensile strength, low weight, stiffness, and elastic modulus per unit density. These materials are also utilized in the creation of innovative, high-temperature-tolerant devices for a range of industrial uses. We are applying a Density functional theory via full potential linearized augmented plane wave approach, which has been applied to the analysis of the intermetallic compound, to these materials. The WIEN2k code was utilized to conduct these computations, which examined several quantum mechanical calculations grounded in the density functional theory of crystalline solids. We can obtain the precise ground state characteristics of the materials using this method. The ground state properties can be studied using several exchange potential approximations, such as the modified Becke Johnson, local density approximation, and generalized gradient

approximation (GGA). First, the generalized gradient approximation, which has a space group of Pm-3m, was used to optimize the structure (221). To obtain ground state properties, the energy volume data has been fitted to Birch Murnaghan equation of state. Similarly, the E-V data for nonmagnetic and ferromagnetic phases, considering the CsCl type structure has also been obtained. The E-V curves further revealed that BeAg and BeAu intermetallic compounds are found stable in nonmagnetic phase. On the other hand, BeFe intermetallic compound is stable in the ferromagnetic phase. This indicates the various spin electronic states, such as spin up and spin down electrons. Moving on to Mg-based intermetallic, the MgLu and MgHf intermetallic compounds' energy volume curves show stability in the non-magnetic phase. Following the discovery of a stable structure, the electronic characteristics of these compounds were calculated using spin polarization and the generalized gradient approximation. We analyze the spin using these computations, demonstrating the metallic character of our materials. Using the Pauling Slater rule, we also computed the magnetic moments for these compounds and discovered the direction in which they are localized with regard to one another. This demonstrates that the BeFe Intermetallic complex is ferromagnetic by nature.

We examine elasticity, a deformation field resulting from a stress field and caused by applied forces, and other mechanical properties under stress in order to verify the mechanical stability of compounds. The WIEN2k Code incorporates the Charpin method, which is used for these computations. In order to determine the bulk modulus, shear modulus, Young's modulus, Poisson ratio, Cauchy's pressure, anisotropic ratio, B/G ratio, and melting temperatures, it is imperative that we consider the mechanical properties of the materials. We use the Pugh criterion to determine the B/G ratio in order to examine the materials' ductility and brittleness characteristics. In order to further analyze the cubic system, the geometrical symmetry reduces the 21 dependent elastic constants to just three independent elastic constants, C_{ij} (C_{11} , C_{12} , and C_{44}). The mechanical and thermodynamic properties of the solids are revealed by these elastic constants. We utilize the Birch-Murnaghan equation of state to compute the thermodynamic properties in order to better comprehend the compound's thermodynamic behavior. We have calculated a few thermodynamic properties that depend on temperature and pressure, such as the Debye temperature, bulk modulus,

thermal expansion coefficient, entropy, and molar heat capacity at constant volume. The noteworthy physical amount the lattice vibration of the solids, or Debye temperature, provides information about how the electrical resistivity of metals varies with temperature. The average sound velocity, which is further determined by longitudinal and transverse velocity, is used to calculate the Debye temperature. The present work opens a scope for the theoreticians and experimentalists to testify our findings and proceed further for technological applications.

ACKNOWLEDGEMENTS

It gives me an immense debt of gratitude to express my sincere thanks to my HOS, Dr. Kailash Chandra Juglan, Professor & Head, School of Chemical Engineering and Physical Sciences, Lovely Professional University, Phagwara, for providing me the opportunity to carry out research. I would like to express our heartfelt gratitude to our Head of Department (HOD) Dr. Mukesh Kumar, Professor & Head, School of Chemical Engineering and Physical Sciences, Lovely Professional University, Phagwara for providing me an opportunity to undertake this research and for his continuous support and encouragement throughout the work. It gives me an immense depth of gratitude to express my sincere thanks to my supervisor, Dr. Vipul Srivastava, Professor, Department of Physics, Lovely Professional University, Phagwara, for providing me the opportunity to carry out research under his excellent guidance. His vision, dynamism, motivation and sincerity have deeply inspired me. I am very grateful for his persistent encouragement, wholehearted cooperation, care and patience throughout the course of Ph.D. I feel very fortunate to get a chance to work under his patient supervision. I remain in debt for his kind sustenance during my personal difficult times. I am also thankful to the creators and upholders of the WIEN2k Code, as made this research valuable and possible. I am extremely grateful to Dr. Navdeep Kaur and Dr. Preeti Kumari for always showing positive and helping nature.

Finally, I would like to acknowledge the most important person of my life- my parents Mr. Kewal Kumar, Kanchan, brother Amritpal Singh and my husband Pushwinder Kumar, daughter Avleen Kaur, father-in-law Dharam Pal, mother-in-law Kamlesh Devi, and brother-in-law Ravinder Kumar who has been the pillar to my strength, the encouragement towards my goals, the root to which I have based my life on. They always promote hard work and nurture my dreams with their invaluable understanding of life.

CONTENTS

List of figures	xi
List of tables	xiv
List of abbreviations	xvi
List of symbols	xviii
Chapter 1. Introduction	1
1.1. Intermetallic compounds	2
1.2 B2 Structure	4
1.3. Literature review	4
1.3. Research motivation and objectives	18
1.3.1. Research motivation	18
1.3.2. Research objectives	19
1.4. Thesis outline	20
References	22
Chapter 2. Method of calculations	27
2.1. Density functional theory	27
2.1.1. First Hohenberg and Kohn (HK) Theorem	28

2.1.2. Second Hohenberg and Kohn (HK) Theorem	28
2.1.3. Hartree-Fock (HF) method	30
2.1.4. Post- Hartree-Fock (HF) method	31
2.2. Generalized gradient approximation	32
2.3. FP-LAPW method	34
2.4. Elastic and mechanical stability	35
2.5. Thermodynamic stability	39
References	41
Chapter 3. A Computational Modeling on thermodynamic performances of BeX(X=Ag, Au, Fe) intermetallics	46
3.1. Introduction	46
3.2. Structural properties	47
3.3. Electronic properties	50
3.4. Elastic and mechanical properties	53
3.5. Thermodynamic properties	56
3.6. Conclusion	63
References	65
Chapter 4. Unveiling the mechanical and thermodynamic properties of MgX (X=Lu, Hf) intermetallic compounds at elevated temperature	68

4.1. Introduction	68
4.2. Structural properties	71
4.3. Electronic properties	74
4.4. Elastic and mechanical properties	76
4.5. Thermodynamic properties	80
4.6. Conclusion	84
References	86
Chapter 5. Structural, magnetic and thermodynamic properties of intermetallic compound CuZn: A first principles study	94
5.1. Introduction	94
5.2. Structural properties	95
5.3. Electronic properties	96
5.4. Thermodynamic properties	98
5.5. Conclusion	103
References	104
Chapter 6. Conclusion and future perspectives	104
6.1. Conclusion	104
6.2. Future perspectives	110
List of publications	112

List of conferences attended

113

List of figures

Figure 1.1: Classification of Alloy	2
Figure 1.2: B2 structure of binary intermetallic compounds	4
Figure 3.1: BeX (X=Ag, Au, and Fe) intermetallics with an optimized crystal structure in the Pm-3m structure	48
Figure 3.2: Variation of total energy as a function of cell volume of BeX (X=Ag, Au, Fe) intermetallics in Pm-3m structure (a) BeAg (b) BeAu (c) BeFe	49
Figure 3.3: Band structure of BeX(X=Ag, Au, Fe) intermetallics (a) BeAg (b) BeAu (c) BeFe up spin (d) BeFe Down spin	51
Figure 3.4: Total Density of states of BeX(X=Ag, Au, Fe) intermetallics (a) BeAg (b) BeAu (c) BeFe	52
Figure 3.5: Partial density of states of BeAg intermetallic (a) Be (b) Ag	53
Figure 3.6: Partial density of states of BeAu intermetallic (a) Be (b) Au	53
Figure 3.7: Partial density of states of BeAu intermetallic (a) Be (b) Fe	53
Figure 3.8: Variation of unit cell volume of BeX(X=Ag, Au, Fe) intermetallics with temperature (a) BeAg (b) BeAu (c) BeFe	57
Figure 3.9: Variation of bulk modulus of BeX(X=Ag, Au, Fe) intermetallics with temperature (a) BeAg (b) BeAu (c) BeFe	58
Figure 3.10: Variation of molar heat capacity at constant volume of BeX(X=Ag, Au, Fe) intermetallics with temperature (a) BeAg (b) BeAu (c) BeFe	59
Figure 3.11: Variation of Grüneisen constant of BeX(X=Ag, Au, Fe) intermetallics with temperature (a) BeAg (b) BeAu (c) BeFe	60
Figure 3.12: Variation of thermal expansion coefficient of BeX(X=Ag, Au, Fe) intermetallics with temperature (a) BeAg (b) BeAu (c) BeFe	61
Figure 3.13: Variation of Debye temperature of BeX(X=Ag, Au, Fe) intermetallics with temperature (a) BeAg (b) BeAu (c) BeFe	62
Figure 3.14: Variation of Entropy of BeX(X=Ag, Au, Fe) intermetallics with temperature (a) BeAg (b) BeAu (c) BeFe	63

Figure 4.1: Crystal structure of MgX(X= Hf, Lu) intermetallics in Pm-3m space group.	71
Figure 4.2: Variation of total energy as a function of cell volume of MgX(X=Lu, Hf) intermetallics in Pm-3m structure.	73
Figure 4.3: Band structure of MgX(X=Lu, Hf) intermetallics (a) MgLu (b) MgHf	75
Figure 4.4: Density of states (DOS) for MgX (X=Hf and Lu) intermetallics (a) Combined orbitals depiction as total DOS (TDOS) for Mg, Lu and Hf (b) different orbitals depiction as partial DOS (PDOS) for Mg, Lu and Hf.	76
Figure 4.5: Variation of thermodynamic parameters with temperature and pressure for MgLu intermetallic	81
Figure 4.6: Variation of thermodynamic parameters with temperature and pressure for MgHf intermetallic	82
Figure 5.1: Crystal structure of CuZn intermetallic in Pm-3m space group.	96
Figure 5.2: Variation of total energy as a function of cell volume of CuZn intermetallic in Pm-3m structure.	96
Figure 5.3: Band structure of CuZn intermetallic compound.	97
Figure 5.4: Density of states (TDOS) for CuZn intermetallic compound (a) Total density of states for CuZn (b) PDOS for Cu atoms (c) PDOS for Zn atoms	98
Figure 5.5: Variation of unit cell volume of CuZn intermetallic with temperature and pressure	99
Figure 5.6: Variation of bulk modulus of CuZn intermetallic with temperature and pressure.	99
Figure 5.7: Variation of molar heat capacity at a constant volume of CuZn intermetallic with temperature and pressure.	100
Figure 5.8: Variation of Grüneisen constant of CuZn intermetallic with temperature and pressure.	100
Figure 5.9: Variation of thermal expansion coefficient of CuZn intermetallic with temperature and pressure.	101

Figure 5.10: Variation of Debye temperature of CuZn intermetallic with 102
temperature and pressure.

Figure 5.11: Variation of entropy of CuZn intermetallic with 102
temperature and pressure.

List of Tables

Table 3.1 Ground state properties unit cell volume V_0 , lattice parameter a_0 , bulk modulus B_0 , first order pressure derivative of bulk modulus B'_0 and equilibrium total energy E_0 , cohesive energy E_{Coh} of BeX (X=Ag, Au, Fe) intermetallics at 0GPa and 0K.	50
Table 3.2: Calculated elastic and mechanical properties for BeX(X=Ag, Au, Fe) intermetallics at 0 GPa and 0 K: elastic constants C_{11} , C_{12} , C_{44} , Bulk Modulus B, Voigt Shear Modulus G_V , Reuss Shear Modulus G_R , Shear Modulus G, Young's Modulus E, Anisotropy Ratio A, Cauchy Pressure $C_{12}-C_{44}$, Bulk modulus to Shear modulus ratio B/G, Poisson Ratio σ , longitudinal velocity V_l , transverse velocity V_t , Average velocity V_m , Debye Temperature θ_D , Melting Temperature T_m .	55
Table 4.1: Structural information of MgX(X=Lu, Hf) intermetallics at a glance.	72
Table 4.2: Calculated ground state properties: unit cell volume V_0 , lattice parameter a_0 , bulk modulus B_0 , first order pressure derivative of bulk modulus B'_0 and equilibrium total energy E_0 of MgX (X=Lu, Hf) intermetallics at 0GPa and 0K	74
Table 4.3: Calculated elastic and Mechanical properties for MgX(X=Lu, Hf) intermetallics at 0 GPa and 0 K, elastic constants C_{11} , C_{12} , C_{44} , Bulk Modulus B, Voigt Shear Modulus G_V , Reuss Shear Modulus G_R , Shear Modulus G, Young's Modulus E, Anisotropy Ratio A, Cauchy Pressure $C_{12}-C_{44}$, Bulk Modulus to shear Modulus ratio B/G, Poisson Ratio σ , longitudinal velocity V_l , transverse velocity V_t , Average velocity V_m , Debye temperature θ_D , Melting Temperature T_m .	78
Table 6.1: Calculated ground state properties: unit cell volume V_0 , lattice parameter a_0 , bulk modulus B_0 , first order pressure derivative of bulk modulus B'_0 and equilibrium total energy E_0 of MgX (X=Lu, Hf) intermetallics at 0GPa and 0K.	107

Table 6.2: Calculated elastic and mechanical properties for BeX(X=Ag, 108
 Au, Fe) intermetallics at 0 GPa and 0 K: elastic constants C_{11} , C_{12} , C_{44} ,
 Bulk Modulus B, Voigt Shear Modulus G_V , Reuss Shear Modulus G_R ,
 Shear Modulus G, Young's Modulus E, Anisotropy Ratio A, Cauchy
 Pressure $C_{12}-C_{44}$, Bulk modulus to Shear modulus ratio B/G, Poisson
 Ratio σ , longitudinal velocity V_l , transverse velocity V_t , Average
 velocity V_m , Debye Temperature θ_D , Melting Temperature T_m .

Table 6.3: Calculated thermodynamic properties like Volume V (a.u.³), 110
 Bulk Modulus B (GPa), Molar heat capacity at constant volume C_V (J K⁻¹
¹ m⁻¹), Grüneisen constant γ , thermal expansion coefficient α (10⁻⁵ K⁻¹),
 Debye temperature θ_D (K).

List of Abbreviations

APW	Augmented plane wave
CB	Conduction band
CC	Coupled cluster
CI	Configuration interaction
DFT	Density functional theory
EOS	Equation of state
FM	Ferromagnetic
FP-LAPW	Full potential linearized augmented plane wave
GGA	Generalized gradient approximation
GMR	Giant magnetoresistive
GS	Ground-state
HEG	Homogeneous electron gas
HF	Hartree-Fock
HK	Hohenberg and Kohn
HP	Hartree product
IMC	Intermetallic compound
IR	Interstitial regions
KS	Kohn and Sham
LDA	Local density approximation
mBJ	Modified Becke-Johnson
MM	Magnetic moment
MP	Møller-Plesset perturbation theory
MR	Magnetoresistive
MT	Muffin-tin
PBE	Perdew-Burke-Ernzerhof
PDOS	Partial density of states
PM	Paramagnetic

QHA	Quasi harmonic Debye approximation
TMR	Tunneling magnetoresistive
TDOS	Total density of states
VB	Valence band
VR	Vacuum region
VRH	Voigt-Reuss-Hill
XC	Exchange-correlation

List of Symbols

A	Anisotropy
Ag	Silver
Au	Gold
a_0	Lattice Constant
α	Thermal expansion coefficient
B	Bulk modulus
B'	Pressure derivative of bulk modulus
Be	Beryllium
B_s	Adiabatic Bulk modulus
B/G	Pugh's ratio
BCC	Body centered cubic
C_p	Molar Heat capacity at constant pressure
Cu	Copper
C_v	Molar Heat capacity at constant volume
CP	Chauchy Pressure
E	Young's modulus
E_f	Fermi level
E_0	Equilibrium energy
E_{form}	Formation energy
E_{Tot}	Total energy
E_{XC}	Exchange -correlation energy
G	Shear modulus
G_R	Reuss shear modulus
G_v	Voigt shear modulus
γ	Grüneisen parameter
h	Plank's constant

Hf	Hafnium
K_B	Boltzmann's constant
Lu	Lutetium
Mg	Magnesium
M_{Tot}	Total magnetic moment
$n(r)$	Electron density
P	Pressure
Σ	Poisson's ratio
T	Temperature
τ	Relaxation time
T_m	Melting temperature
θ_D	Debye temperature
V	Volume
V_0	Equilibrium volume
v_l	Longitudinal elastic wave velocity
v_m	Average sound velocity
v_t	Transverse elastic wave velocity
V_{XC}	Exchange -correlation potential
Zn	Zinc
ZT	Figure of merit

Chapter 1

Introduction

There are a lot of entities that are formed in a certain manner if we look around. They resemble several materials in diverse ways, such as semiconductor devices, magnetic materials, intermetallic compounds, polymerizations, and shapes. The materials science has generated a plethora of technologies in recent years. They have a significant impact. There is a plethora of fundamental features that might be explored further with full effort. Theorists and experimenters have explored a wide range of disciplines, including physics, chemistry, engineering, manufacturing, and numerous other fields.

The periodic table, which presents a wealth of combinations between metals, non-metals, rare earth metals, alkaline earth metals, halogens, and noble gaseous states, is one of the primary sources of information for materials science discoveries. It's commonly referred to as a compound or substance when we combine any of these. There are several instances of the diverse materials that are utilized in daily life, vehicle engines, and spacecraft.

A compound called an alloy is created when two or more atoms of different substances are mixed. An alloy requires at least one metal element to produce. Possessing very beneficial qualities in the materials such as optical, electrically conductive and thermal differ from the other pure metals in their characteristics because of their high strength and extreme hardness. Unlike other materials that have covalent bonding, the alloys' atoms are bonded by a pure metallic connection. It is entirely dependent upon the compound's chemical characteristics [1]. Different constituents have been created, and their mass percentages are typically used to measure them. The atomic fraction is easily found for numerous scientific disciplines. Classification of the alloys is given below

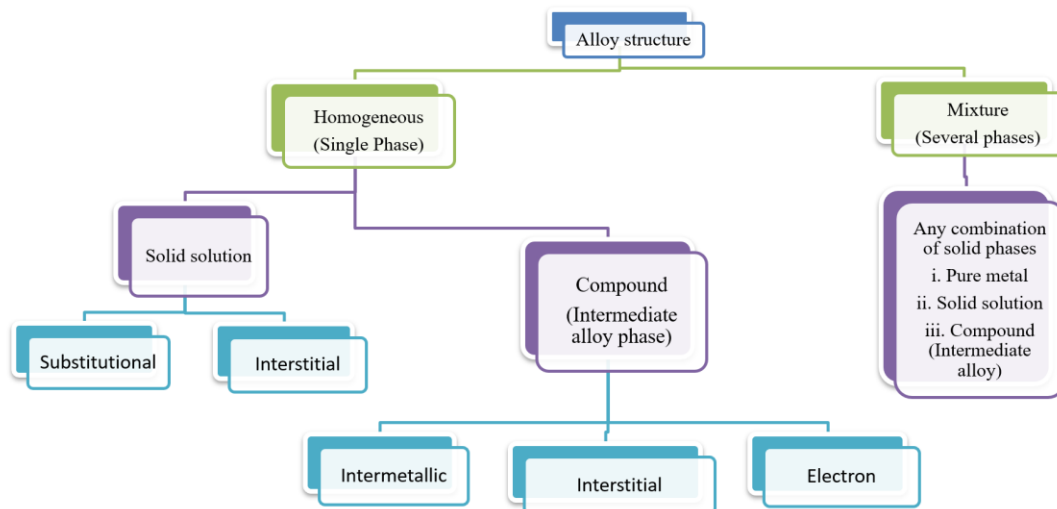


Figure 1.1: Classification of alloys

Classification of the alloys can be defined as the substitution of alloys and specifically interstitial alloys, which are formed entirely by the arrangement of the atoms. We further characterize these interstitial alloys as belonging to two types: homogeneous and heterogeneous. Lines representing a single phase make up the homogeneous, whereas two or more phases make up the heterogeneous. Intermetallic compounds are another name for heterogeneous substances. It can be solid solutions, which are often composed of metallic elements and contain metallic grains, sometimes referred to as crystals that have the same metal composition.

Additionally, the mixture contains a certain number of grains, also referred to as the materials' microstructures. These alloys, which are generally referred to as primary metals, have a variety of uses in the industrial sector, such as aerospace, and in the medical field, where they are used in surgical instruments. One major alloy is beryllium copper alloy, used in non-sparking tools [1].

1.1. Intermetallic compounds

We are primarily concerned with the intermetallic compounds. Metallic alloys are commonly classified as intermetallic compounds. They have solid-state geometry and are long-range organized. In general, these intermetallics perform well at high temperatures [2-4]. The majority of intermetallics are inherently brittle and hard. First, the Hume-Rothery scientist provides us with data on intermetallic compounds that are both stoichiometric and non-stoichiometric [5].

Following that, a scientist by the name of Schulze made a fresh discovery in 1967 [5], providing us with details about solid sides that have two or more metallic parts taken into consideration because their crystallographic structure differs from that of the other constituent particles.

Within the intermetallic compound, which is both homogeneous and heterogeneous, a reporter possesses solid solutions of metallic elements or other interstitial compounds that are typically disregarded. Nitrides and carbides are two such examples. However, one sort of intermetallic compound that is typically generated by a metal is called an interstitial intermetallic compound, which is generally included. These are used in several industries, including semiconductors, biomedicine, energy, and transportation. Furthermore, in order to exploit existing alloys to build new alloys with stronger behaviors, scientists and engineers are attempting to improve their qualities. Electronic gadgets and the aircraft industry both use ceramics made of nitrides, oxides, and carbides. Because of their strength, low friction, and lightweight nature, ceramics are highly prized. When a heat source is removed, ceramic tiles can act as a heat shield and quickly recover to their usual temperature. Covering and packing materials are comprised primarily of carbon and contain hydrogen, oxygen, and other non-metallic components. These materials are known as organic polymers. Most polymer materials can function as electrical insulators and can be employed in that role. Semiconductors, which are the building blocks of digital electronics and are used to make flip-flops, diodes, microprocessors, and other devices, are frequently stiff and brittle. Furthermore, the addition of other elements such as nickel, chromium, and vanadium enhance the unique characteristics of carbon steel. Numerous electronic qualities are further employed in a variety of fields. Additionally, there are certain magnetic qualities that are widely employed in computer chips, cell phones, and other devices like digital timepieces and pocket calculators. The satellite for communication is an additional benefit.

1.2. B2 Structure

Intermetallic compounds are stable in the B2 phase, which is typically exemplified by the combination of Iron and Aluminium, as the number of atoms is equal to that of two metals. Two interpenetrating cubic lattices create them [6].

Intermetallic compounds exhibit a wide range of structural properties characterized by their ordered atomic arrangements, which depend on their lattice types, such as body-centered cubic (BCC), hexagonal close-packed (HCP), and face-centered cubic (FCC) structures. Among these, some intermetallic compounds crystallize in the B2 structure, which corresponds to a body-centered arrangement similar to that of cesium chloride (CsCl). Binary intermetallic compounds with the B₂ structure adopt a body-centered cubic lattice and belong to space group 221 (Pm-3m). This ordered structure features two different types of atoms alternating at the corners and the center of the cubic unit cell, resulting in distinct physical and chemical properties compared to disordered alloys.

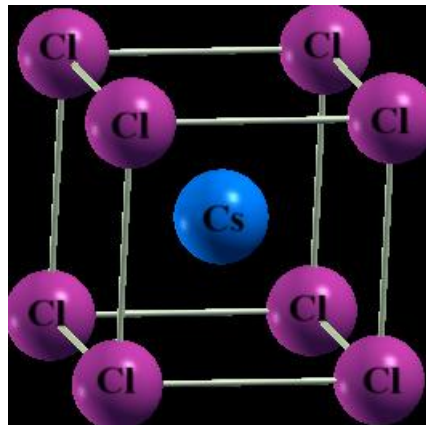


Figure 1.2: B₂ structure of binary intermetallic compounds

1.3. Review of Literature

R.R. Hasiguti, et al. examined various properties done for the TiNi intermetallic compound, in which they explained about the internal friction and some other properties under temperature range of 170°-800°C. They form a graphical representation of an internal friction curve having a well-defined peak range from -70° to 600°C, and also represent a variation of the peak at a particular temperature, is 350 °C results small variation in peaks and a calculation for sharp variation in peaks around

-50° to 40°C. They also calculated the crystal structure according to Wang and have a mechanical property, elastic modulus, which shows a positive value of the temperature coefficient [7].

K. N. Tu, et al. investigated N-Si Samples. In which they form a formation of thin film. They calculated the samples of Ni-Si. These calculations are done for the binary systems only. In the sample, these intermetallic compound Ni forms of film on a silicon substrate at a temperature range from 400° Celsius, and for NiSi₂ show the stable transformation can be annealed. After that, they form a lattice image. After that, they form a lattice image from an epitaxial interface of NiSi on the silicon substrate. In the bulk modulus NiSi diffusion couples which they show the growth of the dominant but irregular in shape [8].

Y. Kimura et al. performed microstructure calculations for binary compounds and investigated the mechanical properties of various intermetallic compounds with a B₂ crystal structure, focusing on Co–Al systems. Their results showed that cobalt-rich compositions were first examined in the stable phase region, with particular interest in thermal analysis using the X-ray copy dispersion method. Most of these intermetallic compounds underwent microstructural treatments followed by hot rolling, which minimized the energy required for compressive states exhibiting plastic strain. These properties were evaluated at room temperature for cobalt alloy compositions ranging from 72 to 76 at.% Co [9].

The study examined NiAl, FeAl, and CoAl—all B₂ structured intermetallic compounds—by combining thermodynamic modeling with experimental measurements of lattice parameters and bulk densities to determine point defect concentrations across varying compositions and temperatures by L. M. Pike, et al.. A key outcome was the correlation between defect type and mechanical hardening:

- Vacancies were shown to be significantly stronger hardeners than antisite defects.
- Hardening rates were linked to lattice dilation effects, with vacancy-induced dilation being especially influential.

According to this method, they gave the vacancy approach due to the interstitial solutions and having given the many anti-site defects for the magnitude having a lattice dilation [10].

In this paper, T. Fukuda et al. studied the systematic stability of intermetallic compounds relevant to Ti-Ni shape memory alloys using first-principles calculations. They also analyzed the electronic states involved in structural formation, employing the muffin-tin orbital method for these calculations. Additionally, the authors calculated the electron density of states, identifying the Fermi energy level and observing a decrease in the density of states across successive regions from the B₂ to R mapping B₁₉ structure. They reported that the number of valence electrons increases for Ti₃Ni₄, whereas it decreases for TiNi₂. Interestingly, when substituting Cu for Ni, Ti₃Ni₄ does not form, while TiNi₂ remains stable and can be formed [11].

A general computational scheme for analyzing defects in intermetallic compounds (IMCs) has been described in terms of chemical bond formation properties. In this context, N. Bornsen et al. investigated bonding orbitals as well as antibonding hybrid orbitals. These calculations contribute significantly to the total energy associated with atomic interactions and the localization of atomic orbitals. The study primarily focuses on B₂ phases, where defect energies are largely influenced by the properties of transition metals and aluminum. Structural stability analyses of compounds such as FeAl, CoAl, and NiAl indicate that some previously held hypotheses about these materials are not fully valid, as they exhibit notable covalent characteristics. Methods like this are particularly appealing for defect studies; however, they require careful validation to avoid misinterpretation. The computational scheme presented in this paper offers a useful tool for investigating the complex defect behavior observed in B₂ aluminides [12].

In this paper, J.B. Yang et al. investigated MnBi alloys in their low-temperature phase, which exhibit a notably high coercivity value of 2.4 Tesla. The alloys show a positive temperature coefficient above this high coercivity, with a temperature range up to 400 K. These alloys behave as permanent magnets at specific elevated temperatures, with operational temperatures ranging from 150 K to 300 K. The study also provides insights into spin orientation, which is perpendicular to the principal axis. According to their calculations, the magnetic moment of Mn is -15 Bohr magnetons, attributed to the hybridization between Mn and Bi atoms. Additionally, the paper reports volume expansion due to increasing interatomic distances among Mn atoms, which is influenced by their magnetic moments [13].

According to this paper, the structural and electronic properties of the compounds were investigated using first-principles methods. The study concluded that the elastic properties were analyzed for six different binary systems. Subsequently, B. Wen et al. calculated the lattice parameters for the compound Al_5Ru_2 , which were found to be in good agreement with experimental results. The detailed structural parameters indicated that the high-energy states of these compounds corresponded to a metastable phase rather than a fully stable one. The authors also determined the absolute heat of formation, finding values exceeding 30 kJ per mole of atoms. Their results showed that the strength of chemical bonding between Al and Ru increases with higher Ru concentration, leading to an increase in the system's bulk modulus. Additionally, the indirect bandgap of the semiconductor was calculated to be 0.168 eV [14].

In this paper, D. Shi et al. studied the structural properties of Al–Ni intermetallic compounds and examined their elastic and electronic properties. All calculations were performed using density functional theory (DFT). The computed values at absolute temperature indicate the bonding characteristics between Al and Ni atoms, showing that chemical bonding is the primary interaction. The compounds generally exhibit single-crystal elastic constants, which provide insight into their mechanical stability. Analysis of the electronic structure confirms that these intermetallic compounds are stable and behave as conductors. Mechanical properties were evaluated using the Voigt approximation, along with the Reuss–Hill method for more accurate estimates. Among the studied compounds, AlNi , Al_3Ni , AlNi_3 , and Al_3Ni_5 are ductile, while Al_4Ni_3 and Al_3Ni_2 are brittle. The calculated heat formation for these compounds was 47.5 kJ/mol per atom [15].

R. P. Singh et al. conducted a first-principles study of intermetallic compounds containing copper and zinc. They employed the full-potential augmented plane wave (FP-APW) method along with the local orbital approach (APW + lo) within the framework of density functional theory (DFT). Elastic properties were evaluated using exchange-correlation probabilities, while lattice parameters and their pressure derivatives were determined through an optimization method. From the electronic structure calculations, it was observed that in rare-earth intermetallics based on copper and zinc, electronic conduction is primarily governed by the 3d orbitals of Cu and Zn [16].

The structural, thermal, elastic, and electronic properties of intermetallic compounds LuX (X = Mg, Cu, Ag, Au, Zn, Cd, and Hg) have been studied by G. Pagare et al. Mechanical properties calculations have also been performed for these compounds. All calculations were carried out using the ab initio method, which was generally based on the full potential linearized augmented plane wave (FP-LAPW) approach. The study first analyzed the magnetic properties using the generalized gradient approximation (GGA). Ground-state properties were also calculated, and optimization was performed to determine the lattice parameters. The bulk modulus and its pressure derivatives were obtained for the CsCl (B₂) crystal structure. These calculations, conducted within the FP-LAPW framework using GGA, provide detailed insights into the compounds properties. For the LuX compounds, the electronic band structure plots indicate that these materials are metallic and stable in the CsCl phase. The elasticity results further confirm their metallic behavior and reveal trends in their mechanical stability [17].

An investigation by H. Devi et al. into the morphological, electronic, and flexible properties based on thermal compounds of monpnictides where (CmX; X=N, P, As, Sb, and Bi) is performed. The first principles method calculation by higher pressure, which one based on DFT. They also show the GGA coupling with some corrections. Our results demonstrate that their ambient NaCl (B₁) type changes from a structural phase to a CsCl (B₂) type structural phase. They show the structural phase of CmN is 111.80, CmSb is 7.52, CmP is 36.81, CmAs is 22.08, and CmBi is 7.14 GPa using LSDA, respectively. Custom parameters have also been reported in phases B₁ and B₂. The calculated band structure indicates that all CmX have phase B₁. They show the majority metal for spin, and the half metal shows for the minority. Most of the thermal properties were predicted from the constants of elasticity. They also calculated the shear ratio of B/G_H of these compounds, having a density of states. [18].

J. Du et al. had already performed first-principles calculations for binary compounds such as Cu-Zr, which exhibit intermetallic character. These studies investigated the mechanical properties of the compounds, showing that variations in Zr concentration influence the mass density proportionally. All Cu-Zr intermetallic compounds studied are ductile and mechanically stable. From these calculations, it is evident that the stability constants derived from first-principles confirm the binary nature of compounds like Cu₅Zr, Cu₅₁Zr₁₄, Cu₂Zr, Cu₁₀Zr₇, Cu₈Zr₃, CuZr, Cu₅Zr₈, and Cu₂Zr.

Structural and electronic properties were extensively analyzed, and optimization of lattice parameters yielded values in good agreement with both experimental data and previous theoretical studies. The mass density shows a decreasing trend with increasing Zr concentration. Polycrystalline Cu-Zr intermetallic alloys exhibit reduced elastic moduli. Heat formation calculations for the eight Cu-Zr compounds are negative, indicating stability. Among these, CuZr exhibits an indirect bandgap of 0.227 eV, behaving like a semiconductor, whereas the remaining seven intermetallic compounds demonstrate good metallic conductivity [19].

In this study, we concluded that several properties can be used to assess the structural stability of the ZrAl intermetallic compound. The analysis showed that two atoms were stable in the (110) crystallographic plane. Elastic property calculations indicate that the formation enthalpy of ZrAl₂ is negative, signifying a thermodynamically stable compound. Y. H. Duan et al. also calculated the direct band gap of Zr₂Al₃ to be 0.053 eV. This suggests strong covalent bonding between the atoms, particularly involving the two aluminum atoms in the (110) plane. Such phase characteristics contribute to the overall stability of the Zr–Al system [20].

In this paper, several properties were calculated using the GGA approximation. The studied structure was found to be stable for the compound in the B₂ phase. Thermodynamic properties such as Poisson's ratio, bulk modulus, and isotropic ratio were calculated for OsAl and OsSi compounds using GGA. N. Acharya et al. also investigated electronic properties, providing insights into the various spin states. A graphical representation of the density of states was plotted, where the Fermi energy separated the energy states. Additionally, the elastic constants C₁₁, C₁₂, and C₄₄ were determined. Using these constants, the Debye temperature was calculated, offering valuable information about the compounds. The metallic nature of the materials was also demonstrated through the plotted electronic states [21].

E. Jain et al. carried out calculations using ab-initio methods within the framework of Density Functional Theory (DFT). They investigated CuX compounds, where X = Sc and X = Pd, both of which adopt a B₂ phase structure (space group Pm-3m, No. 221). These structures exhibit stability similar to the cubic cesium chloride type. The correlation potential was examined using three different approximations: PBE-GGA, WC-GGA, and PBEsol-GGA. The study determined several ground-state parameters,

including the pressure derivative of the bulk modulus, lattice parameter, and the optimized volume–energy relationship. Electronic structure calculations and density of states (DOS) plots revealed the metallic nature of the compounds. Independent elastic constants were computed, from which mechanical properties such as average sound velocity and longitudinal velocity were derived. The authors also evaluated thermal properties, including the Debye temperature [22].

In this paper, G. Pagare et al. calculated extensive properties, including the thermal conductivity, of BeX ($X = \text{Co, Ni, Cu, and Pd}$) intermetallic compounds. These materials exhibit strong resistance to environmental relaxation and stress. All parameters were computed using the FP-LAPW approximation method. From structural optimizations, the authors determined the stability criteria for both non-magnetic (NM) and ferromagnetic (FM) states. BeCo was found to be stable in the FM state, while the other compounds were stable in the NM state. The electronic band structure analysis revealed the metallic nature of these compounds, along with differences between spin states and their respective contributions to the overall properties. Additionally, the ductility and brittleness of the compounds were assessed, indicating which materials can better withstand stress and compression while retaining their intrinsic properties [23].

In this paper, W. C. Hu et al. studied the structural, elastic, and mechanical properties of Sr–Zn intermetallic compounds using the pseudopotential method. The formation enthalpy results indicate the structural stability of the compounds, with all intermediate phases stabilized by negative enthalpy values. The analysis showed that these compounds are more stable in hexagonal structures. Thermodynamic properties were also examined. Mechanical behavior analysis, based on Pugh’s criterion, revealed that the compound is brittle. Furthermore, the electronic structure and density of states (DOS) plots, particularly highlighting the Zn d-states, confirm that the Sr–Zn compounds exhibit metallic behavior [24].

In this paper, the mechanical and electronic properties of Fe–Al intermetallic compounds were investigated using density functional theory (DFT). Cohesive energies and formation enthalpies were also calculated. Y. Liu et al. further evaluate the thermal stability of these compounds, reporting that Fe_3Al had the largest bulk modulus of 233.2 GPa, while FeAl exhibit the highest Young’s modulus of 296.2 GPa.

The variation in Debye temperature shows that Fe_2Al_5 has the highest value at 667.8 K, whereas Fe_3Al had the lowest at 516.6 K. Analysis of the bonding properties reveals that Fe–Al binary intermetallic compounds are predominantly characterized by covalent and metallic bonding [25].

We concluded from this paper; there were structural properties that had been investigated by using different methods that were stable in the Orthorhombic structures and more. J. Wu, et al. also calculated some planarity projections which were in the 3D phase. These were characterized by using the FCC and HCP methods of the nanostructure materials, which were represented in the deposition of the different nanocrystalline stabilities, structure of the compound. They also calculate the pseudo-potential for the ultra-soft compounds. The general representation showed the binary compounds, behavior by using the CASTEP method. The cohesive energy calculations gave a Negative value for the compounds. To check the thermal stability of the compound, they calculated the formation energy. Elastic constant parameters had been determined by using the stress method, they were based on Hooke's law. Some elastic parameters have been determined by the Lagrangian strain behavior, which was done by the tensors, matrix method. They also gave information about the localization and delocalization of the orbitals. The value for the bulk modulus was 317.9 GPa for the compound $\text{Fe}_{11}\text{Si}_5$. Some temperature-dependent energy also gave information about the orderliness of the materials [26].

The combination of first-principles calculations with Boltzmann theory had been applied to study the thermoelectric properties of the intermetallic compound YbAl_3 . Using interpolation techniques based on density functional perturbation theory, the behavior of the compound can be accurately predicted. The study reveals a significant heating effect, which play an important role in electron transport and phonon density scattering. In this work, the electrical transport properties were investigated through first-principles calculations, where energy dependence was analyzed with respect to the relaxation time. J. Liang et al. demonstrated that the thermoelectric performance, particularly the power factor, can be enhanced through nanostructuring of the compound, leading to reduced thermal conductivity and improved efficiency for potential thermoelectric applications [27].

The mechanical properties of Ni–Ti intermetallic systems were investigated using first-principles calculations. Y.F. Li et al. reported that crystallographic variations along different transformation directions were analyzed, focusing on Ni₃Ti and NiTi₂ to better understand the isotropic structural characteristics. From these analyses, the stability and formation of the intermetallic compounds were examined. The results indicated that these compounds exhibit anisotropy and are generally hard and brittle in nature. They also explored the shock resistance of these materials when combined with ceramic phases, achieving a mixture with enhanced mechanical performance. The order of hardness was found to decrease as follows: Ni₃Ti > B₂NiTi > B₁₉'NiTi > NiTi₂ and Ni₃Ti. Furthermore, Ni₃Ti was shown to mix evenly with iron-based alloys and ZTA (zirconia-toughened alumina) ceramics, improving composite behavior [28].

In this paper, R. Iqbal et al. investigated some compounds based on DFT was calculated to verify the structural, electronic structure of the compound in series ScTM (TM = Cu, Ag, Au, and Pd). From the variation of result elasticity of the given compound gives the value of Power factor of $200 \times 10^2 \text{ W/cmK}^2$ was obtained for the content. The Calculated Variable properties based on the elastic constants adhere to the criteria of Stability of the mechanical properties, which suggested formation of stable compounds was in mechanical equilibrium. B/G ratio predicts the inferiority of the natural resources of these compounds. Distortion of anisotropic continuity indicates the property of anisotropic apart from ScPd, except value was almost unity. A larger value of B/C₄₄ gave a higher order of plastic deformation of the compound to other materials [29].

In this paper, we understand the structural formation of the compound, mechanical and thermodynamic properties by A. Benmakhlouf et al. The variation of CuSc intermetallic compound under temperature and variable pressure could be calculated pseudo potential approach, which was inbuilt in the DFT. At equilibrium conditions, the structural parameter was determined in this paper. The mechanical properties criteria could be studied under the pressure that varies from 0 GPa to 12 GPa. This mechanical stability further helps to calculate the various thermodynamic properties like specific heat capacity; the Debye temperature variable rises from 0 Kelvin to 1000 Kelvin. The calculation of the optimized cubic lattice parameter is 3.261 angstrom. The stability criteria for the occurrence of the different variable phase transitions in the

B₂ structural property, which comes at 25.5 GPa at a given room temperature, and having studied 0 pressure. The calculated value for the bulk modulus, which was isothermally stable in the material, is 80.86 GPa, and the calculated value of the Grüneisen parameters is approximately 2.04 [30].

In this paper, they study Cu-Li intermetallic for the different stable phases. The study of these compounds was done only at atmospheric pressure. The structured properties in the Fmmm Cu₁Li₂, Fd-3m Cu₂Li₁, and P1-Cu₇Li₁ were identified. The electronic structure properties showed the behavior of the bonding for copper-Copper was covalent bonding, and the formation of copper-lithium bonds results the ionic bonding. The bonding formation of the compound was due to the 3d states of the copper element which was stable in the phase, which were above structural application. J. Yu, et al. also calculated the effect of the concentration on the copper element systematically formation for the compound. This covalent bond revealed the information about the Poisson ratio factor, which generally varied from 0.25 to 0.35. Some elastic modelling and hardness, which were done by the Vickers method, gave valuable information about the ductility and brutality of the compound. They also calculated the anisotropic ratio for the compound. The study gave the information about whether the compound was more elastic or less elastic, and also gave the information about the compressibility factors [31].

In this paper, the results of first-principles calculations on the Mg–X intermetallic compounds were presented. The study focuses on metastable phases within a balanced geometric configuration and examines the effects of pressure. The phonon dispersion spectra of various compounds were analyzed using multiple linear-response techniques. The spectra show no anomalies in the ground state. Phonon and elastic properties indicated that the compounds can exist in C₁₄, C11_b, D0₁₉, D0_c, and LI₂ structural phases. These elastic constants provide criteria for determining the metastability of the compounds, revealed conditions under which they remain stable under certain pressure ranges. The electronic structure analysis showed that Mg–X intermetallics exhibit metallic character, as confirmed by the bonding characteristics. According to S. Ramesh Kumar et al., most Mg–X intermetallic compounds display both electronic and physical features that were strongly linked to their stability stage,

making them valuable for understanding the fundamental physics and stability mechanisms of such systems [32].

In this paper, the mechanical properties of some chalcogenides were calculated. There were some thermal properties of terbium chalcogenides, TbX (X=S, Se) compounds, done by the DFT method. In this paper, some ground-state parameters were calculated by using the WIEN2k code. The equation of state would be calculated by using the Birch-Murnaghan. S.N. Tripathi et al. gave us the magnetic properties of the compound, which are stable in the FM phase. They also calculated that the magnetic moment over the compound value was $5.44 \mu_B$ and $5.57 \mu_B$. They also calculate some electronic properties, which gave us the information about the Spin states of the compound, in which they were the major contributions for the electrons of the Tb to crossover the Fermi level due to 4f electronic states. Some magnetic properties were calculated, which gave us the information about how significant a factor is in the latest technologies, with the help of the fabrication of devices. These calculations were done by the Charpin method takes us the information of the material, how material was rigid and the stiffness. They also calculated some of the thermal properties, which gives valuable results [33].

In this paper, F. Sun et al. gave us the excellent properties of the binary compound. These calculations were performed using the CASTEP method. They gave us the information about the stability of the compound. This compound was similar to our compound, which showed an intermetallic. The microstructure properties would be calculated for this compound. The study also calculated the structure stability in the orthorhombic and tetragonal Phases. They calculated the eight compounds based on Al-La, which were in the binary form the properties of Al-La. They also calculated the solid-state properties, identified monotonic states corresponding to the highest (but negative) formation energy values. The enthalpy was evaluated using the convex hull approach, providing insights into the metastable and spin states. Cohesive energy was determined, with its value found to decrease, and temperature-dependent binding properties were also investigated. Some intermetallic compounds (IMCs) were found to exist in a single phase but as single crystals, with results reported only under uniaxial stress conditions. The crystalline behavior was analyzed using the Voigt–Reuss–Hill (VRH) approximation. Additionally, the study provided macroscopic-level

information on thermal properties and examined the periodicity of the compound, which yielded valuable results about the work function [34].

In this paper, Y. Pan et al. studied Cr–Si binary compounds, which were silicides, and calculated various functional properties based on their intermetallic nature. These properties were analyzed due to their relevance in modern technologies, particularly in semiconductor devices. The authors evaluated several high-temperature-dependent characteristics relevant for industrial applications. The shear modulus of the compound was found to be comparatively high, and bulk properties of other related metals were also determined. They investigated the thermoelectric potential and applicability of these compounds in high-temperature industries. Corrosion resistance measurements revealed that the material possesses magnetic properties but has a poor corrosion resistance coefficient. Additional calculations on heat-related parameters provided significant insights into the thermal properties of the compounds. However, the study concluded that Cr–Si silicides exhibit poor heat resistance. The authors suggested that large-scale applications could be further explored using density functional theory (DFT) [35].

In this paper, the authors concluded that the magnesium-based alloy had vast applications in the automobile sector. According to Y. Zhou et al., the alloy exhibit high heat resistance, making it suitable for devices where thermal stability was essential. This property further enhances the alloys ability to resist deformation. Calculations under pressure provided insights into the phonon dispersion behavior, as well as data relevant to the rail transit applications of the material. Due to its lightweight nature, the alloy demonstrates excellent casting ability, enabling its use in the production of components for transportation and aerospace engineering. The authors also investigated solidification behavior, noting that it can be altered or controlled through temperature-dependent processes. Additionally, they examined the weakening of texture in the compound, which provided valuable information on the deformation mechanisms of magnesium alloys. The study further discusses how the alloy can store and release energy during deformation, offering insights into system stability. Several primary methods were proposed to improve the elastic and mechanical stability of the compound, including approaches based on high-solubility vector strengthening and controlled solidification techniques [36].

In this paper, some rare earth elements had been investigated, detailed information about the hardness of the material and the further investigation of the compound based on the thermal investigation properties. In this paper, some new investigations had done based on the high-density coherent sources, which were used for the treatment of the ageing of the compound heat treatment. T. Liu, et al. had high melting properties, which revealed information about the ductility and the expansivity of the value at a lower temperature. They were further giving us the information on how the material is a highly strengthening phase formation. Calculation was done systematically to form and refine the valuable results. The all-relationship method of the aluminum rare earth elements, which calculated the finishing for different, different conventional ranges. The material under the hierarchy of the crystal structures provided information about the different elastic constants, which were significant factors. If the larger value, it means the bonding between the atoms was very strong and had directed values, which were a directional state of bonding. The stability criteria for these compounds were in the decreasing order Al_2RE , Al_3RE , $AlRE$, $Al_{11}RE_3$, $AlRE_2$, and $AlRE_3$ [37].

The investigations in this paper, involved thermodynamics, had various applications based on the first principles theory. The key was the excellent result, had the illustrations that were further used in the high-performance devices for the solidification of the material. Y. Xu, et al. had a very high yield strength. The information about the optimization of the compound revealed the information about how material is reduced in the form of when the titanium ions are dissolved in the form of the copper matrices. The thermal conductivity of the compound provided information about the determination of the material, which was in the form of the minimum energy value. All these calculations gave the information about the pseudopotential having a depth iron core variable information. They calculated the crystal structures for the CuTi compounds and found a very high value for enthalpy, which was positive in the states. Some thermal properties would be investigated by using these methods and having a decreased order, which showed $CuTi > Cu_4Ti_3 > CuTi_2 > Cu_2Ti > Cu_4Ti > Cu_3Ti_2$. [38].

There was Ti-Co based on the intermetallic properties investigated, which provided the information about the phase stability of the compounds, and the information about the bonding properties, which were further used in the device fabrications. This study

revealed information about how the compound was thermodynamically formed and its stability. F. Zeng, et al. gave information about the 3d phases. They calculated the charge-based properties, which provided information about the spin states of the material. They gave us the information about the bonding, which shows that the strength is strong and bonded. The extensive research for titanium-based alloys, resulting the more strengthened compounds and had a melting point at a very low temperature. The authors formed thin films based on the coatings, which were further formed of the $\text{Ti}_6\text{Al}_4\text{V}$. The compound is stable in the gamma faces at very high temperatures for the device. Fabrication and the solidification of the devices make the solidification of the devices, which also forms the different phases, like laves phases. The crystallite of the compound and calculated the displacement vector, which helped us to study the phonon transformation frequencies [39].

In this paper, the various stabilities of the intermetallic compound had been investigated. We also know about the hydrostatic pressure based on the Vickers hardness of the compounds of the material AuAl . X. Han, et al. also calculated the anisotropic ratio, which provided information about the rigidity and the toughness of the compound. An isotropic ratio was decreased in the form, which means the value of the Debye temperature and the hardness of the compound was increased. These calculated results also provided information about the low rigidity of the compound. All these calculations had been done by using the first principles method. The bonding properties of the gold wire particles also gave the informational properties about the compound [40].

From this paper, it was concluded that the phase stability structure of the materials was established. The elastic properties of the intermetallic compounds were calculated using density functional theory (DFT) based on first-principles calculations. Y. Ling et al. studied Al-Pr compounds. First, they calculated the optimized lattice parameters and examined the energy minimization process to determine the structural stability of the compounds. Their results for Al_2Pr indicated the strongest bond formation among the alloy particles, and they also calculated the cohesive energy of the compounds. Furthermore, they computed the elastic parameters for the $\alpha\text{-AlPr}_3$ compound, which exhibited the highest anisotropic values, while for Al_2Pr , the results suggest that it was isotropic in nature [41].

The binary system diagrams had studied at higher pressures. D. Shi et al. reported the phase diagram of the Ta–Sb system, calculated using density functional theory (DFT). Computational screening of intermetallic compounds was performed to identify non-centrosymmetric superconductors at their critical temperatures. The thermal and mechanical properties of this compound were also calculated, revealing excellent thermal conductivity. The study further demonstrated that high-pressure exploration of different structures, along with potential surface calculations, can guide the design of metallic compounds [42].

In this paper, Intermetallic compounds for two or more metallic elements with a possible structure of the compound in the B2 phase and having a cesium chloride space group 221 Pm-3m Crystal structures. In this paper, the super ductility and Lower specific gravity of this compound under favorable conditions for aerospace applications. There were some alloys, Al-Ni, Al-Ti, and Al-Fe, which gave impressive properties like a melting point that results in higher temperatures. M. A. Bouchentouf also calculates the resistance property, which provided excellent corrosion enhancement, and also had low-density compounds. This application was suitable for aircraft gas, which was used for turbine blades. These calculations were done by the ab-initio method [43].

1.4. Research motivation and objectives

1.4.1. Research motivation

This present works is motivated by some interesting facts which are building block ups upcoming technologies. Before the commencement of the present work, many research articles were studied. The motivation towards the Intermetallic compounds forced me to explore some novel materials for their fascinating physical performances and extraordinary technological applications. These compounds allow the development of smaller, more adaptable, and more durable electronic devices. Overall, the motivation behind studying Intermetallic compounds lies in their unique properties, multifunctionality, potential applications, and energy efficiency. By exploring and exploiting the properties of Intermetallic compounds, researchers aim to develop new technologies and contribute to scientific progress in various fields.

1.4.2. Research objectives

The Intermetallic compounds, like Be-based, Mg-based, and Cu-based Intermetallic compounds, would be investigated. The efforts would be made

1. Optimization of the structure of the proposed intermetallic compounds by establishing energy-volume relationship.
2. Plotting of various electronic states as band structure and density of states to ascertain materials metallic nature.
3. Study of numerous thermophysical properties under pressure and temperature by using Quasi – Harmonic Debye model as implemented in WIEN2k.
4. Study of different mechanical properties by using Charpin method as implemented in WIEN2k.

1.4.3. Thesis outline

Intermetallic compounds are currently a topic of interest for both theoretical and experimental researchers due to their increasing significance. This work aims to investigate the structural, electrical, mechanical, elastic, and thermodynamic properties of IMCs based on Be, Mg, and Cu, as well as potential applications. The result is that the thesis is organized into six chapters.

Chapter 1 presents information about the intermetallic compounds. This chapter has also covered the categorization of alloys and their potential transformation into intermetallic compounds. Additionally, they have talked about their stable, optimized structural phase, which is often the B2 phase. A thorough literature evaluation is provided in light of these. We may formulate the research problem and study objectives in light of the review of the literature.

Chapter 2 provides a thorough explanation of how the code utilized in the current study was calculated. Since density functional theory (DFT) is used in the current study's electronic structure calculations, a brief introduction to DFT, along with an appropriate methodology and potentials used, is included. The Charpin approach has been given as a means of computing mechanical and elastic parameters. In addition, a quasi-harmonic model has been proposed to investigate the thermophysical properties of the materials.

In Chapter 3, results are shown for the selected materials' various physical attributes. Among these materials are Be-based intermetallics, such as BeAg, BeAu, and BeFe. The LAPW approach has been used to offer potentially intriguing results on mechanical, thermodynamic, and electronic structural features. GGA approximations have also been used to analyze the magnetic stability of these compounds. The nature of bonding has also been examined, along with its elastic characteristics in the face of external forces and deformations. The findings of the work have been published in SCI indexed Journal of Chemical Thermodynamics vol. 188, pp 107175, 2024.

In Chapter 4, the magnesium-based intermetallics (MgLu and MgHf) have been described in terms of their structural, thermodynamic, elastic, and mechanical properties. The Debye quasi-harmonic model and the Charpin method are used in the investigation. It is discovered that both intermetallic compounds are stable in the non-magnetic phase of the CsCl prototype structure. They demonstrate a metallic quality in their electrical band structure by utilizing the most suitable generalized gradient approximation. In addition, bulk to shear modulus ratios, elastic moduli, and Cauchy pressure are calculated. It is discovered that MgLu and MgHf exhibit ductile and brittle natures, respectively.

In Chapter 5, calculations have been made for a number of thermophysical parameters, including bulk modulus, unit cell volume, Debye temperature, molar heat capacity at constant volume, and thermal expansion coefficient of CuZn. The results have been published in Scopus-indexed proceedings- AIP Conference Proceedings vol 2800, pp 020153, 2023.

In Chapter 6, concluding remarks in the form of a summary are presented along with the scope of this study.

References

1. Callister, W.D. (2007). *Materials Science and Engineering: An Introduction*. 7th edition, John Wiley and Sons. Inc. New York, Section 4.3 and Chapter 9.
2. Askeland, Donald R.; Wright, Wendelin J. (2015). 11-2 Intermetallic Compounds. *The science and engineering of materials* (Seventh edition). Boston, 387–389.
3. Panel On Intermetallic Alloy Development, Commission On Engineering And Technical Systems (1997). *Intermetallic alloy development a program evaluation*. National Academies Press, 10.
4. Soboyejo, W. O. (2003). *Intermetallics. Mechanical properties of engineered materials*. Marcel Dekker.
5. Hume-Rothery, W. (1955) [1948]. *Electrons, atoms, metals and alloys* (revised ed.). London: Louis Cassier Co., Ltd. 316–317.
6. Wings of steel: An alloy of iron and aluminium is as good as titanium, at a tenth of the cost (2015). *The Economist*. Retrieved February 5, E02715
7. R. R. Hasiguti and K. Lwasaki (1968). Internal Friction and Related Properties of the TiNi Intermetallic compound. *Journal of Applied Physics*, 39, 2182.
8. K.N. Tu, G. Ottaviani, U. Gosele, and H. Foll (1983). Intermetallic compound formation in thin film and in bulk sample of the NiSi binary system. *Journal of Applied Physics*, 54, 758.
9. Y. Kimura, H. Kuriyama, T. Suzuki, Y. Mishima (1994). Microstructure control and mechanical properties of binary Co-Al alloys based on the B2 intermetallic compound CoAl. *Materials Transactions* 35 (3), 182-188.
10. L. M. Pike, Y. A. Chang and C. T. Liu (1997). Point defect concentration and hardening in the binary B2 intermetallics. *Acta Metallurgica*, 45 (9), 3709-3719.
11. T. Fukuda, T. Kakeshita, H. Houjoh, S. Shiraishi, T. Saburi (1999). The electronic structure and stability of the intermetallic compound in the system. *Materials Science and Engineering*, A273-275, 166-169.
12. N. Bornsen, G. Bester, B. Meyer, M. Fahnle (2000). Analysis of the electronic structure of intermetallic compounds, and application to structural defects in B2 phases. *Journal of Alloys and Compounds*, 308, 1-14.

13. J. B. Yang, W. B. Yelon, W. J. James, Q Cai, M Kornecki, S Roy, N. Ali, P. Heritier (2002). Crystal structure, magnetic properties and electronic structure of the MnBi intermetallic compound. *Journal of Physics: Condensed Matter* 14, 6509-6519.
14. B. Wen, J. Zhao, F. Bai, T. Li (2008). First-principle studies of Al-Ru intermetallic compounds. *Intermetallics*, 16, 332-339.
15. D. Shi, B. Wen, R. Melnik, S. Yao, T. Li (2009). First principles study of Al-Ni intermetallic compounds. *Journal of Solid State Chemistry*, 182, 2664-2669.
16. R.P. Singh, R.K. Singh, Shalu, M. Rajagopalan (2012). First-principle study on structural, elastic and electronic properties of binary rare earth intermetallic compounds: GdCu and GdZn. *International Journal of Computational Materials*, 1, 14.
17. G. Pagare, S. S. Chouhan, P. Soni, S.P. Sanyal, M. Rajagopalan (2013). Electronic, elastic and thermal properties of Lutetium intermetallic compounds. *Solid State Sciences*, 18, 141-148.
18. H. Devi, G. Pagare, S. S. Chouhan, S. P. Sanyal (2013). Structural, Electronic, Elastic and thermal properties for curium mononitrides: A First Principles study. *Computational Material Sciences*, 74, 148-159.
19. J. Du, B. Wen, R. Melnik, Y. Kawazoe (2014). Phase stability, elastic and electronic properties of Cu- Zr binary system intermetallic compounds: A First-principles study. *Journal of Alloys and Compounds*, 588, 96-102.
20. Y. H. Duan, B. Huang, Y. Sun, M. J. Peng, S. G. Zhou (2014). Stability, elastic properties and electronic properties of the stable Zr-Al intermetallic compounds: A first-principles investigation *Journal of Alloys and Compounds*, 590, 50-60.
21. N. Acharya, B. Fatima, S. S. Chouhan, S. P. Sanyal (2014). First Principles study on structural, electronic, elastic and thermal properties of OsAl and OsSi. *Advanced Materials Research*, 1047, 71-77.
22. E. Jain, G. Pagare, S.S. Chouhan, S.P. Sanyal (2014). Structural , electronic, elastic and thermal properties of some transition metal CuX (X= Sc and Pd) intermetallics: A FP-LAPW study. *Computational Materials Science*, 83, 64-69.

23. G. Pagare, E. Jain, S.P. Sanyal (2015). Density functional investigation on electronic structure and elastic properties of BeX at high pressure. *Indian Journal of Physics*, 64-70.
24. W. C. Hu, Y. Liu, D. J. Li, H. L. Jin, Y. X. Xu, C. S. Xu, X. Q. Zeng (2015). Structural, anisotropic elastic and electronic properties of Sr-Zn binary system. *Intermetallic compounds: A first principles study. Computational Materials Science*, 99, 381-389.
25. Y. Liu, X. Y. Chong, Y. Jiang, R. Zhou, J. Feng (2016). Mechanical properties and electronic structures of FeAl Intermetallic. *Physica B: Physics of Condensed Matter*.
26. J. Wu, X. Y. Chong, Y. Jiang, J. Feng (2017). Stability, electronic structure, mechanical and thermodynamic properties of Fe- Si binary compounds. *Journal of Alloys and Compounds*, 693, 859-870.
27. J. Liang, D. Fan, P. Jiang, H. Liu, W. Zhao (2017). First-principles study of the thermoelectric properties of intermetallic compound YbAl₃. *Intermetallics*, 87, 27-30.
28. Y. F. Li, S.L. Tang, Y.M. Gao, S.Q. Ma, Q. L. Zheng Y.H. Cheng (2017). Mechanical and thermodynamic properties of intermetallic compounds in the Ni-Ti system. *International Journal of Modern Physics B* 31, 1750161.
29. R. Iqbal, M.Bilal, S. J. Asadabadi, H. A. R. Aliabad, I. Ahmad (2018). Theoretical investigation of thermoelectric and elastic properties of intermetallic compounds ScTm (TM= Cu, Ag, Au and Pd). *International Journal of Modern Physics B*, 2, 1850004.
30. A. Benmakhlouf, A. Benmakhlouf, O. Allaoui, Salah Daoud (2018). Theoretical study of elastic and thermodynamic properties of CuSc intermetallic compound under high pressure. *Chinese Journal of Physics*, 11.
31. J. Yu, D. Zhou, C. Pu, X. Tang, F. Zhang (2018). Prediction of Stable Cu-Li Binary Intermetallics from First-Principles Calculations: Stoichiometries, Crystal Structures, and Physical Properties. *Journal of Alloys and compounds*, 8388, 32520.
32. S. Rameshkumar, G. Jaiganesh, V. Jayalakshmi (2019). Structural, Phonon, elastic, thermodynamic and electronic properties of Mg-X (X=La, Nd, Sm)

- intermetallics: The First principles study. *Journal of Magnesium and Alloys*, 7, 166-185.
33. S. N. tripathi, Vipul Srivastava, S.P. Sanyal (2019). First Principle Mechanical and Thermodynamic Properties of Some TbX (X=S, Se) Compounds. *Journal of Superconductivity and Novel Magnetism*.
 34. F. Sun, G. Zhang, X. Ren, M. Wang, H. Xu, Y. Fu, Y. Tang, D. Li (2020). First-principles studies on phase stability, anisotropic elastic and electronic Properties of Al-La binary system intermetallic compounds. *Materials Today Communications*, 24, 101101.
 35. Y. Pan, D.I. Pu, E.D. Yu (2021). Structural, electronic, mechanical and thermodynamic properties of Cr-Si binary silicides from first-principles investigation. *Vacuum*, 185, 11024.
 36. Y. Zhou, Y. Lin, H. Wang, Q. Dong, J. Tan (2022). First-principles study on the elastic anisotropy and thermal properties of Mg–Y compounds. *Journal of Physics and Chemistry of Solids*, 171, 111034.
 37. T. Liu, T. Ma, Y. Li, Y. Ren, W. Liu (2020). Stable, mechanical and thermodynamic properties of Al-RE intermetallics: a First principles Study. *Journal of Rare Earths*.
 38. Y. Xu , M. Tian , C. Hu , Z. Han , S. Zhou , Y. Cao (2022). Structural, electronic, mechanical, and thermodynamic properties of Cu–Ti intermetallic compounds: First-principles calculations. *Solid State Communications*, 352, 114814.
 39. F. Zeng, M. Chen, H. Wang, H. Peng, B. Li, J. Huang (2023). First-Principles Investigation on Phase Stability, Mechanical Properties, Bonding Characteristic and Slip Properties of Ti-Co Binary Intermetallic Compounds. *Molecular Diversity Preservation International*, 13, 628.
 40. X. Han, M. Liu, X. Zhou (2023). Calculation of Mechanical Properties, Electronic Properties, and Thermodynamic Properties of AuAl Crystal: First-Principles Calculation. *Journal of Applied Physics*, 58, Issue 8.
 41. Y. Ling, W. Liu, X. Zou, H. Yan (2023). Phase stability and elastic properties of Al–Pr intermetallic compounds from first principles calculations. *Physica B: Condensed Matter*, 663, 415001.

42. D. Shi, J. Song, Y. Qin, X. Chen, S. Du (2024). A computational screening of Ta-Sb intermetallic at high pressure. *Journal of Applied Physics*, 135, 1444401.
43. M. A. Bouchentouf, A. Abdiche, D. Ghaffor, A. Mokadem, N. Beloufa, S. Bekheira (2024). Effect of SB addition on the mechanical, electronic and thermodynamic properties of intermetallic B2-NiAl: first principles study. *Annals of west university of Timisoara physics*, LXVI.

Chapter 2

Method of calculations

In this chapter, we first considered some computational approaches to investigate the intermetallic compounds in terms of various properties. By computational methods, we calculate most of the independent particle approximation, which directly deals with many-body problems. Physical Sciences, Chemistry, Materials Sciences, Chemical Engineering, and other related disciplines encompass a wide range of fields. Technologies that can reduce development time and cost before entering the laboratory process are necessary. The importance of computational theoretical approaches that can handle any atomic arrangement without introducing experimental parameters, increases in this context.

2.1. Density functional theory

Quantum mechanical approach has been done, which is a purely computational method based on the Density functional theory. In recent decades, DFT [1] is the most accurate practical approach and has been used to initiate various scientific results. These investigations are based on the electronic structures in the formation of the many-body systems. So, our calculations have been done by using this theory; we can easily determine by functionals, that is, functions of another function of many many-electron system. This method provides the information based on computational physics and chemistry, which are available in the field of condensed matter physics. This theory approximation is used to calculate the exchange potential and also gives detailed criteria information about the correlation of the interacting particles having the potential. If we look at the cost of the computational method for this compound, this is very low as compared to the other traditional methods like Hartree-Fock theory, which depend upon the electron correlation potentials, which are in the descendant's form. This method has come out as the most accurate theoretical approach and has been used to produce various scientific results. There are several examples available that surefire

the contribution of DFT in generating essential information, which would be impractical to discover through experiments.

First, in computational material science, DFT calculations are performed using the ab-initio approach. Higher-order parameters are not necessary for the computation of the material behavior, which is dependent on the basic material properties. The atoms' inter-electronic interactions are represented by this DFT approach. The potential system that underpins the density functional theory is created by adding up all of the exterior potentials (V_{ext}), which are further dictated by the system's elemental composition, structure, and effective potential (V_{eff}). The Schrodinger-like equation, also referred to as the Kohn-Sham equations, is utilized for n electrons of the materials [2].

The Thomas-Fermi model serves as the foundation for both the structural and electrical theories of materials. Walter Kohn and Pierre Hohenberg initially framed the DFT theory within the parameters of the two Hohenberg-Kohn theorems [3]. Using the HK theorems, we can quickly determine the non-degeneracy of the ground state energy in the absence of a magnetic field [4-5].

2.1.1. First Hohenberg and Kohn (HK) Theorem

We determine the electronic system's ground state properties using the Hohenberg-Kohn theorem [6]. These three spatial coordinates determine the electron density. First, we establish the foundation for the body problem of an electron with $3N$ spatial coordinates by determining the ground state properties with ease. This theorem extends the time-dependent density functional theory's (TDDFT) description of the excited state. This confirms that there is an injective mapping between the GS electron density and wave function.

Further, the derivation for computing the required density was done by Kohn and Sham (KS) [7]. Hence, the combined theoretical and computational work done by Hohenberg, Kohn, and Sham gave the current realization of DFT. Since they provided the rationale for utilizing electron density rather than the many-body wave function, Walker and Kohn were awarded the 1998 Nobel Prize in Chemistry for their pioneering work.

2.1.2. Second Hohenberg and Kohn (HK) Theorem

The functional energy of the system is defined by this theorem. It indicates that the system's energy functional is minimized by the ground state electron density.

Specifically, if the initial functional form $n(r)$ is known and would match the electron density $n_{KS}(r)$, computed through the KS equation, then that would be the GS electron density. This GS density would further help to calculate the value of the total energy volume. Therefore, KS thought of a way to derive a set of equations, each of which correlated to a single electron, to find the appropriate electron density.

$$\left[\frac{\hbar^2 \nabla^2}{2m} + V_N(r) + V_H(r) + V_{XC}(r) \right] \psi_i(r) = E_i \psi_i(r) \quad (2.1)$$

Here, V_N is representing a nuclear potential that describes electron-atomic nuclei interaction and V_H is a Hartree potential.

$$V_H(r) = e^2 \int \frac{n(r')}{|r - r'|} d^3r' \quad (2.2)$$

The coulomb repulsion inside an electron of one of the KS equations is indicated by the potential above, and total $n(r)$ originated from all electrons in a problem. Additionally, this potential indicates the relationship between the HF and KS methods. Exchange-correlation potential (V_{XC}), defined as a functional derivative (δ) of exchange-correlation energy (E_{XC}), is the third term in equation (2.1).

$$V_{XC}(r) = \frac{\delta E_{XC}(r)}{\delta n(r)} \quad (2.3)$$

The HF method created a system that represented the wave function as an orbital slater determinant, often known as a KS determinant. But for such systems XC potential is unknown and can only be derived from the free electron gas as shown below:

$$V_{XC}(r) = V_{XC}^{electron\ gas}(n(r)) \quad (2.4)$$

The above relation is directed towards the approximation of XC functional by using local density, hence it is also called as local density approximation (LDA). It examined how $n(r)$ matched the homogeneous electron gas (HEG) in terms of correspondence [7]. Further, the same value for states, KS, proposed an equality assumption between each small volume of the system and the volume of HEG. Although LDA sustained its workability in solid-state physics, another functional known as generalized gradient approximation (GGA) gave another breakthrough. In computational chemistry and materials science, both LDA and GGA are widely used approximations; however, GGA has some revolutionary features. The LDA approximation in principle is imperative and noticeable for systems with a low spatially varying $n(r)$, but fails to describe several features of d and f orbital compounds, and it also overestimates the binding energies [8]. LDA assumes the XC electron density to be uniform throughout the system, but GGA takes its gradient (varying electron density). The incorporation of gradient terms in GGA (explained in the subsequent heading) provides more accurate and efficient results of bond lengths and energies as compared to LDA, which is itself in describing the systems with strong $n(r)$ variations. Moreover, LDA tends to underestimate the band gaps and thus gives poor descriptions of electronic structures. However, GGA methods provide better and more accurate results for band gaps. In addition, when compared to experimental results, LDA underestimates the lattice parameter because it does not account for the complete range of interactions within the atoms. Conversely, GGA incorporates the fraction of exact XC to increase the lattice parameter's accuracy [1-13].

The density functional theory, which works on the electron density ($n(r)$) of the states for many bodies. Some computational methods for the available theories are discussed below

2.1.3. Hartree-Fock (HF) method

The method of this approximation is further used to calculate the behavior of a many-body electronic system, such as atoms and molecules. In this method, first of all, we considered an independent motion of the electrons, which involves building up a wavefunction $\Psi(r_i)$ of the N electrons that have to be considered. The wavefunction Ψ

(r_i) of the system is equal to the product individual electron's wave function $\chi_i(r_i)$. The consideration of the spin coordinate of the N number of the system having a symbol $\chi(r)$ is also known as the spin-orbital interactions [11].

$$\psi(r_i) = \chi_1(r_1)\chi_2(r_2)\chi_3(r_3) \cdots \chi_N(r_N) \quad (2.5)$$

This equation is also known as the “Hartree product” (HP). These equations state that the flow of the electronic wave function is not consistent with the indistinguishability of the electrons. The antisymmetric principle of a wavefunction changes its sign into the exchanging electrons is also known as the fermion, based on the Pauli Exclusion Principle. But HP does not change its sign with the exchanging of two electrons for N number of electrons of the wave function because the Slater determinant is a way to satisfy the antisymmetric principle.

$$\psi(r_1, r_2, r_3 \cdots r_N) = \frac{1}{\sqrt{N!}} \begin{vmatrix} \chi_1(r_1) & \chi_2(r_1) & \cdots & \chi_N(r_1) \\ \chi_1(r_2) & \chi_2(r_2) & \cdots & \chi_N(r_2) \\ \vdots & \vdots & \ddots & \vdots \\ \chi_1(r_N) & \chi_2(r_N) & \cdots & \chi_N(r_N) \end{vmatrix} \quad (2.6)$$

Nonetheless, this determinant—also referred to as the Fermi correlation—provides us with information regarding the correlation of the electrons in the uncorrelated wave function. Thus, the HF method does not consider the opposite spins of the electrons for the uncorrelated wave function. This method was found that feasibility of the molecule containing 10 to 20 atoms becomes computationally infeasible for the larger system.

2.1.4. Post-Hartree-Fock (HF) method

This improved version of the HF method is predicated on electronic correlation, which incorporates electron repulsions more effectively than the HF method does, which gives the average repulsion. In this method, there is only a single reference determinant present, and it also includes the configuration interaction (CI), coupled cluster (CC), and Moller-Plesset perturbation theory (MP) [1]. These method gives the information about the multiple variants, such as CCSD, the calculations include the excitation of single electrons (S) and two electrons, (D: double). However, if there are three electrons present, and calculations are named as CCSDT. The addition of a tiny perturbation based on the HF's Hamiltonian operator forms the basis of this theory. These method gives the accurate result, but their cost of the molecules over 20 atoms, which is also a big constraint [12], and also suffer from the truncation of the excitation

level of the atoms. Therefore, these methods have limits for a small system, and that's why they are computationally demanding.

Due to these drawbacks, DFT came to the spotlight and addressed these shortcomings of the HF method and post-HF method by using the electron density as the basis [8,13]. After the study of these things, first of all, the question comes to our mind, why do we need electron density over wave function, and where did it come from? This started from where the hunt for the ground state energy began through the time-dependent wave equation calculations. The electron-electron interactions, which are crucial for the derivation of the equation, are also included in the Hamiltonian for this equation [8]. Hence, that's why the wavefunction for individual electrons is directly linked to the function of the other electrons. And it is very hard to describe the discovery of the wavefunctions for the given set of coordinates, $r_1, r_2 \dots r_N$ and the likelihood of discovering N electrons at a specific set of coordinates was considered the defined probability is also named as $n(r)$, at a point in the space and formulated as:

$$n(r) = 2 \sum_i \psi_i^*(r) \psi_i(r) \quad (2.7)$$

From the equation, $\psi_i(r)$, this shows that the individual electron wave function has a position at r , and the factor 2 shows that the Pauli exclusion principle. This gives the physical observable quantity for the three coordinate functions. However, the wave function depends on the $3N$ spatial coordinates, and it is very complicated to handle.

2.2. Generalized gradient approximation

Being advanced to LDA, GGA favors the calculations in a way of improves total energies and also gives the structural energy differences [14-16]. In this approximation, since E_{XC} is dependent on both the gradients and the local electron densities, its expression in terms of spin-polarization is as follows:

$$E_{XC}^{GGA}[n^\uparrow, n^\downarrow] = \int f(n^\uparrow, n^\downarrow, \nabla n^\uparrow, \nabla n^\downarrow) d^3r \quad (2.8)$$

As mentioned in equation (2.8), E_{XC} of GGA includes a gradient of the first order, which helps to extract the information through various GGA functions. Such as Becke [B3LYP] [17, 18], Perdew-Wang [PW91] [19], and the most recent one is Perdew-Burke Ernzerhof [PBE] [20]. B3LYP has already been used as a DFT functional for

molecules containing transition metals and has shown prominent results for various chemical systems and their properties. However, this function has not ensured a uniform density limit. On the other hand, non-empirical PW91 and PBE functionals assured the uniform density limit and became even more special due to their authentic behavior of estimating more physical properties than LDA. As far as the concern is for present work is concerned, we used the PBE functional of GGA to probe the various materials and their properties.

Further, to add to the possible accuracy in the calculations of electronic and magnetic structures, an approach known as DFT+U or LDA/GGA+U was introduced. The term „U“ is a Hubbard correction discovered through the Hubbard model [21]. In this approach, an addition of on-site potential introduces coulomb repulsion between the electronic states, which are strongly correlated to the orbitals that are in *d* and *f* states. DFT+U approximation tends to be applied on the electrons of outer shells (*d* or *f*) to amplify the localization of electrons that provide substantial improvement in the electronic and magnetic properties [22].

Another functional known as modified Becke-Johnson (mBJ), introduced by Taran and Blaha in 2009 [23], actually modified the potential given by Becke and Johnson back in 2006 [24]. Their modifications of using mBJ-exchange in addition to LDA-correlation (mBJLDA) made this one of the best potentials in predicting band gaps, as other, much more expensive and sophisticated theories. Researchers quickly began to take notice of mBJ, which they later demonstrated to be a more accurate version of LDA and PBE functional by showing accurate band gap results [25]. Additionally, this XC potential is a semi-local, orbitally independent potential and can yield remarkable results of band gap and magnetic moment, which can compete with the expensive hybrid or GW approaches.

2.3. FP-LAPW method

The significance of the full potential linearized augmented plane wave method [26] (FP-LAPW) in estimating the physical, or specifically electronic properties, has increased significantly. This focuses on the theory of density functionals. It is an all-electron approach that can be used to calculate the properties of any element in the periodic table, including multi-atomic systems. As of late, this technique has been incorporated into a new front aimed at solving the density functional equations for crystalline solids, one-dimensional systems, and ultrathin films [27]. Furthermore, the FP-LAPW method is based on DFT for the treatment of V_{XC} . Though FP-LAPW still has relatively high memory and compute requirements, and its implementation is only suitable for rather complex systems, it is successfully implemented in the widely used WIEN2k code given by Blaha and his co-workers [28], written in FORTRAN 90 with the LINEX operating system. This implementation makes substantial advancements in the method, particularly in terms of speed, ubiquity, ease of use, and new functionality. It is also among the most accurate methods for determining band structure [28].

However, the method was initially developed from the augmented plane wave (APW) approach [29, 30], where Andersen [31] introduced additional advancement. Further, the linearized APW (LAPW) technique made it simple to handle the crystal potentials with a range of forms by aligning the variational problems' linear-algebraic formulation with the original formulation's convergence properties. Hence, the invention of FP-LAPW bulk film codes [26] was made possible by the consideration of the potentials and charge densities [32, 33]. By dividing a unit cell, the FP-LAPW method offers a basis set for the total energy, ground state density, and (KS) eigenvalues of many-electron systems, making it a crucial tool for solving KS equations. This approach divides a unit cell into three regions.

- i. Muffin-tin (MT) spheres that do not overlap, with atomic sites positioned around the radius, or RMT. The linear combination of radial wave functions, spherical harmonics, and their derivatives defines the basis function for each atom in this region. MT spheres are typically made to virtually fill every available space.
- ii. Interstitial regions (IR) in which the basis function comprises plane waves that relate to the MT's spherical harmonics and radial functions.

- iii. Vacuum region (VR), which is supposedly written in terms of cylindrical coordinates.

The merger of these basis sets is controlled by individual parameters, $R_{MT} \times K_{max} = 6 - 9$, where, R_{MT} is an MT radius and the largest K vector magnitude is known as K_{max} . On the other hand, the full-potential LAPW approach (FP-LAPW) handles charge density and potential inside defined regions without utilizing any shape approximations, where potential is defined as:

$$V(r) = \begin{cases} \sum_{lm} V_{lm}(\vec{r}) Y_{lm}(\hat{r}) & \text{Muffin - Tin} \\ \sum_k V_k e^{iKr} & \text{interstitial region} \end{cases} \quad (2.9)$$

where the MT approximation is bound to zero value of l and m, which leads to the spherical rate and IR region constituents zero value of K that corresponds to the volumetric rate.

2.4. Elastic and mechanical stability

Since mechanical properties are crucial to the final processing and use of materials, they must be taken into account when utilizing them commercially. These characteristics increase the effectiveness of the search by examining the behavior of the materials under external pressure. Mechanical parameters, followed by elastic constants, allow us to learn more about materials, such as their capacity to flex when a force is applied, and to assess the materials' stability in the face of external strain. Elastic constants are useful in determining the crystalline systems' mechanical stability, structural stability, ductility, chemical bonding, anisotropy, and possible phase transitions [34-36]. Elastic constants also assist in finding mechanical parameters, which are necessary for industrial purposes as well as basic research [37, 38].

The concept of elasticity was first explained by Robert Hooke, and an expression is known as Hooke's law [39, 40].

$$\sigma_i = C_{ij}\epsilon_j \quad (2.10)$$

With sufficiently small strains, the rule specified a direct relationship between stress (σ_i) and strain (ϵ_j), where the proportionality constant (C_{ij}) refers to the elastic constants. In contrast to cubic symmetry, which is represented by three unique elastic parameters denoted as C_{11} , C_{12} , and C_{44} , many independent components having a constant value of elastic tensor have varying numbers of elastic constants and frequently rely on the symmetrical behavior of the materials. These constants give precise details about mechanical behavior, such as material stability, elasticity, ductility, anisotropy, etc.

Moreover, several methods are there to determine elastic constants, and one of them is the Charpin method [41] as implemented in the WIEN2k code. In this, Voigt-Reuss-Hill (VRH) approximation [42-44] assists in regulating the various moduli within the stability criteria for cubic symmetry [45]. The Born stability criterion, also known as the Born and Huang criteria [46], is typically applied to the mechanical stability of cubic structural materials. The constraints are delineated by the following equations:

$$\left\{ \begin{array}{l} C_{11} > 0, C_{44} > 0 \\ \frac{1}{2}(C_{11} - C_{12}) > 0 \\ \frac{1}{3}(C_{11} + 2C_{12}) > 0 \end{array} \right\} \quad (2.11)$$

In equation (2.11), the variables, $(C_{11} + 2C_{12})$, $(C_{11} - C_{12})$, and C_{44} degeneracy, two-fold degeneracy, and three-fold degeneracy are denoted, respectively. Conversely, cubic instability of the materials is indicated by negative values of these parameters [47]. Mechanical properties such as shear modulus (G), which can be computed through the VRH approximation using the following formulas, function as a material's synthetic twist indicator.

$$G_v = \frac{1}{5} (C_{11} - C_{12} + 3C_{44}) \quad (2.12)$$

$$G_R = \frac{5(C_{11} - C_{12})C_{44}}{3(C_{11} - C_{12}) + 4C_{44}} \quad (2.13)$$

Given that G_V and G_R represent Voigt's and Reuss's shear moduli in this instance, G is equal to:

$$G = \frac{G_V + G_R}{2} \quad (2.14)$$

Three well-defined elastic constants can be used to estimate bulk modulus (B), which measures a material's resistance to fracture and indicates how hard it is.

$$B = \frac{1}{3}(C_{11} + 2C_{12}) \quad (2.15)$$

A material's brittleness and ductility are assessed by Pugh's ratio (B/G), which depends on its equilibrium value (1.75). The poor malleability of the material is demonstrated by a bigger B/G , which indicates that the substance is brittle, and the lower value indicates that the substance is ductile [48]. Additionally, Young's modulus (E), which assesses a material's stiffness by examining its internal extension and contraction in response to tension and compression, is described as follows:

$$E = \frac{9BG}{3B+G} \quad (2.16)$$

Poisson's ratio (σ), which is defined as the ratio of relative contraction to relative expansion, is explained by equation (2.17), which also explains atomic bonding in materials. This parameter has critical values to define atomic bonding, such as, materials will have covalent bonding if ν is 0.1, for ionic materials it is 0.25, and ranges between 0.33 to 0.25 for metallic materials. Apart from this, Cauchy's pressure (CP) also defines atomic bonding. Other than this, atomic bonding is defined by Cauchy's pressure (CP). If the value for ($C_{12} > C_{44}$) is positive, then it suggests non-directional

metallic bonding, whereas negative values ($C_{12} < C_{44}$) denote covalent bonding among materials.

$$\sigma = \frac{3B-2G}{2(3B-G)} \quad (2.17)$$

$$CP = (C_{12} - C_{44}) \quad (2.18)$$

When a material deviates from its equilibrium value, it develops imperfections and microcracks, which are referred to as anisotropy (A) ($A=1$). When anisotropy differs from unity ($A>1$), there is a greater chance of fractures and defects occurring during the synthesis or crystal formation process. If A factor has a value less than or equal to unity, then the material is isotropic or otherwise anisotropic. Its value can be calculated by [49]

$$A = \frac{2C_{44}}{C_{11} - C_{12}} \quad (2.19)$$

Further, an imperative parameter that brings resourceful information about materials is the Debye temperature (Θ_D). It helps to reveal the thermal characteristics of materials at high temperatures or pressure. It can be derived using the following equation from the average sound velocity (v_m): [50]

$$\theta_D = \frac{h}{K_B} \left[\frac{3}{4\pi V_a} \right]^{1/3} v_m \quad (2.20)$$

where h , V_a , K_B , are referred to as Planck's constant, average atomic volume, and Boltzmann's constant, respectively. Moreover, v_m is given by:

$$v_m = \left[\frac{1}{3} \left(\frac{2}{v_t^3} + \frac{1}{v_l^3} \right) \right]^{-\frac{1}{3}} \quad (2.21)$$

where the transverse v_t , longitudinal v_l , and elastic wave velocities indicated in equation (2.21) can be calculated using the following equations.

$$v_t = \left(\frac{G}{\rho} \right)^{1/2} \quad (2.22)$$

$$v_l = \left(\frac{3B + 4G}{3\rho} \right)^{1/2} \quad (2.23)$$

2.5. Thermodynamic stability

The Gibbs2 package uses the Quasi-Harmonic Debye approximation (QHA) [51-53], successfully predicts the thermal expansion in the materials through its geometrical dependency on temperature and phonon frequencies [54]. There are several instances in the literature that demonstrate how well QHA predicts the thermodynamic characteristics of solids [55-57]. The QHA accounts for the solid material's thermal expansion and thermal transport characteristics at low and high-temperature limitations. Therefore, by incorporating the results of an E-V curve into Birch-Murnaghan's, which are calculated by using the calculation of EOS [58]. Thus, it is possible to study various thermodynamic parameters across a specific pressure and temperature range.

$$E(V) = E_0 + \frac{BV}{B'(B' - 1)} \left[B \left(1 - \frac{V_0}{V} \right) + \left(\frac{V_0}{V} \right)^{B'} - 1 \right] \quad (2.24)$$

Here, E_0 and V_0 represent equilibrium energy and volume, and B' represents the pressure derivative of B . A minimized Gibbs function at constant pressure (P) and temperature (T) is obtained using the given QHA method and is defined as follows:

$$\left[\frac{\partial G^*(V; P, T)}{\partial V} \right]_{P,T} = 0 \quad (2.25)$$

Here, $G^*(V; P, T)$ is:

$$G^*(V, P, T) = E(V) + PV + F_{vib}(\theta_D(V); T) \quad \text{nnn} \quad (2.26)$$

where the parameters E , F_{vib} , and θ_D are defined as static energy, vibrational Helmholtz free energy, and Debye temperature. Moreover, F_{vib} in terms of Boltzmann constant (K_B) and Debye integral, $D\left(\frac{\theta_D}{T}\right)$,

$$F_{vib}[\theta_D(V); T] = NK_B T \left[\frac{9\theta_D}{8T} + 3 \ln \left(1 - e^{-\frac{\theta_D}{T}} \right) - D\left(\frac{\theta_D}{T}\right) \right] \quad (2.27)$$

The thermodynamical parameter θ_D and its relationship to Poisson's ratio $f(v)$ represent phase transition, hardness, and lattice vibrations in solid materials, while equation (2.28) shows the adiabatic bulk modulus (B_S).

$$\theta_D = \frac{h}{k} \left[6\pi^2 V^{1/2} n \right]^{1/3} f(v) \sqrt{\frac{B_S}{M}} \quad (2.28)$$

Further, if the temperature is below θ_D , then the material's lattice vibrations are stimulated by acoustic vibration; however, they are insignificant at temperatures beyond θ_D .

References

1. Sholl, D. S., & Steckel, J. A. (2022). Density functional theory: a practical introduction. John Wiley & Sons.
2. Hanaor, D. A., Assadi, M. H., Li, S., Yu, A., & Sorrell, C. C. (2012). Ab initio study of phase stability in doped TiO₂. *Computational Mechanics*, 50, 185-194.
3. Hohenberg, P., & Kohn, W. (1964). Inhomogeneous electron gas. *Physical review*, 136(3B), B864.
4. Levy, M. (1979). Universal variational functionals of electron densities, first-order density matrices, and natural spin-orbitals and solution of the v-representability problem. *Proceedings of the National Academy of Sciences*, 76(12), 6062-6065.
5. Vignale, G., & Rasolt, M. (1987). Density-functional theory in strong magnetic fields. *Physical review letters*, 59(20), 2360.
6. Hohenberg, P., & Kohn, W. (1964). Inhomogeneous electron gas. *Physical review*, 136(3B), B864.
7. Kohn, W., & Sham, L. J. (1965). Self-consistent equations including exchange and correlation effects. *Physical review*, 140(4A), A1133.
8. Koch, W., & Holthausen, M. C. (2015). A chemist's guide to density functional theory. John Wiley & Sons.
9. Honkala, K., Hellman, A., Remediakis, I. N., Logadottir, A., Carlsson, A., Dahl, S., Christensen, C.H. and Nørskov, J.K., (2005). Ammonia synthesis from firstprinciples calculations. *Science*, 307(5709), 555-558.
10. Schweinfest, R., Paxton, A. T., & Finnis, M. W. (2004). Bismuth embrittlement of copper is an atomic size effect. *Nature*, 432(7020), 1008-1011.
11. Slater, J. C. (1951). A simplification of the Hartree-Fock method. *Physical review*, 81(3), 385.
12. Orio, M., Pantazis, D. A., & Neese, F. (2009). Density functional theory. *Photosynthesis research*, 102(2), 443-453.
13. Parr, R. G. (1989). W. Yang Density functional theory of atoms and molecules. Oxford University Press, 1, 1989.

14. Perdew, J. P., Chevary, J. A., Vosko, S. H., Jackson, K. A., Pederson, M. R., Singh, D. J., & Fiolhais, C. (1993). Erratum: Atoms, molecules, solids, and surfaces: Applications of the generalized gradient approximation for exchange and correlation. *Physical Review B*, 48(7), 4978.
15. Becke, A. D. (1992). Density-functional thermochemistry. I. The effect of the exchange-only gradient correction. *The Journal of chemical physics*, 96(3), 2155-2160.
16. Hammer, B., Jacobsen, K. W., & Nørskov, J. K. (1993). Role of nonlocal exchange correlation in activated adsorption. *Physical review letters*, 70(25), 3971.
17. Becke, A. D. (1988). Density-functional exchange-energy approximation with correct asymptotic behavior. *Physical review A*, 38(6), 3098.
18. Lee, C., Yang, W., & Parr, R. G. (1988). Development of the Colle-Salvetti correlation-energy formula into a functional of the electron density. *Physical review B*, 37(2), 785.
19. Perdew, J. P., & Wang, Y. (1992). Accurate and simple analytic representation of the electron-gas correlation energy. *Physical review B*, 45(23), 13244.
20. Perdew, J. P., Burke, K., & Ernzerhof, M. (1996). Generalized gradient approximation made simple. *Physical review letters*, 77(18), 3865.
21. Hubbard, J. (1963). Electron correlations in narrow energy bands. *Proceedings of the Royal Society of London. Series A. Mathematical and Physical Sciences*, 276(1365), 238-257.
22. Tompsett, D. A., Middlemiss, D. S., & Islam, M. S. (2012). Importance of anisotropic Coulomb interactions and exchange to the band gap and antiferromagnetism of βMnO_2 from DFT+ U. *Physical Review B*, 86(20), 205126.
23. Tran, F., & Blaha, P. (2009). Accurate band gaps of semiconductors and insulators with a semilocal exchange-correlation potential. *Physical review letters*, 102(22), 226401.
24. Becke, A. D., & Johnson, E. R. (2006). A simple effective potential for exchange. *The Journal of chemical physics*, 124(22), 221101.

25. Tran, F., Blaha, P., & Schwarz, K. (2007). Band gap calculations with Becke–Johnson exchange potential. *Journal of Physics: Condensed Matter*, 19(19), 196208.
26. Wimmer, E., Krakauer, H., Weinert, M., & Freeman, A. J. (1981). Full-potential selfconsistent linearized-augmented-plane-wave method for calculating the electronic structure of molecules and surfaces: O₂ molecule. *Physical Review B*, 24(2), 864.
27. Singh, D. J., & Nordstrom, L. (2006). *Planewaves, Pseudopotentials, and the LAPW method*. Springer Science & Business Media.
28. Blaha, P., Schwarz, K., Madsen, G. K., Kvasnicka, D., & Luitz, J. (2001). WIEN2k. An augmented plane wave+local orbitals program for calculating crystal properties, (Vol. 60).
29. Slater, J. C. (1937). Wave functions in a periodic potential. *Physical Review*, 51(10), 846.
30. Slater, J. C. (1964). Energy band calculations by the augmented plane wave method. In *Advances in quantum chemistry* (Vol. 1, pp. 35-58). Academic Press.
31. Andersen, O. K. (1975). Linear methods in band theory. *Physical Review B*, 12(8), 3060.
32. Weinert, M. (1981). Solution of Poisson's equation: Beyond Ewald.type methods. *Journal of Mathematical Physics*, 22(11), 2433-2439.
33. Hamann, D. R. (1979). Semiconductor charge densities with hard-core and soft-core pseudopotentials. *Physical Review Letters*, 42(10), 662.
34. Gilman, J. J. (2009). *Chemistry and physics of mechanical hardness*. (vol 5) John Wiley & Sons.
35. Gilman, J. J. (2003). *Electronic basis of the strength of materials*. Cambridge University Press.
36. Sen, K. D. (Ed.) (1997). *Chemical Hardness In: Structure and Bonding* (Vol 80) NewYork: Springer, Verlag, Berlin, Heidelberg.
37. Blum, C. G., Ouadi, S., Fecher, G. H., Balke, B., Kozina, X., Stryganyuk, G., Ueda, S., Kobayashi, K., Felser, C., Wurmehl, S., & Büchner, B. (2011). Exploring the details of the martensite–austenite phase transition of the shape memory Heusler compound Mn₂NiGa by hard x-ray photoelectron

- spectroscopy, magnetic and transport measurements. *Applied Physics Letters*, 98(25), 252501.
38. Winterlik, J., Balke, B., Fecher, G. H., Felser, C., Alves, M. C., Bernardi, F., & Morais, J. (2008). Structural, electronic, and magnetic properties of tetragonal Mn_{3-x}Ga : Experiments and first-principles calculations. *Physical Review B*, 77(5), 054406.
 39. Huntington, H. B. (1958). The elastic constants of crystals. In *Solid state physics* (Vol. 7, pp. 213-351). Academic Press.
 40. Alam, M. A., Hadi, M. A., Nasir, M. T., Roknuzzaman, M., Parvin, F., Zilani, K., MA Islam, A.K. & Naqib, S. H. (2016). Structural, elastic, and electronic properties of newly discovered Li_2PtSi_3 superconductor: Effect of transition metals. *Journal of Superconductivity and Novel Magnetism*, 29(10), 2503-2508.
 41. Charpin, T. (2001). A package for calculating elastic tensors of cubic phase using WIEN. Laboratory of Geometrix, Paris.
 42. Voigt, W. (1928). *Lehrbuch der Kristallphysik* (Leipzig: Teubner). *Advances in Earth Science*.
 43. Reuss, A. J. Z. A. M. M. (1929). Calculation of the flow limits of mixed crystals on the basis of the plasticity of monocrystals. *Z. Angew. Math. Mech*, 9, 49-58.
 44. Hill, R. (1952). The elastic behaviour of a crystalline aggregate. *Proceedings of the Physical Society. Section A*, 65(5), 349.
 45. Sin'Ko, G. V., & Smirnov, N. A. (2002). Ab initio calculations of elastic constants and thermodynamic properties of bcc, fcc, and hcp Al crystals under pressure. *Journal of Physics: Condensed Matter*, 14(29), 6989.
 46. Born, M., & Huang, K. (1954). *Dynamical Theory of Crystal Lattices*, Clarendon Press, Oxford.
 47. Ram, M., Saxena, A., Aly, A. E., & Shankar, A. (2020). Half-metallicity in new Heusler alloys Mn_2ScZ (Z= Si, Ge, Sn).
 48. Pugh, S. F. (1954). XCII. Relations between the elastic moduli and the plastic properties of polycrystalline pure metals. *The London, Edinburgh, and Dublin Philosophical Magazine and Journal of Science*, 45(367), 823-843.

49. Tvergaard, V., & Hutchinson, J. W. (1988). Microcracking in ceramics induced by thermal expansion or elastic anisotropy. *Journal of the American Ceramic Society*, 71(3), 157-166.
50. Schreiber, E., Anderson, O. L., Soga, N., & Bell, J. F. (1975). Elastic constants and their measurement.
51. Blanco, M. A., Francisco, E., & Luana, V. (2004). GIBBS: isothermal-isobaric thermodynamics of solids from energy curves using a quasi-harmonic Debye model. *Computer Physics Communications*, 158(1), 57-72.
52. Otero-de-la-Roza, A., & Luaña, V. (2011). Gibbs2: A new version of the quasiharmonic model code. I. Robust treatment of the static data. *Computer Physics Communications*, 182(8), 1708-1720.
53. Otero-de-la-Roza, A., Abbasi-Pérez, D., & Luaña, V. (2011). Gibbs2: A new version of the quasiharmonic model code. II. Models for solid-state thermodynamics, features and implementation. *Computer Physics Communications*, 182(10), 2232-2248.
54. Joshi, H., Vu, T. V., Hieu, N. N., Khenata, R., & Rai, D. P. (2021). Mechanical and thermodynamical properties of Fe₂CoAl a full-Heusler alloy under hydrostatic pressure: A DFT study. *Materials Chemistry and Physics*, 270, 124792.
55. Chen, X. J., Zhang, C., Meng, Y., Zhang, R. Q., Lin, H. Q., Struzhkin, V. V., & Mao, H. K. (2011). β -tin \rightarrow I m m a \rightarrow sh Phase Transitions of Germanium. *Physical Review Letters*, 106(13), 135502.
56. Umemoto, K., Wentzcovitch, R. M., Saito, S., & Miyake, T. (2010). Body-Centered Tetragonal C₄: A Viable sp³ Carbon Allotrope. *Physical review letters*, 104(12), 125504.
57. Wood, B. C., & Marzari, N. (2009). Dynamics and thermodynamics of a novel phase of NaAlH₄. *Physical review letters*, 103(18), 185901.
58. Murnaghan, F. D. (1944). The compressibility of media under extreme pressures. *Proceedings of the National Academy of Sciences*, 30(9), 244-247.

Chapter 3

A Computational Modeling on thermodynamic performances of BeX(X=Ag, Au, Fe) intermetallics

The current study uses computational quantum mechanical modeling within the framework of DFT to report the thermodynamics of BeX (X=Ag, Au, Fe) intermetallics in terms of their unit cell volume, bulk moduli, molar heat capacity at constant volume, Grüneisen parameter, thermal expansion coefficient, and Debye temperature. The thermodynamic parameters were examined between 0 and 1200 K in temperature and between 0 and 40 GPa in pressure. For the intermetallics under consideration, the molar heat capacity at constant volume obeyed the Debye T³ law, and at a given temperature, the Dulong-Petit limit was reached. Additionally, Debye temperatures for BeX (Ag, Au, Fe) were estimated to be 430 K, 335 K, and 661 K, respectively, at 0 K and 0 GPa to comprehend the highest modes of vibration in the materials. Additionally, the thermal expansion coefficient illustrated the strength of atomic bonding by describing how the materials expanded and contracted in response to temperature changes. Its high value suggested that the solids' low melting temperature was caused by weak atomic bonding.

3.1. Introduction

For the past few decades, there has been a lot of interest in the electronic, structural, thermodynamic, and mechanical properties of intermetallics [1–20]. The intermetallics that are formed through the alloying of elements from the II group and the transition metal group possess unique physical properties. There aren't many experimental studies in the literature on these intermetallics at high pressures and temperatures. On the other hand, these intermetallic studies are now reasonably possible and have been documented in the literature [1-5, 7-11, 14-20], thanks to the development of new quantum mechanical modeling and high-speed computational facilities. Intermetallics with various physical properties and applications, such as binary [1–12], ternary [18,19], and quaternary [20], are of interest. Low weight and high strength are needed

for spacecraft and aircraft applications [14]. By estimating the elastic stiffness of the elastic modulus per unit density, the high strength of the materials can be understood. These materials are also needed to fabricate innovative devices that can withstand high temperatures for use in industrial settings [13–15]. A report on the binary intermetallics for flexible Lithium-Ion battery anodes with high performance has been made [16]. Numerous theoretical studies have been reported in this regard [1–11]. Density functional theory was used by Pan et al. [1] to investigate the structural, electronic, mechanical, and thermodynamic properties of Cr–Si binary silicide intermetallics. Using first principles theory, Yu et al. [2] investigated a few Copper-Lithium intermetallics. Numerous binary intermetallics, such as CdRE and Al-RE (RE=rare earth), have been studied by Srivastava et al. [4,9-11].

The primary goal of this study on BeX(X=Ag, Au, and Fe) intermetallics is to provide industrial applications with cutting-edge thermodynamic information, especially at high temperatures and pressures. Therefore, using computational modeling, or the well-known density functional theory, we have presented a theoretical study of BeX (X=Ag, Au, and Fe) intermetallics to know their structure, electronic states, and thermodynamic parameters like stiffness modulus, molar heat capacity at constant volume, thermal expansion coefficient, and Debye temperature in the temperature range of 0-1200 K and pressure range of 0-40 GPa [21].

3.2. Structural Phase Stability

Like the other intermetallics under investigation, the BeAg, BeAu and BeFe intermetallics crystallize in the cubic B2 phase (space group, Pm-3m) [1–11]. Figure 3.1 displays the crystal structure of BeX (X=Ag, Au, and Fe) intermetallics in their cubic phase.

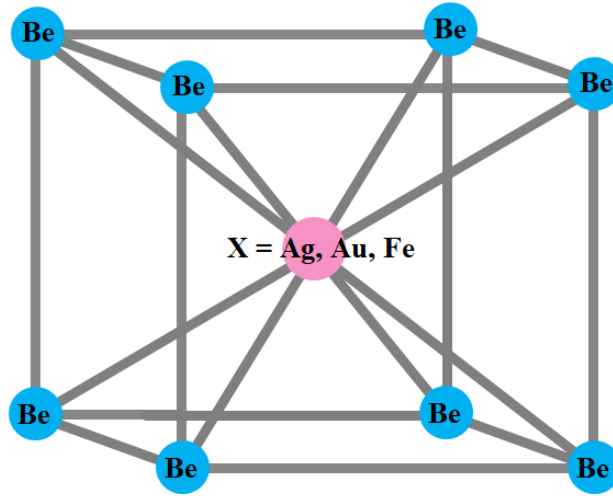


Figure 3.1: BeX (X=Ag, Au, and Fe) intermetallics with an optimized crystal structure in the Pm-3m structure

In the unit cell of the cesium chloride type structure (B2 phase), the Be atoms are located at (0, 0, 0) with RMT = 2.0 a.u., and the Ag or Au atoms are located at (0.5, 0.5, 0.5) with RMT = 2.2 a.u. The atom positions in the BeFe compound are as follows: Be is (0,0,0), with an RMT of 1.8, and Fe is (0.5, 0.5, 0.5), with an RMT of 1.9. The Birch-Murnaghan equation of state was used to fit the total energy versus unit cell volume in order to optimize the structure. In order to determine whether or not the materials have a magnetic effect, we have computed the total energy of the compounds in the ferromagnetic (FM) and non-magnetic (NM) phases. Thus, taking into account the CsCl-type structure, we have shown the variation of total energy (with GGA potential) in NM and FM phases in Figure 3.2 (a, b, and c).

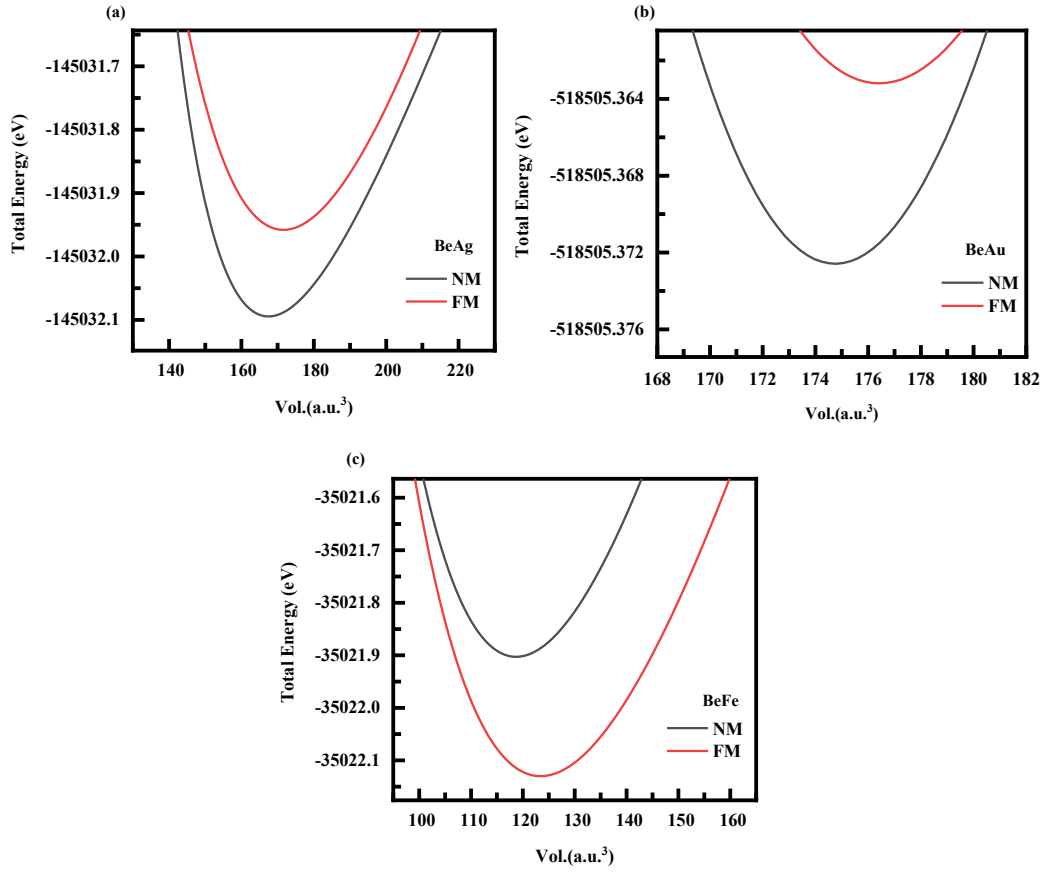


Figure 3.2: Variation of total energy as a function of cell volume of BeX (X=Ag, Au, Fe) intermetallics in Pm-3m structure (a) BeAg (b) BeAu (c) BeFe

The figures for the intermetallic compounds BeAg, BeAu, and BeFe demonstrate that the materials under consideration are stable in the non-magnetic phase due to their lowest energy levels in this phase. According to the Slater-Pauling rule, it is discovered that for the BeFe compound, the total energy is minimum in the ferromagnetic phase, represented in Figure 3.2, with a magnetic moment of 2.06 μ_B . The obtained total energy varies with unit cell volume; under compression, the energy decreases with decreasing volume, and the minimum energy is observed. Table 3.1 shows our calculated ground state properties for the materials under consideration, including the lattice constant (a_0), bulk modulus (B_0), and pressure derivative (B'_0). Additionally, we computed BeAg and BeAu cohesive energies using

$$E_{Coh}^{BeX} = \frac{[(E_{Be} + E_{Ag/Au})_{atom} - (E_{BeX(X=Ag,Au)})_{bulk}]}{n} \quad (3.1)$$

where $(E_{Be})_{atom}$, $(E_{Ag/Au})_{atom}$ are the bulk (isolated) energies of atoms of beryllium, silver, and gold, respectively. BeX (X=Ag, Au) solid's total energy is represented by

$(E_{BeX(X=Ag,Au)})_{bulk}$. The amount of energy required to divide a solid's atoms into distinct atomic species is referred to as the cohesive energy. Along with melting point, boiling point, solubility, and other variables, it is one of the primary physical parameters used to measure the thermal stability of materials. Table 3.1 displays the cohesive energy values that were computed. The materials in the B2 Phase exhibit thermal stability, as evidenced by the positive cohesive energy values. Regarding the structural details found in the literature for the materials under investigation, the crystallographic data for AuBe with cP8 phase (space group, P213; prototype FeSi) are reported [22]. Regarding AgBe, the phase diagram provided in Predel, B. [23] does not report such a phase. This may be caused by the phase's inherent instability or by the lack of experimental identification in the body of literature currently in publication.

Table 3.1 Ground state properties unit cell volume V_0 , lattice parameter a_0 , bulk modulus B_0 , first order pressure derivative of bulk modulus B'_0 , and equilibrium total energy E_0 , cohesive energy E_{Coh} of BeX (X=Ag, Au, Fe) intermetallics at 0GPa and 0K.

Solid	V_0 (a.u. ³)	a_0 (Å)	B_0 (GPa)	B'_0	E_0 (x10 ² eV)	E_{Coh} (eV/atom)
BeAg	173.39	2.92	119.27	8.66	-1450.32	2.47
BeAu	175.88	2.97	150.01	6.87	-5185.05	0.84
BeFe	123.30	2.63	177.38	4.33	-350.22	-

1 a.u. = 0.52917 Å; 1 Å = 10⁻¹⁰ m

3.3. Electronic properties

We have plotted band structures in Figure 3.3 (a,b,c,d) to help understand the behavior of different electronic states in BeAg, BeAu, and BeFe intermetallics. Using the GGA potential and the optimized lattice parameter (found in Table 3.1) of the stable structure, the electronic band structures are produced. The figure shows that the metallic behavior of BeAg and BeAu is demonstrated by the crossover of the Be '-s' and '-p' states close to the Fermi level (E_F).

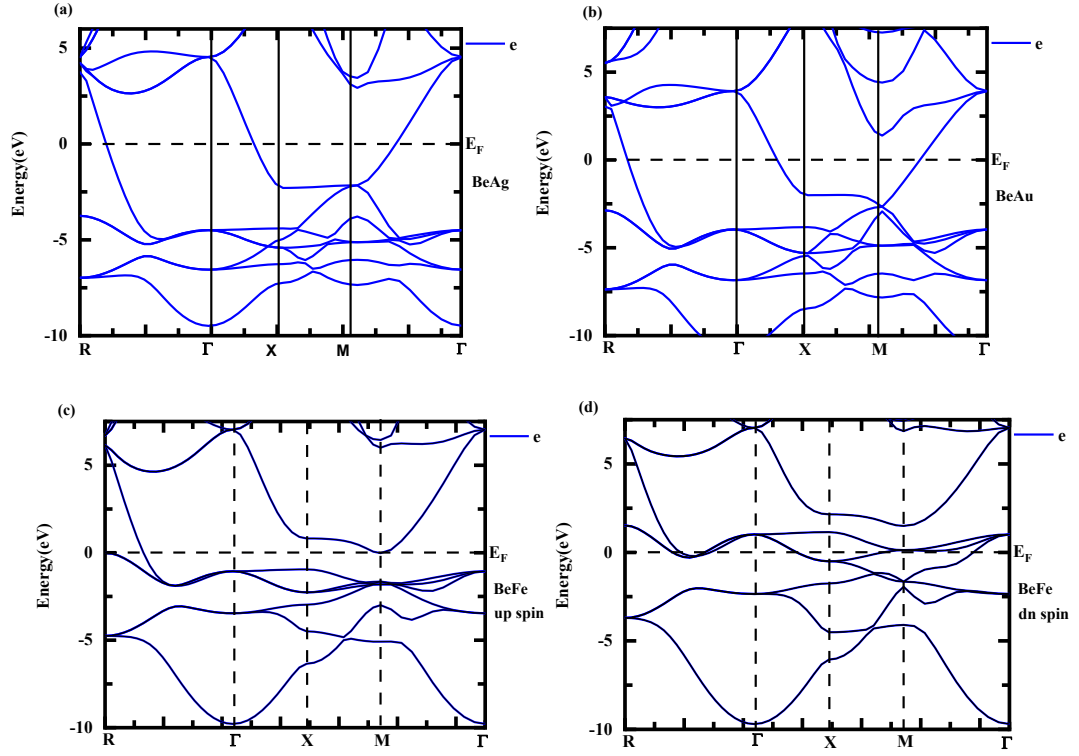


Figure 3.3: Band structure of BeX(X=Ag, Au, Fe) intermetallics (a) BeAg (b) BeAu (c) BeFe up spin (d) BeFe Down spin

Figure 3.3 (c,d) shows the electronic band structure of FM, which was plotted to help understand the behavior of different electronic states in the BeFe compound. BeFe in its stable configuration state, which we present as the Pm-3m structure with GGA approximations. The figure shows that the crossover of different electronic states at the ‘ Γ ’ and ‘ X ’ points illustrates the metallic behavior of BeFe in the spin-up case close to the Fermi level (E_F). Likewise, in the spin-down scenario close to the Fermi level (E_F), the metallic behavior of BeFe is further highlighted by the crossover of different electronic states at the ‘ Γ ’ and ‘ X ’ points. As a result, its metallic behavior is visible in the entire band profile.

In addition, the total density of states (TDOS) and partial density of states (PDOS) in the Pm-3m structure are computed and shown in Figures 3.4 (a,b,c), 3.5 (a,b), 3.6 (a, b), and 3.7 (a.b), respectively, to help comprehend the elemental contribution of various electronic states. Total DOS and PDOS show the crossover of Be-‘s’, Be-‘p’ states with small Ag- and Au-‘d’ states close to the Fermi level.

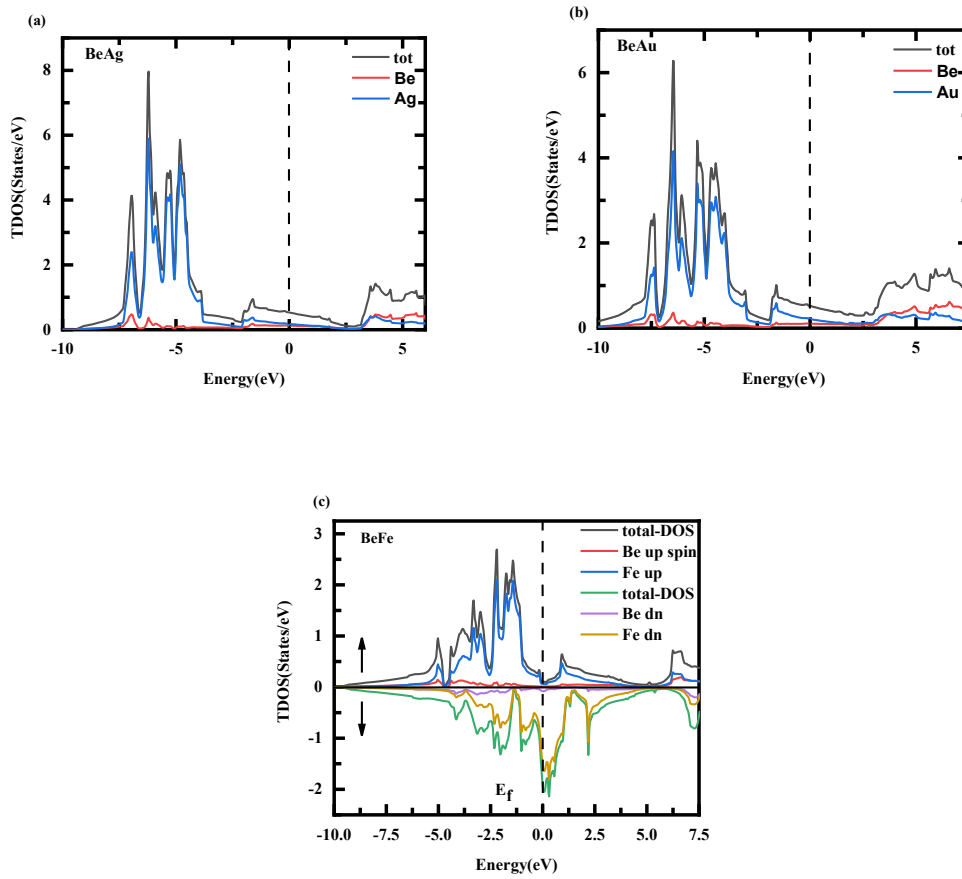


Figure 3.4. Total Density of states of BeX(X=Ag, Au, Fe) intermetallics (a) BeAg
(b) BeAu (c) BeFe

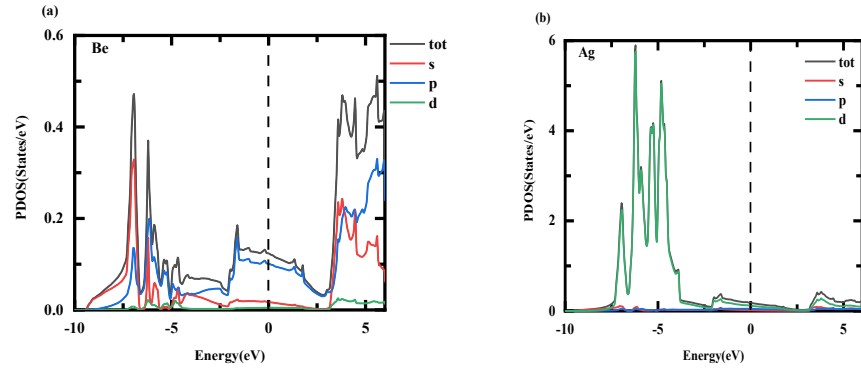


Figure 3.5: Partial density of states of BeAg intermetallic (a) Be (b) Ag

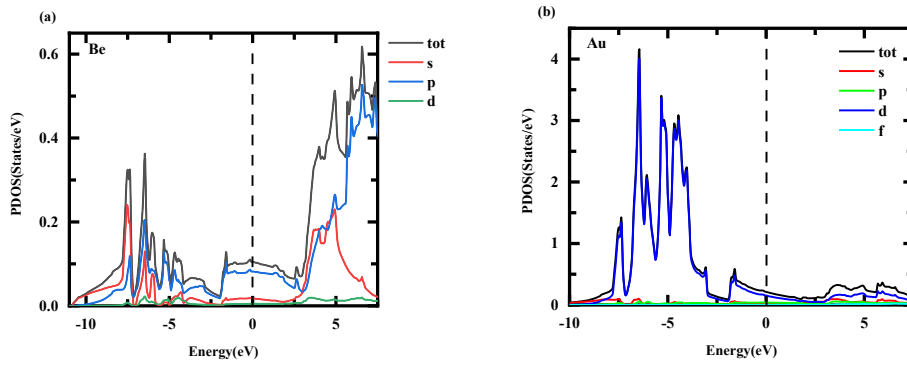


Figure 3.6: Partial density of states of BeAu intermetallic (a) Be (b) Au

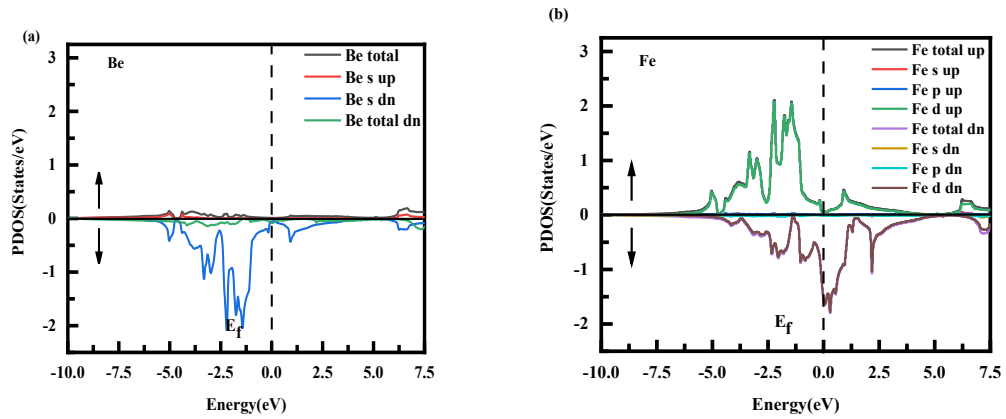


Figure 3.7: Partial density of states of BeAu intermetallic (a) Be (b) Fe

3.4. Elastic and Mechanical properties:

Materials are frequently compressed for structural stability, so it's critical to understand the behavior of materials under stress. In this context, mechanical properties for the ductile and brittle nature of BeAg, BeAu, and BeFe have been calculated, including

Young's modulus (E), bulk modulus (B), shear modulus (G), elastic constants (C), Poisson ratio (σ), anisotropic ratio (A), and B/G ratio. The values that were calculated are listed in Table 3.2.

Using the Charpin method embedded in the WIEN2k code, the elastic constants C_{11} , C_{12} , and C_{44} , along with their corresponding values, are calculated as follows: 165.82 GPa, 105.76 GPa, and 83.80 GPa for BeAg; 202.06 GPa, 132.65 GPa, and 39.09 GPa for BeAu; and 263.27 GPa, 135.71 GPa, and 141.87 GPa for BeFe intermetallic compound. A variety of mechanical and thermal properties can be calculated with an understanding of the elastic constants.

The anisotropic ratio ($A = \frac{2C_{44}}{C_{11} - C_{12}}$) is defined through the application of elastic constants. Anisotropic material is defined as having an A value greater than 1, but isotropic material is defined as having an A value less than or equal to 1. Regarding BeX (X=Ag, Au, and Fe), the values of A are 2.79, 1.13, and 2.22, respectively, indicating the anisotropy in the crystals. The Poisson ratio (σ) calculation is very helpful in understanding the bonding properties or forces between the atoms in BeX (X=Ag, Au, Fe).

A covalent bond would have a value of $\sigma = 0.1$, whereas an ionic bond would have a value of $\sigma = 0.25$. If the bonding nature is metallic, the value of $\sigma = 0.33$. For BeAg and BeAu, our computed Poisson ratio values are 0.30 and 0.39, respectively, indicating weak and strong metallic bonding in the materials. We have calculated the Poisson ratio to be 0.25 BeFe, indicating that the material is ionic. Taking into account the bulk-to-shear modulus ratio, or B/G, brittle and ductile behavior can also be clarified.

The Pugh criteria state that a material is deemed brittle if its B/G value is less than 1.75 and ductile if it is greater than 1.75. In this instance, its value is computed to be 2.15 and 4.02, indicating that BeAg and BeAu are ductile, and its value is computed to be 1.71 for BeFe, indicating that it is brittle. Cauchy pressure ($C_{12} - C_{44}$), however, once more determines the materials' ductile/brittle behavior. For a negative value, the material would behave brittly, and for a positive value, it would behave ductility. BeAg and BeAu, whose computed values are 21.96 GPa and 93.55 GPa, respectively, are similar to ductile nature. According to the report, the calculated value for BeFe is -

6.16 GPa shown in Table 3.2, is similar to a brittle nature.

Table 3.2: Calculated elastic and mechanical properties for BeX(X=Ag, Au, Fe) intermetallics at 0 GPa and 0 K: elastic constants C_{11} , C_{12} , C_{44} , Bulk Modulus B, Voigt Shear Modulus G_V , Reuss Shear Modulus G_R , Shear Modulus G, Young's Modulus E, Anisotropy Ratio A, Cauchy Pressure $C_{12}-C_{44}$, Bulk modulus to Shear modulus ratio B/G, Poisson Ratio σ , longitudinal velocity V_l , transverse velocity V_t , Average velocity V_m , Debye Temperature θ_D , Melting Temperature T_m .

1 GPa = 10^9 Pa

Properties	BeAg	BeAu	BeFe
C_{11} (GPa)	165.82	202.06	263.27
C_{12} (GPa)	105.76	132.65	135.71
C_{44} (GPa)	83.80	39.09	141.87
B (GPa)	119.27	150.01	175.69
G_V	62.29	37.34	110.63
G_R	48.83	37.21	95.23
G (GPa)	55.56	37.28	102.93
E (GPa)	144.32	103.28	258.35
A	2.79	1.13	2.22
$C_{12}-C_{44}$ (GPa)	21.96	93.55	-6.16
B/G ratio	2.15	4.02	1.71
σ	0.30	0.39	0.25
V_l (m s ⁻¹)	5053.92	3485.81	7285.38
V_t (m s ⁻¹)	2697.73	1679.76	4178.28
V_m (m s ⁻¹)	3012.83	1888.26	4641.37
θ_D (K)	384.38	239.45	661.13
T_m (K)	1178.17	1337.09	2109.16

Furthermore, we used equation 16 as provided in Section 2 to estimate the melting temperature (T_m) for BeX (where X=Ag, Au, or Fe). Experimental research is made

possible by the calculated values of T_m , which are 1178.17 K and 1337.09 K for BeAg and BeAu, and 2109.16 K for the BeFe compound, respectively.

3.5. Thermodynamic properties

A full-potential linearized augmented plane-wave method (FP-LAPW) [25] based on DFT as implemented in the WIEN2k code [24] is used to investigate BeX(X=Ag, Au, Fe) concerning various thermodynamic parameters like volume (V), bulk moduli (B), molar heat capacity at constant volume (C_v), Grüneisen parameter (γ), thermal expansion coefficient (α), and Debye temperature (θ_D). Utilizing the quasi-harmonic Debye model, the thermophysical performances of the BeX(X=Ag, Au, and Fe) compound are calculated. This provides important insights into the different behaviors of solids at different temperatures and pressures. We have used the quasi-harmonic Debye model to calculate various thermodynamic variables under temperature (0 K to 1200 K) and pressure (0 GPa to 40 GPa) in order to make BeX(X=Ag, Au, Fe) materials suitable for industrial applications. Figures 3.7–3.13, which calculate the thermodynamic variables for BeX (X=Ag, Au, Fe), include volume (V), bulk moduli (B), molar heat capacity at constant volume (C_v), and Grüneisen parameter (γ). Nonetheless, Figure 3.7 (a,b,c) shows how unit cell volume varies with temperature and pressure. The figures clearly show that, for a given pressure value, cell volume increases with rising temperature; conversely, for a given temperature value, cell volume decreases with rising pressure. It is clear from such behavior in solids [1–11] that temperature causes a solid to expand while pressure compresses it.

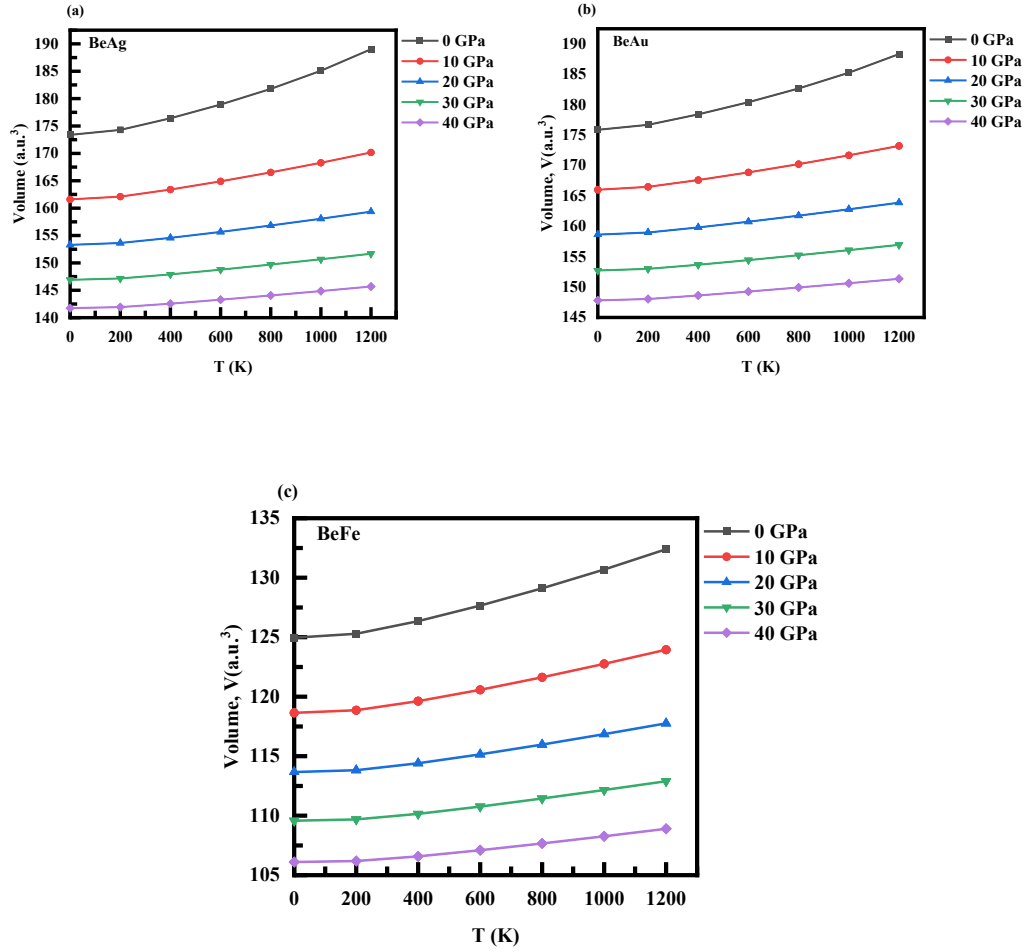


Figure 3.8: Variation of unit cell volume of BeX(X=Ag, Au, Fe) intermetallics with temperature (a) BeAg (b) BeAu (c) BeFe

Figure 3.8 (a,b,c) shows the bulk modulus variation as a function of temperature and pressure. As observed in the case of variation of volume under temperature and pressure, it is evident from the figures that variation of the bulk modulus under temperature and pressure has the opposite effect of γ . The bulk modulus rises with increasing pressure and falls with increasing temperature, as shown in Figure 3.8. The reason for this variation in the B value with temperature and pressure is that the former increases hardness while the latter decreases it. Second, while pressure has the opposite effect, rising temperatures also result in rising unit cell volumes and interatomic distances. Additionally, we computed its value at 298 K and 0 GPa to be 115 and 140 or 172.95 GPa for BeX (X=Ag, Au, and Fe), respectively.

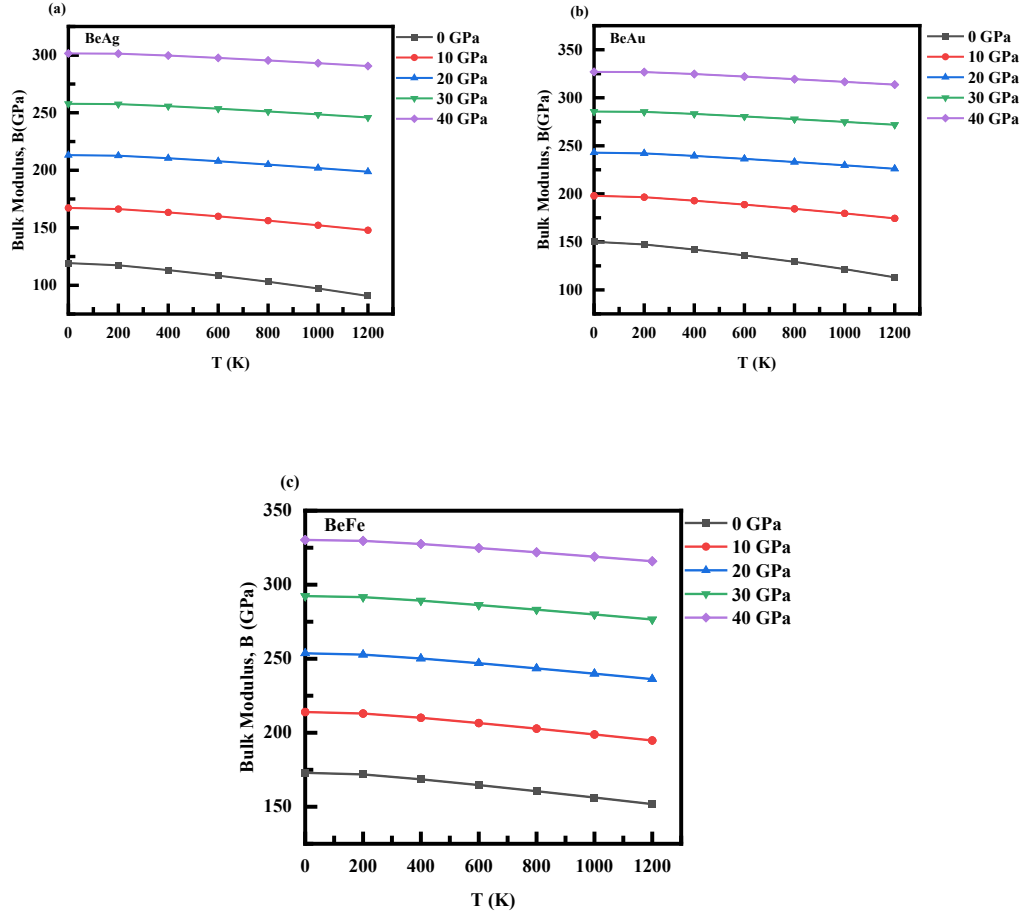


Figure 3.9: Variation of bulk modulus of BeX(X=Ag, Au, Fe) intermetallics with temperature (a) BeAg (b) BeAu (c) BeFe

In addition, the molar heat capacity at C_v is computed, which measures the motion of molecules and offers details on phase transition and lattice vibration. Figure 3.9 illustrates how the C_v increases quickly at lower temperature values, ranging from 0 to 200 K. A gradual increase in C_v is seen above 200 K, and it reaches the well-known Dulong-Petit limit at 600 K, when it becomes constant. For BeX (X=Ag, Au, and Fe), the computed value of C_v at 1200 K and 0 GPa is $50 \text{ J K}^{-1} \text{ m}^{-1}$.

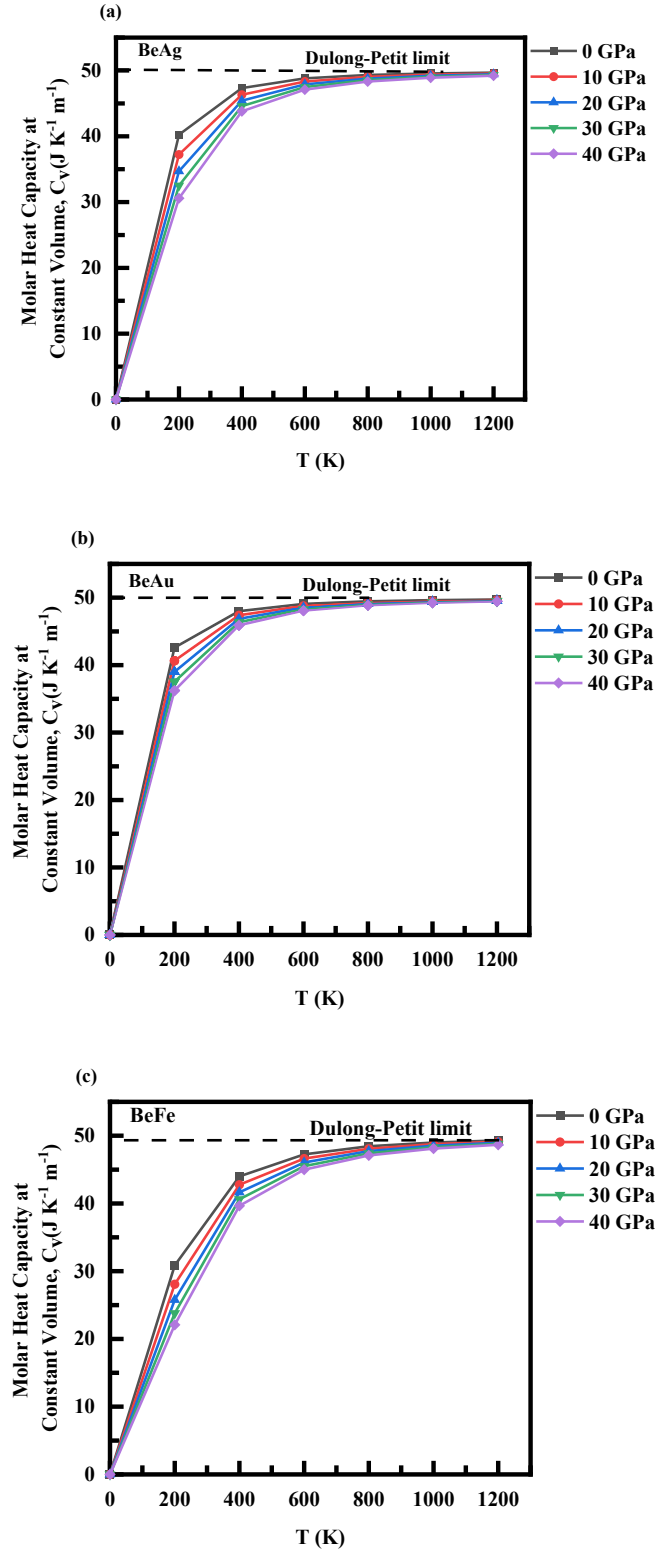


Figure 3.10: Variation of molar heat capacity at constant volume of BeX(X=Ag, Au, Fe) intermetallics with temperature (a) BeAg (b) BeAu (c) BeFe

The anharmonicity in the crystal is expressed by the Grüneisen parameter (γ), which is used to infer the thermodynamic properties of the material at high pressure and temperature. It also explains how vibrational frequencies, or phonon frequencies, are affected by temperature and pressure. According to Figure 3.10 (a,b), the value of γ gradually rises as temperature rises and falls as pressure rises. At 0 K and 0 GPa BeX (X=Ag, Au, and Fe), the Grüneisen parameter values are determined to be 2.32, 2.34, and 1.95, respectively.

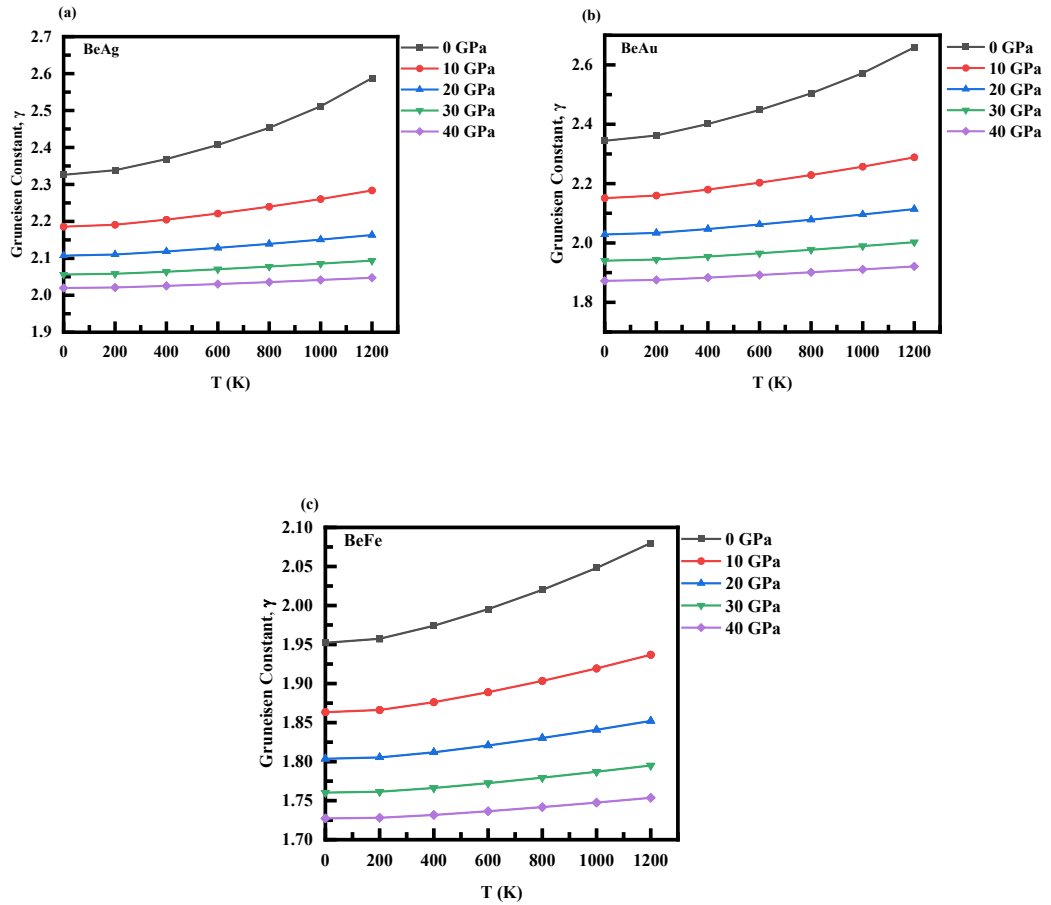


Figure 3.11: Variation of Grüneisen constant of BeX(X=Ag, Au, Fe) intermetallics with temperature (a) BeAg (b) BeAu (c) BeFe

Figure 3.11 (a,b) shows the change in the ' α ' for BeX (X=Ag, Au, and Fe) as a function of temperature and pressure. The value of ' α ' is observed to increase slowly at higher temperatures, although it does so quickly between 0 and 200 K. The primary cause of the slow growth in ' α ' over 200 K is the fact that pressure affects ' α ' in the opposite way. Because C_v drops with pressure and is proportional to ' α ' decreases with increasing pressure for a constant temperature value. The thermal expansion

coefficient values for BeAg and BeAu are 6.17×10^{-5} and $5.0 \times 10^{-5} \text{ K}^{-1}$ at 298 K and 0 GPa, respectively, and $3.18 \times 10^{-5} \text{ K}^{-1}$ at 200 K for the BeFe combination at 200 K and 0 GPa. The thermal expansion coefficient of these materials is positive. For the materials under investigation, we have also computed melting temperatures, and Table 3.2 displays the results. Thermal expansion explains the intermolecular forces. A substance's molecules begin to move faster and with an increase in average kinetic energy when it is heated. The mean spacing between the molecules rises as a result. As a result, the substance's length, area, and volume grow.

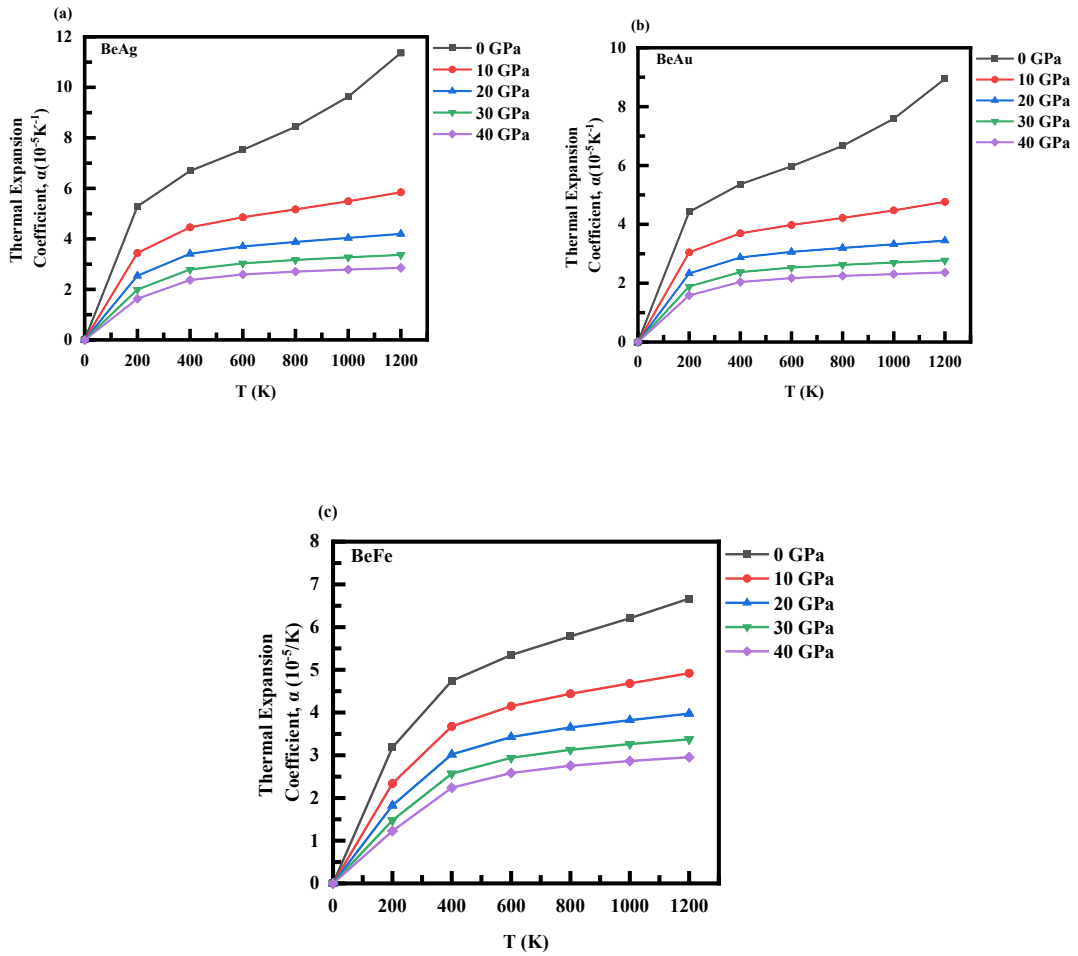


Figure 3.12: Variation of thermal expansion coefficient of BeX(X=Ag, Au, Fe) intermetallics with temperature (a) BeAg (b) BeAu (c) BeFe

Additionally, we computed the θ_D considering the impact of outside temperature and pressure. But Figure 3.12 (a,b,c) shows how it varies with temperature and pressure changes. A good thermodynamic presentation of a material, such as its molar heat capacity at constant volume and thermal expansion, can be obtained from its Debye

temperature. Beyond the θ_D , a crystal exhibits classical characteristics. It is evident from Figure 3.12 that θ_D stays constant between 0 and 200 K, and beyond that point, it exhibits a decreasing trend as temperature increases and a rising trend as pressure increases. Table 3.2 shows the calculated Debye temperature values at 0 K and 0 GPa; however, the values for BeX (X=Ag, Au, and Fe) are calculated at room temperature and zero pressure, which equals 418.54 K, 357.86 K, and 656.66 K, respectively. When compared to other materials that are similar, these examined values are fairly equivalent [1–11].

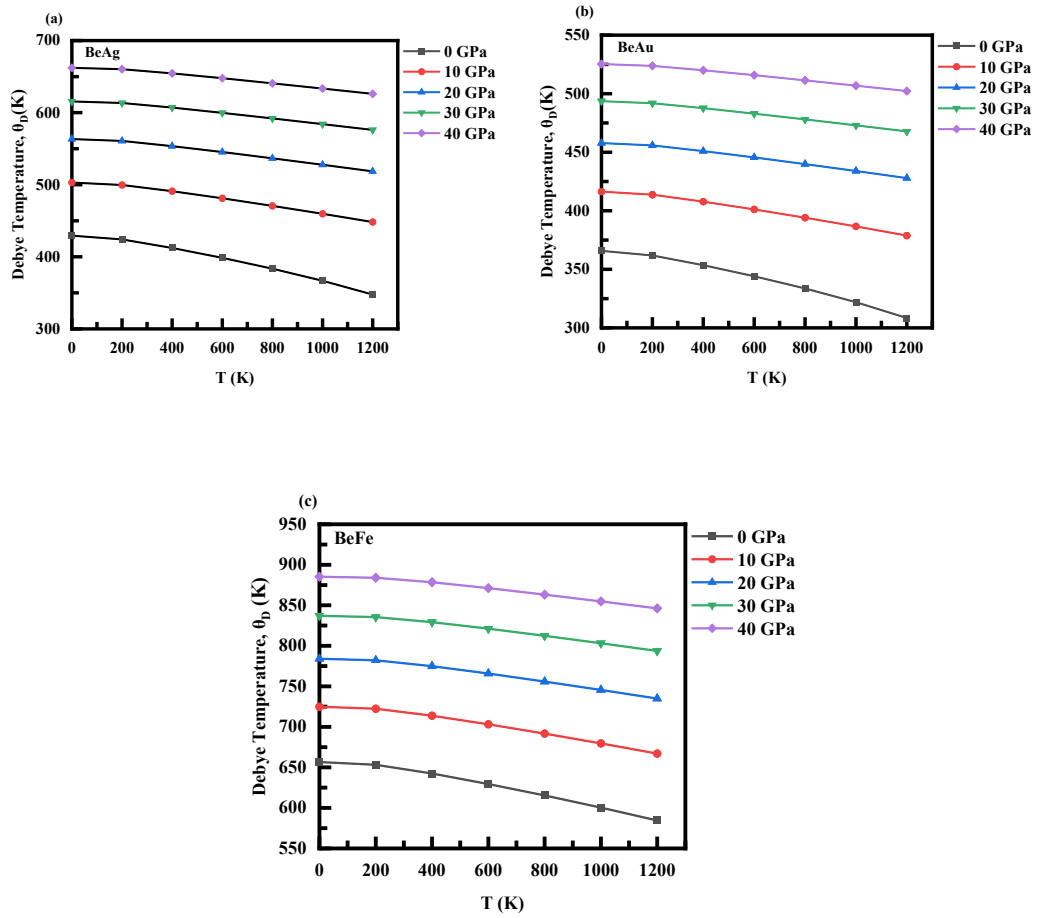


Figure 3.13: Variation of Debye temperature of BeX(X=Ag, Au, Fe) intermetallics with temperature (a) BeAg (b) BeAu (c) BeFe

Lastly, we have computed the entropy as a function of pressure and temperature outside. However, Figure 3.13 (a,b,c) shows how it changes as temperature and pressure change. Entropy provides us with details about the system's disorder. The figure makes it very evident that entropy is zero at 0 K and 0 GPa and begins to grow

exponentially as temperature rises at a certain pressure. The rising entropy value suggests that, at higher temperatures, the degree of disorder in the BeX (X=Ag, Au, and Fe) intermetallic compound is increasing. According to our calculations, at 400 K and 0 GPa, the value for BeAg is $66.31 \text{ mol}^{-1} \text{ K}^{-1}$, the value for BeAu is $73.64 \text{ mol}^{-1} \text{ K}^{-1}$, and the value for the BeFe compound is $45.94 \text{ mol}^{-1} \text{ K}^{-1}$. It should be noted that there is a slight increase in entropy at higher temperatures. This is because the atoms' vibrations are increasing, which causes the system's internal energy to rise.

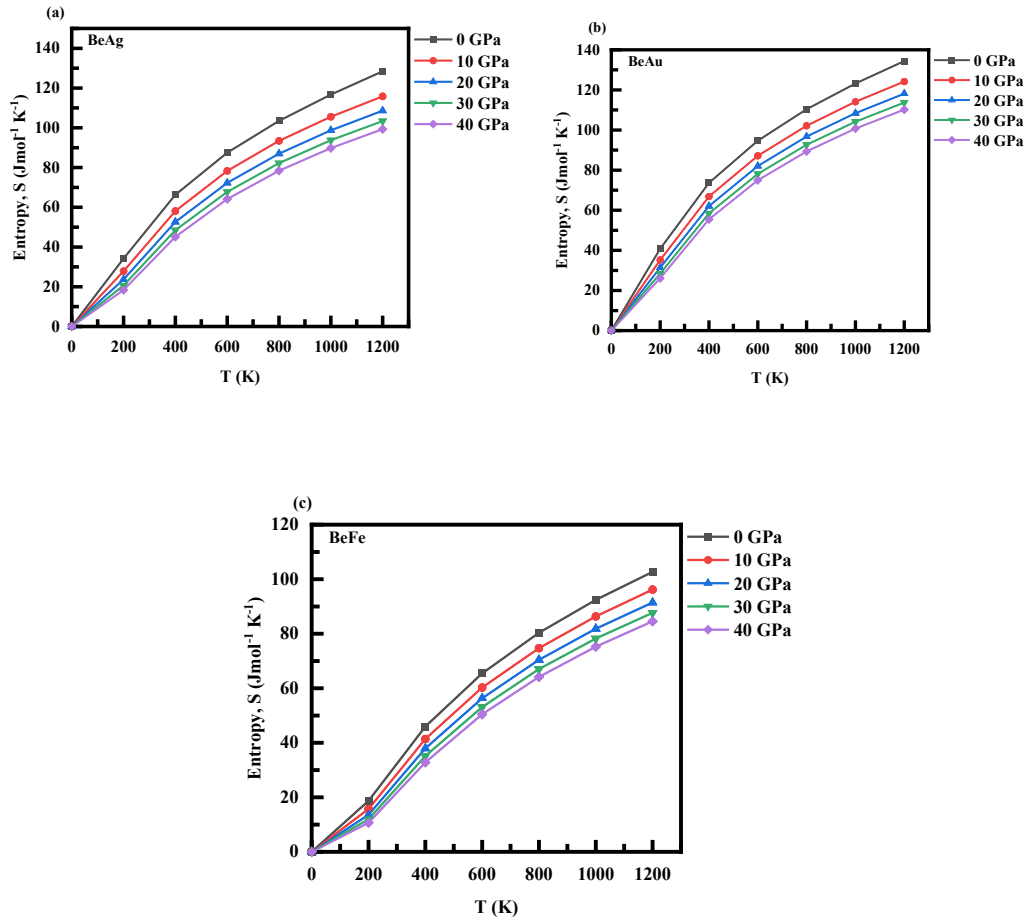


Figure 3.14: Variation of Entropy of BeX(X=Ag, Au, Fe) intermetallics with temperature (a) BeAg (b) BeAu (c) BeFe

4.6. Conclusion:

We present a study employing a quantum mechanical theoretical approach with well-known density functional theory to investigate the structural, electronic, thermophysical, elastic, and mechanical properties of BeX(X=Ag, Au, and Fe) intermetallics under varying temperature and pressure. With optimized lattice

parameters of 2.92 Å, 2.97 Å, and 2.63 Å for BeX (X=Ag, Au, and Fe), respectively, these materials have an initial Pm-3m structure. We have methodically examined temperature-induced studies of bulk modulus, molar heat capacity at constant volume, thermal expansion coefficient, and Debye temperature in order to use these materials for high temperature applications. For BeX (X=Ag, Au, Fe), we predict Debye temperatures of 430 K, 335 K, and 661 K at 0 K and 0 GPa, respectively. All compounds show a $50 \text{ J K}^{-1} \text{ m}^{-1}$ molar heat capacity at constant volume, or the Dulong-Petit limit at high temperatures. Our findings are consistent with comparable binary intermetallics and are solely predictions for the materials under consideration. This study creates more room for experimentation to confirm our findings and create devices that can withstand high temperatures.

References

1. Pan, Y., Pu, D. L., & Yu, E. D. (2021). Structural, electronic, mechanical and thermodynamic properties of Cr–Si binary silicides from first-principles investigations. *Vacuum*, 185, 110024.
2. Yu, J., Zhou, D., Pu, C., Tang, X., & Zhang, F. (2018). Prediction of stable Cu–Li binary intermetallics from first-principles calculations: Stoichiometries, crystal structures, and physical properties. *Journal of Alloys and Compounds*, 766, 640-648.
3. Jain, E., Pagare, G., Chouhan, S. S., & Sanyal, S. P. (2014). Structural, electronic, elastic and thermal properties of some transition metal CuX (X= Sc and Pd) intermetallics: A FP-LAPW study. *Computational materials science*, 83, 64-69.
4. Srivastava, V., Khan, A. A., Rajagopalan, M., & Sanyal, S. P. (2012). Theoretical investigation on first-principles electronic and thermal properties of some CdRE intermetallics. *Physica B: Condensed Matter*, 407(2), 198-203.
5. Devi, H., Pagare, G., Chouhan, S. S., & Sanyal, S. P. (2015). Electronic and high pressure elastic properties of RECd and REHg (RE= Sc, La and Yb) intermetallic compounds. *Journal of Physics and Chemistry of Solids*, 76, 70-81.
6. Reichmann, T. L., Ganesan, R., & Ipser, H. (2014). Thermochemical investigations in the system Cd–Gd. *Journal of alloys and compounds*, 610, 676-683.
7. Benmakhlouf, A., Benmakhlouf, A., Allaoui, O., & Daoud, S. (2019). Theoretical study of elastic and thermodynamic properties of CuSc intermetallic compound under high pressure. *Chinese journal of physics*, 57, 179-188.
8. Benamrani, A., Daoud, S., Salam, M. M. A., & Rekab-Djabri, H. (2021). Structural, elastic and thermodynamic properties of YRh: DFT study. *Materials Today Communications*, 28, 102529.
9. Pagare, G., Srivastava, V., Sanyal, S. P., & Rajagopalan, M. (2011). Electronic and thermal properties of B2-type AlRE intermetallic compounds: A first principles study. *Physica B: Condensed Matter*, 406(3), 449-455.

10. Srivastava, V., Pagare, G., Sanyal, S. P., & Rajagopalan, M. (2009). First principles calculations of Al-rich RE (RE= Ho, Er, Tm and Yb) intermetallic compounds. *physica status solidi (b)*, 246(6), 1206-1214.
11. Srivastava, V., Sanyal, S. P., & Rajagopalan, M. (2008). First principles electronic and thermal properties of some AlRE intermetallics. *Physica B: Condensed Matter*, 403(19-20), 3615-3622.
12. Naka, S., Thomas, M., & Khan, T. (1992). Potential and prospects of some intermetallic compounds for structural applications. *Materials science and technology*, 8(4), 291-298.
13. Fleischer, R. L., Dimiduk, D. M., & Lipsitt, H. A. (1989). Intermetallic compounds for strong high-temperature materials: status and potential. *Annual Review of Materials Science*, 19(1), 231-263.
14. Fleischer, R. L. (1987). High-strength, high-temperature intermetallic compounds. *Journal of materials Science*, 22, 2281-2288.
15. Pope, D. P., & Darolia, R. (1996). High-temperature applications of intermetallic compounds. *MRS Bulletin*, 21(5), 30-36.
16. Fang, Z., Duan, S., Liu, H., Hong, Z., Wu, H., Zhao, F., ... & Wang, J. (2022). Lithium Storage Mechanism and Application of Micron-Sized Lattice-Reversible Binary Intermetallic Compounds as High-Performance Flexible Lithium-Ion Battery Anodes. *Small*, 18(2), 2105172.
17. Benamrani, A., Daoud, S., & Bouarissa, N. (2022). First principles study of structural, elastic, and thermodynamic properties of LiAl_2X (X= Rh, Pd, Ir and Pt) intermetallic compounds. *The European Physical Journal B*, 95(7), 106.
18. Chen, H., Li, X., Chen, Z., Zhang, R., Ma, X., Zheng, F., ... & Lin, X. (2019). Investigation on electronic structures and mechanical properties of Nb-doped TiAl_2 intermetallic compound. *Journal of Alloys and Compounds*, 780, 41-48.
19. Singh, R. P. (2014). First principle study of structural, electronic and thermodynamic behavior of ternary intermetallic compound: CeMgTi . *Journal of Magnesium and Alloys*, 2(4), 349-356.
20. Sharma, R., Dar, S. A., Parveen, N., & Srivastava, V. (2020). A DFT investigation on electronic structure, charge density, mechanical stability and

- thermodynamic properties of XA13 ($\text{X} = \text{Sc, Yb and Lu}$) intermetallic compounds. *Journal of Molecular Graphics and Modelling*, 94, 107463.
21. Schwarz, K., Blaha, P., & Madsen, G. K. (2002). Electronic structure calculations of solids using the WIEN2k package for material sciences. *Computer physics communications*, 147(1-2), 71-76.
 22. Elliott, R. P., & Shunk, F. A. (1982). The Au– Be (Gold-Beryllium) system. *Journal of Phase Equilibria*, 2(4), 478-479.
 23. B. Predel, O. Madelung (ed.) “Ag-Be (Silver-Beryllium) Landolt-Börnstein - Group IV Physical Chemistry 5A (Ac-Au – Au-Zr)” SpringerMaterials (1991).
https://materials.springer.com/lb/docs/sm_lbs_978-3-540-39444-0_14
 24. Blaha, P., Schwarz, K., Madsen, G. K., Kvasnicka, D., & Luitz, J. (2001). WIEN2k. An augmented plane wave+ local orbitals program for calculating crystal properties, 60(1).
 25. Blaha, P., Schwarz, K., Sorantin, P., & Trickey, S. B. (1990). Full-potential, linearized augmented plane wave programs for crystalline systems. *Computer physics communications*, 59(2), 399-415.

Chapter 4

Unveiling the mechanical and thermodynamic properties of MgX (X=Lu, Hf) intermetallic compounds at elevated temperature

This reveals the thermodynamic and mechanical characteristics of intermetallic compounds under high-pressure and temperature conditions. The study is carried out by utilizing the Debye quasi-harmonic model and the Charpin method within the density functional theory framework. Both intermetallic compounds are found stable in the CsCl-prototype structure with a non-magnetic phase. In their electronic band structure, they exhibit a metallic nature with the use of the most appropriate generalized gradient approximation. Further, elastic moduli, bulk to shear modulus ratios, and Cauchy pressure are determined, and it is found that MgLu and MgHf show ductile and brittle nature, respectively. Additionally, for the considered intermetallic compounds, estimates of the molar heat capacity at constant volume (C_V), Grüneisen parameter (γ), thermal expansion coefficient (α), and Debye temperature (θ_D) are made at elevated temperatures up to 700 K and pressures up to 20 GPa. At room temperature and zero pressure, the estimated values of θ_D for MgLu and MgHf are 226.120 K and 284.560 K, respectively. The other reported binary intermetallics and our results agree. It is possible to employ these materials in devices that can withstand temperature changes.

Keywords: DFT, Elastic constants, Debye temperature, elasto-mechanical properties, high temperature

4.1.Introduction

A family of metallic compounds known as intermetallics has a clearly defined and organized structure, frequently exhibiting a stoichiometric ratio of the constituent elements. These substances are not the same as alloys, which are usually made up of a combination of metals without any particular organized structure. Since intermetallic

compounds have so many different properties and applications, they are crucial to materials science and engineering [1-5]. Comprehending and managing the development of intermetallic compounds is essential for customizing materials possessing desirable attributes for certain technological requirements. Researchers persist in investigating methods to enhance these substances and broaden their scope of utilization throughout diverse sectors. Due to their exceptional strength at high temperatures, intermetallics like titanium aluminides (TiAl) and nickel aluminides (NiAl) are employed in aerospace applications, especially in high-temperature devices like exhaust components and turbine rotors [6-9].

The automotive sector is investigating the use of intermetallic composites for lightweight parts. One area of research is the prospect of magnesium-based intermetallics in lightweight alloys, which may lead to an increase in fuel efficiency. Magnesium has an extensive background in the automobile industry. In 1921, Dow Chemical in the United States produced the racing engine pistons for the Indianapolis 500, which marked the first usage of magnesium in automotive technology [10]. Certain intermetallic compounds are used in solder alloys for electronic components. These materials provide good mechanical strength and thermal conductivity, making them suitable for joining electronic circuits [11]. These substances can increase catalytic activity and stability, which helps to convert pollutants more effectively. Pt-based intermetallic compounds are used as Catalysts for the Oxygen Reduction Reaction [12]. The application of intermetallic alloys as prospective fuel cell hydrogen storage materials is being studied. Their reversible ability to collect and exhale hydrogen makes them an attractive candidate for energy storage applications. In proton exchange membrane fuel cells (PEMFCs), conventional carbon-supported Pt nanoparticles were employed to catalyze chemical processes to enhance electrochemical energy conversion [13]. The ordered fct-PtFe particles trapped in porous carbon revealed a novel type of Pt-based catalyst with much-desired activity, durability, and lower Pt usage for practical PEMFC applications, according to the experimental results [13]. Certain intermetallic alloys can be used in surgical implants and equipment because they are biodegradable. Because of their biological compatibility and ability to withstand corrosion, titanium-based intermetallics are utilised, for instance, in orthopaedic implants [14]. It is being considered to use some

intermetallics as structural materials in nuclear reactors. These materials show strong resistance to radiation and stability at elevated temperatures [15]. The development of modern manufacturing processes, such as additive manufacturing (3D printing), that is capable of being utilized for creating complex components with customized properties, depends on an understanding of intermetallic materials.

Thus, intermetallics have vast applications as mentioned above. For these applications lot of physics, chemistry, and mechanics need to be understood. Many studies on different binary intermetallics have been conducted in this regard, and the structural, electronic, thermodynamic, and mechanical properties of these materials have been reported [16–25]. These substances possess a basic CsCl-type (Space group 221, B2 phase) structure. Some Mg-based intermetallics have also been reported for their extraordinary physical properties [26–33]. On the other hand, a few experimental synthesis studies of intermetallics are reported [34–37], which use experimental X-ray diffraction (XRD) and electron-probe microanalysis (EPMA) for the Mg-Ce system. To improve the degradation behavior compared to Mg and Ca alloys, Mg- or Ca-based intermetallic compounds of Mg_2Ca , Mg_2Si , Ca_2Si , and CaMgSi are being researched as potential new candidates for biodegradable implant materials [38,39].

The various intermetallics' stated status has motivated us to perform such a study. Therefore, our goal in studying considered intermetallic materials is to maximize and unlock their special qualities for a variety of uses, including electronics, energy, catalysis, and structural materials. Developments in this area have an impact on a variety of sectors and technologies by facilitating the creation of novel materials with enhanced properties and performance. In this paper, we have studied Mg-based intermetallics, namely MgX ($X = \text{Lu, Hf}$), using the WIEN2k code on the basis of density functional theory [40].

4.2. Structural phase stability:

The cubic B2 phase is where the MgLu and MgHf intermetallics crystallize [66]. Figure 4.1 depicts the crystal structure of MgX intermetallics (X=Lu, Hf) in cubic phase.

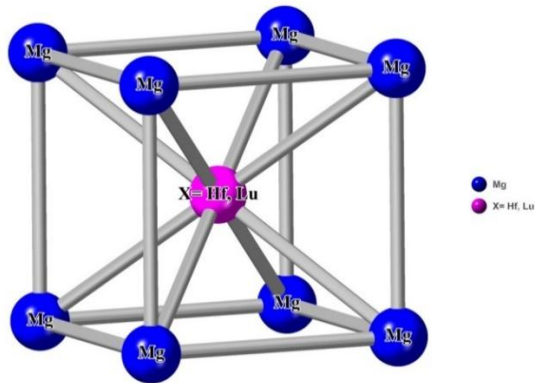


Figure 4.1: Crystal structure of MgX(X= Hf, Lu) intermetallics in Pm-3m space group.

Table 4.1: Structural information of MgX(X=Lu, Hf) intermetallics at a glance.

Intermetallic compound	Structure type	Space group	Pearson symbol	Lattice parameter (Å)	Atomic coordinates / R_{MT}
MgLu	Cubic	$Pm-3m$, (No. 221)	cP2	7.0128	Mg(1a): 0, 0, 0 (0, 0, 0) Lu(1b): 0.5, 0.5, 0.5 (0.5, 0.5, 0.5) Mg: 2.6 a.u. Lu: 2.8 a.u.
MgHf	Cubic	$Pm-3m^a$ (No. 221)	cP2	6.5839	Mg(1a): 0, 0, 0 (0, 0, 0) Hf(1b): 0.5, 0.5, 0.5 (0.5, 0.5, 0.5) Mg: 2.2 a.u. Hf: 2.3 a.u.

^aExp. HfCo [67]

Table 4.1 provides an overview of the positions of the atoms in the unit cell for this structure, along with their RMT values. The Birch-Murnaghan equation of state was used to fit the total energy versus unit cell volume to optimize the structure. To determine whether or not materials have a magnetic effect, we computed the total energy of the compounds in the ferromagnetic (FM) and non-magnetic (NM) phases. As a result, we have shown the variation of total energy (with GGA potential) in the FM and NM phases while considering the CsCl-type structure in Figure 4(a,b). Figure 4(a) makes it evident that there is very little difference between the FM and NM phases, and the estimated spin magnetic moment for MgLu is 0.01004 μ_B . Conversely, it can be observed from Figure 4(b) that the most stable phase for MgHf is the NM phase.

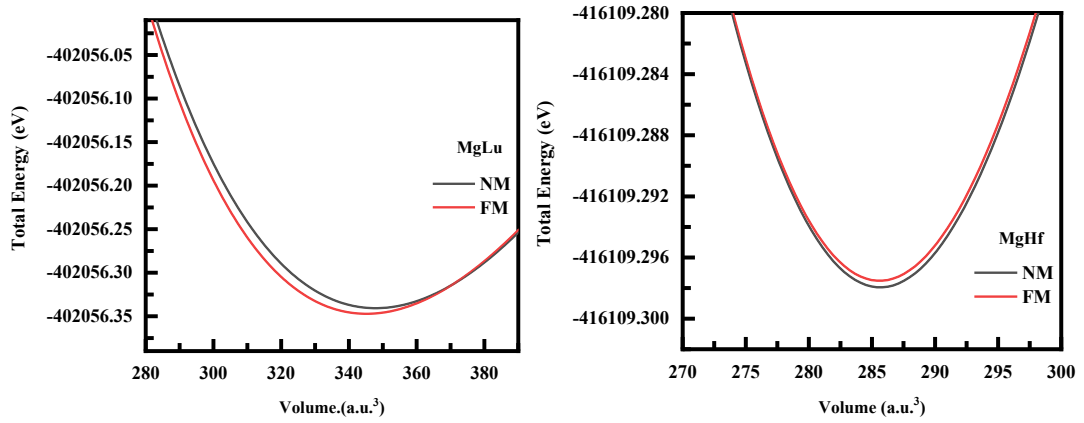


Figure 4.2: Variation of total energy as a function of cell volume of MgX(X=Lu, Hf) intermetallics in Pm-3m structure.

So, present study considered NM phase for both the intermetallics. Table 4.2 presents the ground state properties of the materials under consideration in the Pm-3m phase, including lattice constant (a_0), bulk modulus (B_0) and pressure derivatives (B'_0). These properties are compared to the available data for the same compounds [68,69] and different compounds [70]. There are some other materials in which this CsCl phase is the high-pressure phase [71].

Table 4.2: Calculated ground state properties: unit cell volume V_0 , lattice parameter a_0 , bulk modulus B_0 , first order pressure derivative of bulk modulus B'_0 and equilibrium total energy E_0 of MgX (X=Lu, Hf) intermetallics at 0GPa and 0K

Parameters	MgLu	MgHf
V_0 (a.u. ³)	344.945	285.371
	347.410 ^a	286.873 ^a
a_0 (Å)	3.711	3.484
	3.72 ^a	3.49 ^a , 3.19 ^c
B_0 (GPa)	44.744	76.589
	45.22 ^b	-
B'_0	4.26	3.75
E_0 (x10 ² eV)	-4020.564	-4161.093

^a[68]; ^b[69]; ^cExp.CoHf [70]

4.3.Electronic properties:

For electronic properties, we have computed the results of the band structure and density of states. The electronic properties were investigated by using the GGA approximation [44]. The results of these electronic properties, as stated band structure profile for MgLu and MgHf intermetallics, are displayed in Figure 4.3 (a,b). The electronic band profiles are computed using the optimized lattice parameter, as given in Table 4.1, at absolute temperature and zero GPa.

We have calculated the density of states and band structure results for electronic properties. The GGA approximation was used to investigate the electronic properties [44]. Figure 4.3 (a,b) shows the results of these electronic properties as stated in the band structure profile for the intermetallics MgLu and MgHf. At zero GPa and absolute temperature, the electronic band profiles are calculated with the optimized lattice parameter provided in Table 4.1. Energy (E) of different electronic states on the Y-

axis, with the wave vector (k) pointing in the direction of propagation Fermi level is set to 0 eV for the band structure calculation. These plots show that the valence band and conduction band overlap at the Fermi level, which indicates that the intermetallic compounds MgLu and MgHf are metallic in nature. The metallic nature of the materials under consideration is evident from Figure 4.3 (a,b), where the crossover of the electronic states for MgLu and MgHf from Γ at 0.775 eV to X at 1.223 eV and 0.826 eV to X states at 1.304 eV, respectively, demonstrate this.

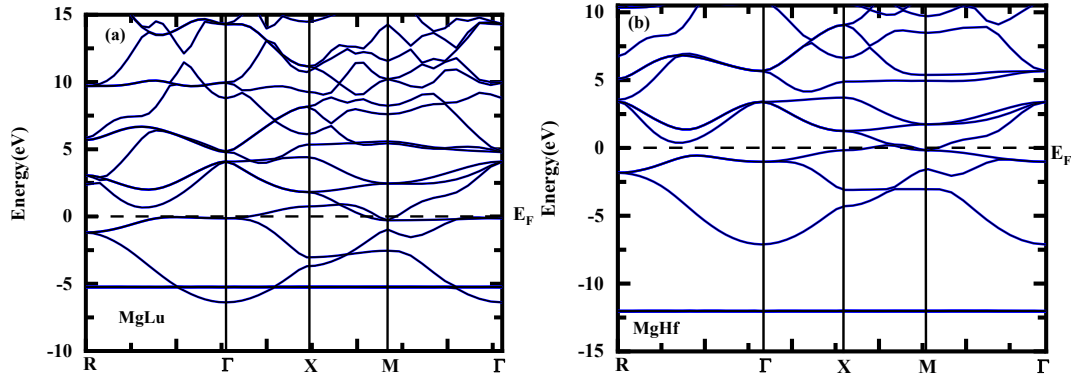
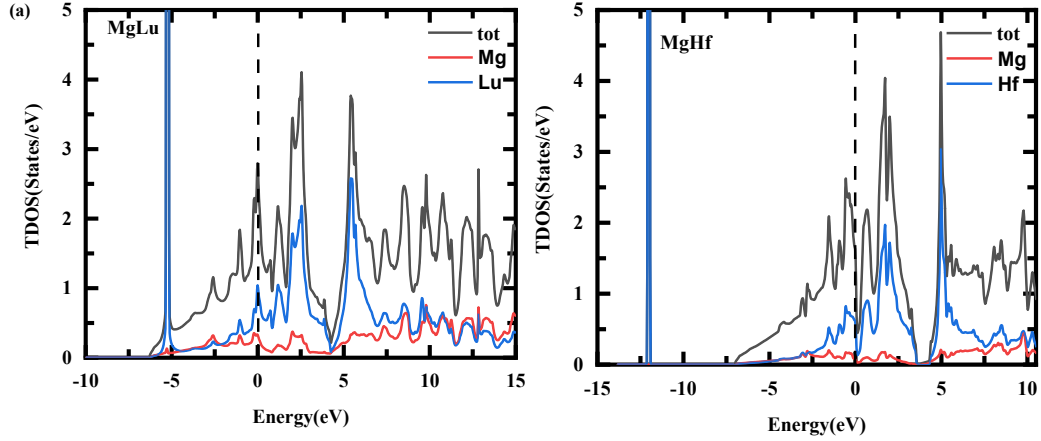


Figure 4.3: Band structure of MgX(X=Lu, Hf) intermetallics (a) MgLu (b) MgHf

In addition, the total density of states (TDOS) and projected density of states (PDOS) in the Pm-3m structure are computed and shown in Figure 4 (a,b) to help comprehend



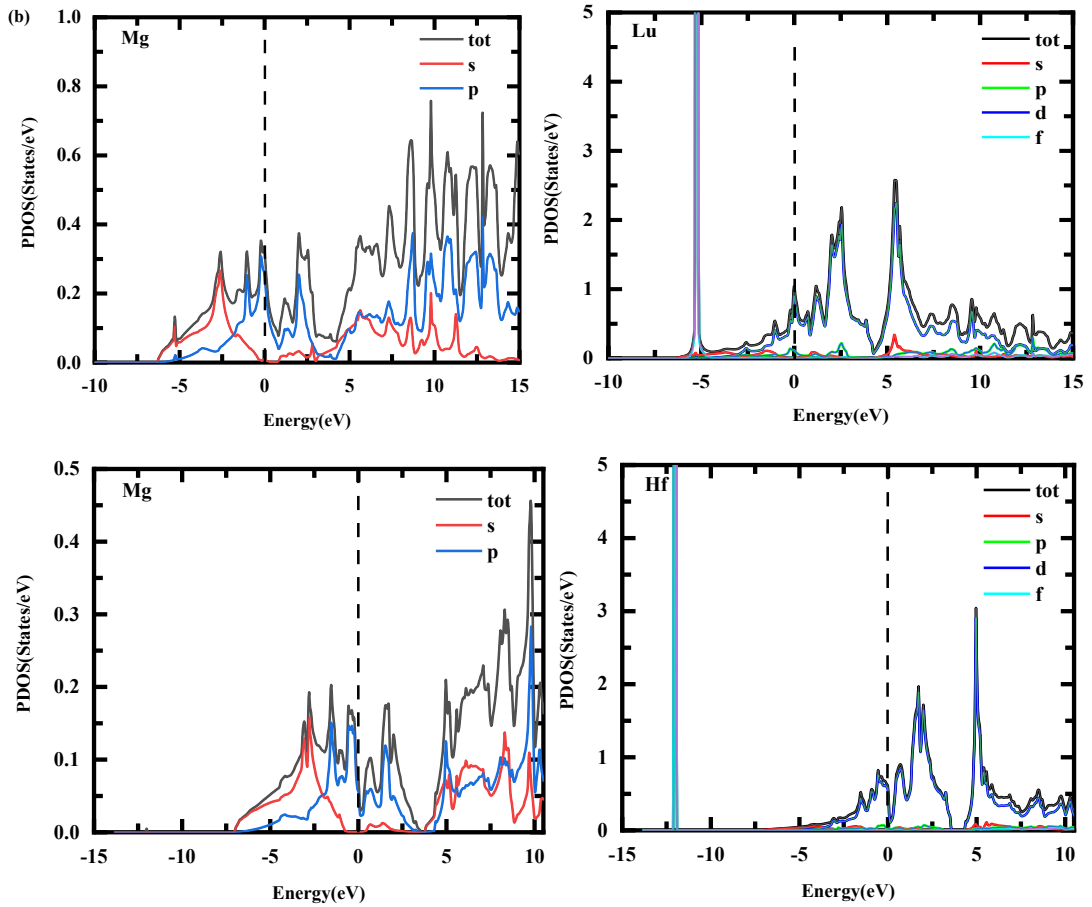


Figure 4.4: Density of states (DOS) for MgX (X=Hf and Lu) intermetallics (a) Combined orbitals depiction as total DOS (TDOS) for Mg, Lu and Hf (b) different orbitals depiction as partial DOS (PDOS) for Mg, Lu and Hf.

The electronic contribution of the E-K diagrams. Figure 4.4 makes this very evident for MgLu and MgHf intermetallic compounds majority of electrons cross over the Fermi level due to the 4f states of Lutetium (Lu) and Hafnium (Hf). In short, we plot a projected density of states graph for MgLu and MgHf intermetallic compounds in Figure 4(b) to comprehend the contribution of electronic states. It is evident that Mg-‘p’ states hybridize with Lu/Hf-‘d’ states at E_f and making them metallic. A sharp localized peak at -5 (-12) eV representing Lu-‘f’ (Hf-‘f’) states in Fig. 4(a,b).

4.4. Elastic and mechanical properties

It is crucial to investigate the structural stability of compound elastic constants in order to comprehend force application. Thus, it is crucial to examine the material that is being

compressed. The behavior of crystals, mechanical stability, ductility, nature of forces, and numerous thermodynamic properties of solids, such as bulk modulus, molar specific heat at constant volume, and Debye temperature, are all provided by the elastic constants. For the ductile and brittle behavior of the MgLu and MgHf intermetallic compounds, we have calculated the various mechanical properties such as Young's modulus (E), bulk modulus (B), shear modulus (G), elastic constants (C_{ij}), Poisson ratio (σ), anisotropic ratio (A), and B/G ratio. Table 4.3 presents the computed values.

Table 4.3: Calculated elastic and Mechanical properties for MgX(X=Lu, Hf) intermetallics at 0 GPa and 0 K. Elastic constants C_{11} , C_{12} , C_{44} , Bulk Modulus B, Voigt Shear Modulus G_V , Reuss Shear Modulus G_R , Shear Modulus G, Young's Modulus E, Anisotropy Ratio A, Cauchy Pressure $C_{12}-C_{44}$, Bulk modulus to Shear modulus ratio B/G, Poisson Ratio σ , longitudinal velocity V_l , transverse velocity V_t , Average velocity V_m , Debye Temperature θ_D , Melting Temperature T_m .

Properties	MgLu	Others	MgHf	Others
C_{11} (GPa)	57.701	56.35 ^a , 52.97 ^b	136.460	-
C_{12} (GPa)	38.179	39.65 ^a , 39.08 ^b	47.166	-
C_{44} (GPa)	35.910	45.54 ^a , 34.6 ^b	85.476	-
B(GPa)	44.7	43.7 ^b	76.8	173 ^c
G_V (GPa)	25.450	23.54 ^b	69.144	-
G_R (GPa)	17.335	13.35 ^b	77.627	-
G(GPa)	21.393	18.44 ^b	65.864	56 ^d
E(GPa)	55.346	48.11 ^b	153.697	151 ^d , 221 ^e , 238 ^e
A	3.679	-	1.914	-
$C_{12}-C_{44}$ (GPa)	2.269	-	-38.310	-
B/G ratio	2.089	2.37 ^b	1.167	-
σ	0.294	0.3 ^b	0.167	-
V_l (m s ⁻¹)	3375.896	-	4547.568	-
V_t (m s ⁻¹)	1824.841	-	2875.848	-
V_m (m s ⁻¹)	2036.660	-	3163.919	-
θ_D (K)	205.346	-	340.685	-
T_m (K)	894.071		1359.615	1913 ^f

^a[69]; ^b[27]; ^c[72]; ^d[73]; ^eExp.[74]; ^f[75]

The elastic constants, namely C_{11} , C_{12} , and C_{44} , have been calculated for MgLu and MgHf using the Charpin method [54] implemented in the WIEN2k code [41]. The estimated values are presented in Table 4.3. Further, with the analysis of elastic constants, some mechanical properties are reported. The bulk modulus (B), which represents the resistance to fracture, values are calculated to be 44.690 GPa and 76.874

GPa, and Young's modulus (E), which indicates stiffness of the material, corresponding values are calculated to be 55.346 GPa and 153.697 GPa for MgLu and MgHf intermetallic compounds by using equation (9), respectively.

The elastic constants C_{11} , C_{12} , and C_{44} , for MgLu and MgHf, have been computed through the application of the Charpin method [54] in the WIEN2k code [41]. Table 4.3 displays the estimated values. Some mechanical properties are reported in addition to the analysis of elastic constants. Using equation (9), the corresponding values for the bulk modulus (B), which represents the resistance to fracture, are calculated to be 44.690 GPa and 76.874 GPa, and the Young's modulus (E), which indicates the stiffness of the material, are calculated to be 55.346 GPa and 153.697 GPa for MgLu and MgHf intermetallic compounds. The plastic twist of the materials is indicated by the shear modulus has also been calculated for corresponding values of 21.393 GPa and 65.864 GPa for MgLu and MgHf intermetallic compounds, respectively, by using the Voigt-Reuss-Hill approximation [58-60].

By using elastic constants, we calculated the anisotropic factor ($A = \frac{2C_{44}}{C_{11} - C_{12}}$) which describes the characteristic behavior of the material in different directions of the structure. Material is classified as isotropic if the value of A is less than 1, but anisotropic if A is greater than 1. The value of A, as determined by MgLu and MgHf intermetallic compounds, is 3.679 and 1.914, which represents that the material is anisotropic. This anisotropic behavior shows the material during the growth process at the micro level some cracks or defects.

Bulk modulus and shear modulus can be used to explain the ductile and brittle behavior of the materials after the elastic constants have been calculated. Pugh's [63] criteria state that the B/G ratio should be calculated. If the value is less than 1.75, the material is deemed brittle, and if the value is greater than 1.75, the material is deemed ductile. If MgLu and MgHf corresponding values are 2.089 and 1.167, which indicate the MgLu intermetallic compound is ductile, and the presence of the MgHf intermetallic compound suggests that the material is brittle. We also compute the Cauchy pressure, $C_{12} - C_{44}$, which further characterizes the materials' brittle and ductile properties. When the material's value is negative, it exhibits brittle behavior; when it is positive, it exhibits ductile behavior. In case of MgLu and MgHf, corresponding values are 2.269

and -38.310, which shows the MgLu intermetallic compound ductile behavior and MgHf intermetallic compound brittle in nature. Further to understand the bonding nature of the materials and forces between the atoms in MgLu and MgHf intermetallics can be discussed by using Poisson ratio (σ). Under uniaxial stress, it is the ratio of lateral to longitudinal strain. Should $\sigma = 0.1$ be the value of bonding nature, it would be covalent; if $\sigma = 0.25$, it would be ionic; and if $\sigma = 0.33$, it would be metallic. We have determined that the Poisson ratio for MgLu is 0.294, which indicates bonding nature of the material would be ionic, and MgHf is 0.167, which indicates bonding nature of the material would be covalent.

Further, we have calculated the melting temperature for MgLu and MgHf intermetallic compounds by using the above equation (16), which is given in Section 2. So, the calculated values of melting temperature for MgLu are 894.071 and for MgHf are 1359.615, which provides room for research using experiments.

4.5. Thermodynamic properties

By using the quasi-harmonic Debye approximation, thermal properties also play a crucial role in providing valuable information about some important parameters, such as unit cell volume (V), bulk modulus (B), molar heat capacity at constant volume (C_v), Grüneisen parameter (γ), thermal expansion coefficient (α), and Debye temperature (θ_D) for MgLu and MgHf intermetallic compounds [49–53]. A full-potential linearized augmented plane-wave method (FP-LAPW) [42] based on density functional theory (DFT) and implemented in the WIEN2k [41] code is utilized to examine these materials. Plots showing the variations in unit cell volume (V), bulk modulus (B), molar heat capacity at constant volume (C_v), Grüneisen parameter (γ), thermal expansion coefficient (α), and Debye temperature (θ_D) under pressure changes from 0 GPa to 20 GPa and temperature ranges from 0 K to 700 K have been executed. For the MgLu and MgHf intermetallic compounds, we have plotted the variation of unit cell volume as a function of temperature and pressure, respectively, in Figures 4.5 and 4.6(a). These graphs make it abundantly evident that unit cell volume rises with rising temperature and falls with rising pressure. The general trend in solids can be attributed to variations in temperature and pressure within the unit cell volume. This tells us that a solid expands with temperature, but compresses under pressure. We have

plotted the bulk modulus variation for the intermetallic compounds MgLu and MgHf as a function of temperature and pressure, respectively, in Figures 4.5 and 4.6(b).

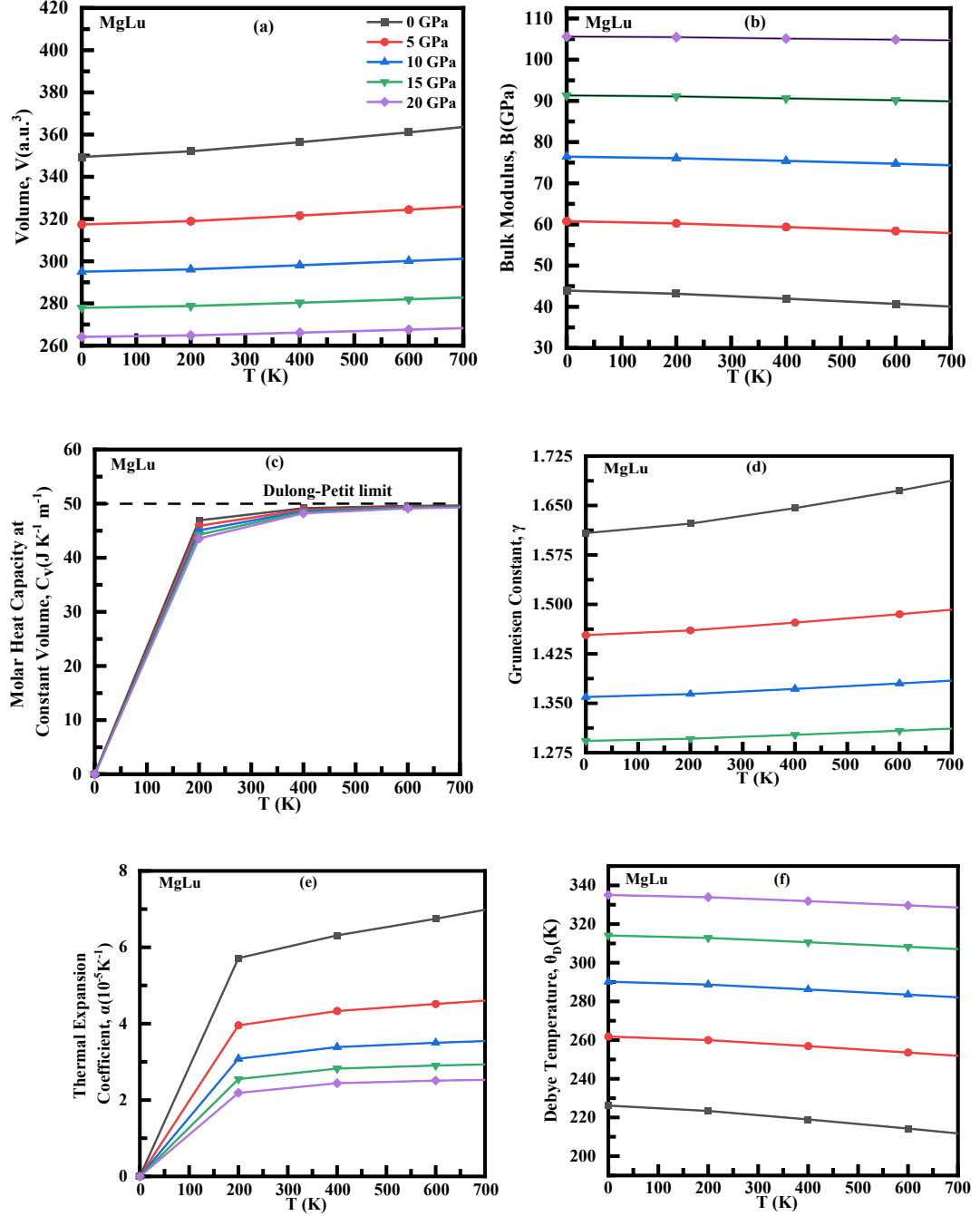


Figure 4.5: Variation of thermodynamic parameters with temperature and pressure for MgLu intermetallic

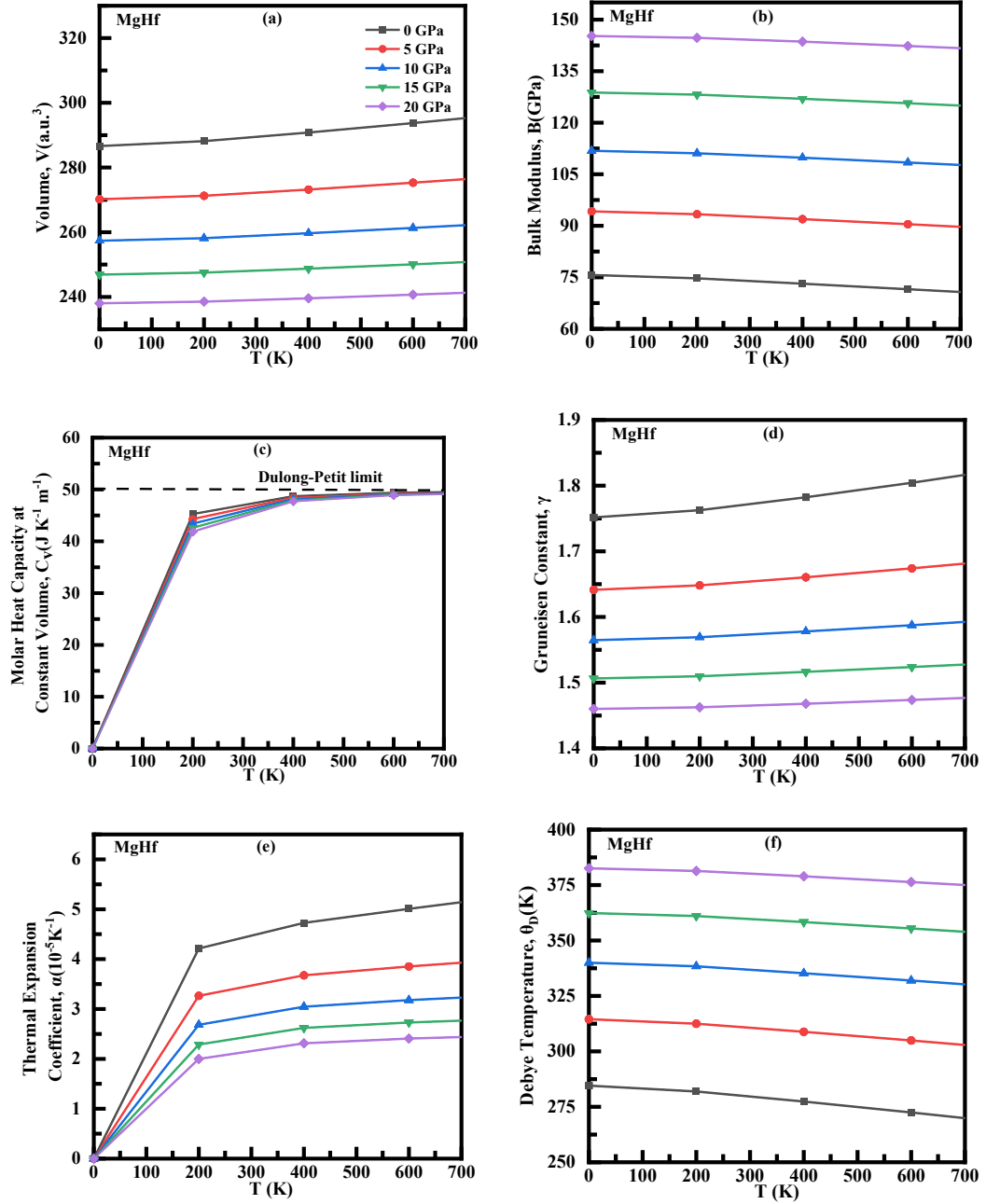


Figure 4.6: Variation of thermodynamic parameters with temperature and pressure for MgHf intermetallic

As observed in the case of variation of volume under temperature and pressure, it is evident from the figures that variation of the bulk modulus under temperature and pressure has the opposite effect of γ . The bulk modulus rises with increasing pressure and falls with increasing temperature, as shown in Figures 4.5 and 4.6 (b). The reason for this variation in the B value with temperature and pressure is that the former

increases hardness while the latter decreases it. Second, while pressure has the opposite effect, rising temperatures also result in rising unit cell volumes and interatomic distances. Although we have shown the calculated bulk modulus values at 0 K and 0 GPa, the values for MgLu and MgHf are calculated at room temperature and zero pressure, which equals 43.939 GPa and 75.676 GPa, respectively.

Moreover, the molar heat capacity at constant volume is computed, and its variation with temperature and pressure is shown in Figures 4.5 and 4.6 (c). C_v measures the motion of molecules and provides information about lattice vibration and phase transition. It is evident from Figures 4.5 and 4.6(c) that the C_v rises quickly at lower temperature values, from 0 to 200 K. A gradual increase in C_v is seen above 200 K, and it reaches the well-known Dulong-Petit limit at 600 K, when it becomes constant. For MgLu and MgHf, the computed value of C_v at 700 K and 0 GPa is $50 \text{ J K}^{-1} \text{ m}^{-1}$. The anharmonicity in the crystal is expressed by the Grüneisen parameter, which is used to infer the thermodynamic properties of the material at high pressure and temperature. It also explains how vibrational frequencies, or phonon frequencies, are affected by temperature and pressure. As a result, we have determined for the first time the pressure and temperature dependence of γ for MgLu and MgHf, which is displayed in Figures 4.5 and 4.6 (d). As temperature rises, γ values gradually decrease, and as pressure rises, they decrease. The Grüneisen parameter values for MgLu and MgHf are determined to be 1.608 and 1.752 at 0 K and 0 GPa, respectively, and 1.646 and 1.782 at 400 K and 0 GPa. The variation of the thermal expansion coefficient (α) with temperature and pressure is depicted in Figures 4.5 and 4.6 (e). The value of α is observed to increase slowly at higher temperatures, but it does so quickly between 0 and 200 K. The primary cause of the slow increase in α above 200 K is the fact that pressure affects α in the opposite way. Because C_v decreases with pressure and is proportional to α decreases with increasing pressure for a fixed temperature value. The coefficient of thermal expansion values are computed to be 6.310×10^{-5} and $4.727 \times 10^{-5} \text{ K}^{-1}$ at 400 K and 0 GPa for MgLu and MgHf, respectively. The thermal expansion coefficient of these materials is positive. Thermal expansion explains the intermolecular forces. Moles of a heated substance have an increase in average kinetic energy, which causes them to accelerate. Consequently, the average distances between the molecules also rise. As a result, the substance's length, area, and volume increase.

Finally, we have computed the variation of Debye temperature (θ_D) under temperature and pressure for MgLu and MgHf are calculated and presented in Figs. 5 and 6 (f), respectively. Atomic vibrations in solids—more precisely, the average energy of these vibrations is connected to the Debye temperature. Atoms fluctuate around their equilibrium positions in a solid material because of thermal energy; they are not static. Because these vibrations are quantized, their possible energy levels are limited to specific discrete values. The temperature at which all possible energy levels are occupied and these quantized vibrational modes become excited is known as the Debye temperature. This temperature is the point at which a solid lattice's specific heat capacity begins to be substantially influenced by the vibrations of its atoms. It is specifically the temperature at which atomic vibrations in a solid lattice cross a particular threshold, which is typically connected to the lattice's quantum mechanical behavior. A crystal exhibits classical behavior above θ_D . It is evident from Figures 4.5 and 4.6 (f) that θ_D is constant between 0 and 200 K, and that above that point, it exhibits a decreasing trend with rising temperature and an increasing trend with rising pressure. The calculated values of Debye temperature at 0 K and 0 GPa have been presented; however, for MgLu and MgHf, the values are calculated at room temperature and zero pressure, which equals 226.120 K and 284.560 K, respectively.

4.6.Conclusion

In summary, DFT theory has been used to investigate the electronic structure, mechanical, and thermodynamic behaviors of MgX (Lu and Hf) intermetallics. These materials were undertaken for the study up to a high temperature of 700K and pressure up to 20 GPa. These materials possess the B2-phase as the optimized phase. The optimized lattice parameter values of 3.711 and 3.484 are reported for MgLu and MgHf, respectively. These results are found to be consistent with values reported in the literature. Additionally, a review of bulk modulus and elastic constants reveals that these materials are not hard and stiff. B/G values of 2.089 and 1.167 for MgLu and MgHf reveal ductile and brittle nature, respectively. To understand the vibrational behavior of the studied materials, Debye temperature, heat capacity, and thermal expansion coefficients are calculated. At calculated Debye temperatures of 226 K and 284 K for MgLu and MgHf, respectively, materials exhibit vibrational energy in the

crystal lattice that reaches a maximum to excite all possible vibrational modes in the material. The materials' specific heat capacity, thermal conductivity, and other properties related to lattice vibrations are further explained. The molar heat capacity for these materials is calculated in the range of 45-48 JK⁻¹m⁻¹. The present study found materials' suitability in temperature-resistive devices, where rapid heating or cooling is required, such as in electronic devices and aerospace, automobile industries.

References

1. Paul, A. R., Mukherjee, M., & Singh, D. (2022). A critical review on the properties of intermetallic compounds and their application in the modern manufacturing. *Crystal Research and Technology*, 57(3), 2100159.
2. Pope, D. P., & Darolia, R. (1996). High-temperature applications of intermetallic compounds. *MRS Bulletin*, 21(5), 30-36.
3. Bauer, J. C., Chen, X., Liu, Q., Phan, T. H., & Schaak, R. E. (2008). Converting nanocrystalline metals into alloys and intermetallic compounds for applications in catalysis. *Journal of Materials Chemistry*, 18(3), 275-282.
4. Fleischer, R. L. (1987). High-strength, high-temperature intermetallic compounds. *Journal of materials Science*, 22, 2281-2288.
5. Fleischer, R. L. (1987). High-strength, high-temperature intermetallic compounds. *Journal of materials Science*, 22, 2281-2288.
6. Pope, D. P., & Ezz, S. S. (1984). Mechanical properties of Ni₃Al and nickel-base alloys with high volume fraction of γ' . *International metals reviews*, 29(1), 136-167.
7. Dimiduk, D. M., Miracle, D. B., & Ward, C. H. (1992). Development of intermetallic materials for aerospace systems. *Materials Science and Technology*, 8(4), 367-375.
8. Aoki, K. (1990). Ductilization of L12 intermetallic compound Ni₃Al by microalloying with boron. *Materials Transactions, JIM*, 31(6), 443-448.
9. Stoloff, N. S., Koch, C. C., Liu, C. T., & Izumi, O. (1987). High-temperature ordered intermetallic alloys II (No. CONF-861207-). *Materials Research Society, Pittsburgh, PA*.
10. Prakash, U. (2018). Intermetallic matrix composites based on iron aluminides. In *Intermetallic Matrix Composites* (pp. 21-35). Woodhead Publishing.
11. Frear, D. R., & Vianco, P. T. (1994). Intermetallic growth and mechanical behavior of low and high melting temperature solder alloys. *Metallurgical and Materials Transactions A*, 25, 1509-1523.
12. Wang, J., Pan, F., Chen, W., Li, B., Yang, D., Ming, P., ... & Zhang, C. (2023). Pt-based intermetallic compound catalysts for the oxygen reduction reaction:

- structural control at the atomic scale to achieve a win–win situation between catalytic activity and stability. *Electrochemical Energy Reviews*, 6(1), 6.
13. Du, X. X., He, Y., Wang, X. X., & Wang, J. N. (2016). Fine-grained and fully ordered intermetallic PtFe catalysts with largely enhanced catalytic activity and durability. *Energy & Environmental Science*, 9(8), 2623-2632.
 14. Li, Y., Yang, C., Zhao, H., Qu, S., Li, X., & Li, Y. (2014). New developments of Ti-based alloys for biomedical applications. *Materials*, 7(3), 1709-1800.
 15. Nikulina, A. V., Konkov, V. F., Peregud, M. M., & Vorobev, E. E. (2018). Effect of molybdenum on properties of zirconium components of nuclear reactor core. *Nuclear Materials and Energy*, 14, 8-13.
 16. Yang, Y., Wang, C., Sun, J., Li, S., Liu, W., Wu, H., & Wang, J. (2021). First-Principles Study of Mechanical and Thermodynamic Properties of Binary and Ternary CoX (X= W and Mo) Intermetallic Compounds. *Materials*, 14(6), 1404.
 17. Liu, T., Ma, T., Li, Y., Ren, Y., & Liu, W. (2022). Stabilities, mechanical and thermodynamic properties of Al–RE intermetallics: A first-principles study. *Journal of Rare Earths*, 40(2), 345-352.
 18. Jayalakshmi, V., Jaiganesh, G., & Rameshkumar, S. (2020). Probing into the global structural prediction, physical and electronic properties of AX (A= Ca, Sr, Ba; X= La, Nd, Sm) binary intermetallic alloys. *Journal of Alloys and Compounds*, 848, 156364.
 19. Wang, R., Wang, S., Wu, X., Lan, M., & Song, T. (2012). First-principles calculations of phonon and thermodynamic properties of AlRE (RE= Y, Gd, Pr, Yb) intermetallic compounds. *Physica Scripta*, 85(3), 035705.
 20. Srivastava, V., Pagare, G., Sanyal, S. P., & Rajagopalan, M. (2009). First principles calculations of Al-rich RE (RE= Ho, Er, Tm and Yb) intermetallic compounds. *physica status solidi (b)*, 246(6), 1206-1214.
 21. Pagare, G., Srivastava, V., Sanyal, S. P., & Rajagopalan, M. (2011). Electronic and thermal properties of B2-type AlRE intermetallic compounds: A first principles study. *Physica B: Condensed Matter*, 406(3), 449-455.

22. Srivastava, V. (2024). A computational modeling on thermodynamic performances of BeX (X= Ag, Au) intermetallics. *The Journal of Chemical Thermodynamics*, 188, 107175.
23. Srivastava, V., Khan, A. A., Rajagopalan, M., & Sanyal, S. P. (2012). Theoretical investigation on first-principles electronic and thermal properties of some CdRE intermetallics. *Physica B: Condensed Matter*, 407(2), 198-203.
24. Fatima, B., Chouhan, S. S., Acharya, N., & Sanyal, S. P. (2014). Theoretical prediction of the electronic structure, bonding behavior and elastic moduli of scandium intermetallics. *Intermetallics*, 53, 129-139.
25. Chouhan, S. S., Pagare, G., Rajagopalan, M., & Sanyal, S. P. (2012). First principles study of structural, electronic, elastic and thermal properties of YX (X= Cd, In, Au, Hg and Tl) intermetallics. *Solid state sciences*, 14(8), 1004-1011.
26. Rameshkumar, S., Jaiganesh, G., & Jayalakshmi, V. (2019). Structural, phonon, elastic, thermodynamic and electronic properties of Mg–X (X= La, Nd, Sm) intermetallics: The first principles study. *Journal of Magnesium and Alloys*, 7(1), 166-185.
27. Zhang, J., Mao, C., Long, C. G., Chen, J., Tang, K., Zhang, M. J., & Peng, P. (2015). Phase stability, elastic properties and electronic structures of Mg–Y intermetallics from first-principles calculations. *Journal of Magnesium and Alloys*, 3(2), 127-133.
28. Boucetta, S. (2014). Theoretical study of elastic, mechanical and thermodynamic properties of MgRh intermetallic compound. *Journal of Magnesium and Alloys*, 2(1), 59-63.
29. Yang, Z., Du, J., Wen, B., Hu, C., & Melnik, R. (2013). First principles studies on the structural, elastic, electronic properties and heats of formation of Mg–AE (AE= Ca, Sr, Ba) intermetallics. *Intermetallics*, 32, 156-161.
30. Du, J., Zhang, A., Guo, Z., Yang, M., Li, M., & Xiong, S. (2018). Atomic cluster structures, phase stability and physicochemical properties of binary Mg-X (X= Ag, Al, Ba, Ca, Gd, Sn, Y and Zn) alloys from ab-initio calculations. *Intermetallics*, 95, 119-129.

31. Wu, Y., Hu, W., & Sun, L. (2007). Elastic constants and thermodynamic properties of Mg–Pr, Mg–Dy, Mg–Y intermetallics with atomistic simulations. *Journal of Physics D: Applied Physics*, 40(23), 7584.
32. Wu, Y., & Hu, W. (2007). Elastic and brittle properties of the B2-MgRE (RE= Sc, Y, Ce, Pr, Nd, Gd, Tb, Dy, Ho, Er) intermetallics. *The European Physical Journal B*, 60, 75-81.
33. Wang, R., Wang, S., Wu, X., Yao, Y., & Liu, A. (2010). Ab initio calculations on the third-order elastic constants for selected B2–MgRE (RE= Y, Tb, Dy, Nd) intermetallics. *Intermetallics*, 18(12), 2472-2476.
34. Zhang, X., Kevorkov, D., & Pekguleryuz, M. O. (2009). Study on the binary intermetallic compounds in the Mg–Ce system. *Intermetallics*, 17(7), 496-503.
35. Pöttgen, R., & Johrendt, D. (2019). *Intermetallics: synthesis, structure, function*. Walter de Gruyter GmbH & Co KG.
36. Lotfi, S., & Brgoch, J. (2020). Discovering intermetallics through synthesis, computation, and data-driven analysis. *Chemistry—A European Journal*, 26(40), 8689-8697.
37. Chen, D., Chen, J., Yan, H., & Chen, Z. (2007). Synthesis of binary and ternary intermetallic powders via a novel reaction ball milling technique. *Materials Science and Engineering: A*, 444(1-2), 1-5.
38. Hagihara, K., Fujii, K., Matsugaki, A., & Nakano, T. (2013). Possibility of Mg- and Ca-based intermetallic compounds as new biodegradable implant materials. *Materials Science and Engineering: C*, 33(7), 4101-4111.
39. Shi, R., Zhu, Z., & Luo, A. A. (2020). Assessing phase equilibria and atomic mobility of intermetallic compounds in aluminum-magnesium alloy system. *Journal of Alloys and Compounds*, 825, 153962.
40. Schwarz, K., Blaha, P., & Madsen, G. K. (2002). Electronic structure calculations of solids using the WIEN2k package for material sciences. *Computer physics communications*, 147(1-2), 71-76.
41. Blaha, P., Schwarz, K., Madsen, G. K., Kvasnicka, D., & Luitz, J. (2001). WIEN2k. An augmented plane wave+ local orbitals program for calculating crystal properties, 60(1).

42. Blaha, P., Schwarz, K., Sorantin, P., & Trickey, S. B. (1990). Full-potential, linearized augmented plane wave programs for crystalline systems. *Computer physics communications*, 59(2), 399-415.
43. Singh, D. J., & Nordstrom, L. (2006). *Planewaves, Pseudopotentials, and the LAPW method*. Springer Science & Business Media.
44. Perdew, J. P., Burke, K., & Ernzerhof, M. (1996). Generalized gradient approximation made simple. *Physical review letters*, 77(18), 3865.
45. Koller, D., Tran, F., & Blaha, P. (2012). Improving the modified Becke-Johnson exchange potential. *Physical Review B*, 85(15), 155109.
46. Räsänen, E., Pittalis, S., & Proetto, C. R. (2010). Universal correction for the Becke–Johnson exchange potential. *The Journal of chemical physics*, 132(4).
47. Tran, F., & Blaha, P. (2009). Accurate band gaps of semiconductors and insulators with a semilocal exchange-correlation potential. *Physical review letters*, 102(22), 226401.
48. Blöchl, P. E., Jepsen, O., & Andersen, O. K. (1994). Improved tetrahedron method for Brillouin-zone integrations. *Physical Review B*, 49(23), 16223.
49. Otero-de-la-Roza, A., Abbasi-Pérez, D., & Luaña, V. (2011). Gibbs2: A new version of the quasiharmonic model code. II. Models for solid-state thermodynamics, features and implementation. *Computer Physics Communications*, 182(10), 2232-2248.
50. Dar, S. A., Srivastava, V., & Sakalle, U. K. (2017). A first-principles calculation on structural, electronic, magnetic, mechanical, and thermodynamic properties of SrAmO₃. *Journal of Superconductivity and Novel Magnetism*, 30(11), 3055-3063.
51. Blanco, M. A., Francisco, E., & Luana, V. G. I. B. B. S. (2004). GIBBS: isothermal-isobaric thermodynamics of solids from energy curves using a quasi-harmonic Debye model. *Computer Physics Communications*, 158(1), 57-72.
52. Tripathi, S. N., Srivastava, V., & Sanyal, S. P. (2019). First principle mechanical and thermodynamic properties of some TbX (X= S, Se) compounds. *Journal of Superconductivity and Novel Magnetism*, 32, 2931-2938.

53. Breidi, A., Allen, J., & Mottura, A. (2018). First-principles modeling of superlattice intrinsic stacking fault energies in Ni₃Al based alloys. *Acta Materialia*, 145, 97-108.
54. Charpin, T. (2001). A package for calculating elastic tensors of cubic phase using WIEN. Laboratory of Geometrix, Paris.
55. Sin'Ko, G. V., & Smirnov, N. A. (2002). Ab initio calculations of elastic constants and thermodynamic properties of bcc, fcc, and hcp Al crystals under pressure. *Journal of Physics: Condensed Matter*, 14(29), 6989.
56. Bhat, T. M., & Gupta, D. C. (2016). Robust thermoelectric performance and high spin polarisation in CoMnTiAl and FeMnTiAl compounds. *RSC Advances*, 6(83), 80302-80309.
57. Mehl, M. J., Klein, B. M., & Papaconstantopoulos, D. A. (1995). Intermetallic compounds: principle and practice. *Principles*, 1, 195-210.
58. Voigt, W. (1928). *Lehrbuch der Kristallphysik* (Textbook of crystal physics). BG Teubner, Leipzig und Berlin.
59. Schreiber, E., Anderson, O. L., Soga, N., & Bell, J. F. (1975). Elastic constants and their measurement.
60. Hill, R. (1952). The elastic behaviour of a crystalline aggregate. *Proceedings of the Physical Society. Section A*, 65(5), 349.
61. Tvergaard, V., & Hutchinson, J. W. (1988). Microcracking in ceramics induced by thermal expansion or elastic anisotropy. *Journal of the American Ceramic Society*, 71(3), 157-166.
62. Anderson, O. L. (1963). A simplified method for calculating the Debye temperature from elastic constants. *Journal of Physics and Chemistry of Solids*, 24(7), 909-917.
63. Pugh, S. F. (1954). XCII. Relations between the elastic moduli and the plastic properties of polycrystalline pure metals. *The London, Edinburgh, and Dublin Philosophical Magazine and Journal of Science*, 45(367), 823-843.
64. Bing, L., Rong-Feng, L., Yong, Y., & Xiang-Dong, Y. (2010). Characterisation of the high-pressure structural transition and elastic properties in boron arsenic. *Chinese Physics B*, 19(7), 076201.

65. Daoud, S., Bioud, N., & Lebga, N. (2013). Elastic and piezoelectric properties, sound velocity and Debye temperature of (B3) boron–bismuth compound under pressure. *Pramana*, 81(5), 885-892.
66. Bioud, N., Sun, X. W., Bouarissa, N., & Daoud, S. (2018). Elastic constants and related properties of compressed rocksalt CuX (X= Cl, Br): Ab initio study. *Zeitschrift Für Naturforschung A*, 73(8), 767-773.
67. Mukai, D., Miyata, H., & Aoki, K. (1999). Hydrogen absorption and desorption properties of Hf-based intermetallic compounds. *Journal of alloys and compounds*, 293, 417-420.
68. Jain, A., Ong, S. P., Hautier, G., Chen, W., Richards, W. D., Dacek, S., ... & Persson, K. A. (2013). Commentary: The Materials Project: A materials genome approach to accelerating materials innovation. *APL materials*, 1(1).
69. Tao, X., Ouyang, Y., Liu, H., Feng, Y., Du, Y., & Jin, Z. (2008). Elastic constants of B2-MgRE (RE= Sc, Y, La–Lu) calculated with first-principles. *Solid state communications*, 148(7-8), 314-318.
70. Lu, X., Cheng, K., Liu, S., Li, K., Zheng, F., & Du, Y. (2015). Experimental investigation of phase equilibria in the Co–Hf system. *Journal of Alloys and Compounds*, 627, 251-260.
71. Singh, A., Srivastava, V., Aynyas, M., & Sanyal, S. P. (2010). Pressure-induced phase transition and electronic structure of curium pnictides: Ab initio calculations. *Journal of nuclear materials*, 401(1-3), 60-64.
72. İyigör, A., Özdoğan, M., Ünsal, M., Örnek, O., & Arıkan, N. (2017). Ab-initio study of the structural, electronic, elastic and vibrational properties of HfX (X= Rh, Ru and Tc). *Philosophical Magazine Letters*, 97(3), 110-117.
73. Lu, W., Li, C., Yi, J., & Li, K. (2018). Stability and elastic properties of B2 Co X (X= Ti, Zr and Hf) intermetallic compounds as a function of pressure. *Philosophical Magazine*, 98(3), 203-218.
74. Li, X., Fang, L., Xu, C., Zhou, Y., Liu, Y., Xu, G., ... & Du, Y. (2023). Interdiffusion behaviors and mechanical properties of Hf-X (X= Nb, Ta) binary systems. *Calphad*, 81, 102548.
75. Guo, Q., & Kleppa, O. J. (1998). Standard enthalpies of formation of some alloys formed between group IV elements and group VIII elements, determined

by high-temperature direct synthesis calorimetry: II. Alloys of (Ti, Zr, Hf) with (Co, Ni). Journal of alloys and compounds, 269(1-2), 181-186.

Chapter 5

Structural, magnetic and thermodynamic properties of intermetallic compound CuZn: A first principles study

Intermetallic compounds are known for their diverse behavior, showing structural, electronic, and Thermodynamic properties that correspond to vivid applications in the industrial and technological field. Density functional theory and the full potential linearized augmented approach, which is a feature of the WIEN2k code, were used in these calculations for CuZn. thermodynamic quantities using the quasi-harmonic Debye model, such as specific heat at constant volume C_V . Molecule motion, lattice vibration, and phase transition are all explained by specific heat at constant volume (C_V). The temperature range is 0 K to 1000 K, and the pressure range is 0 GPa to 40 GPa for the C_V plotted within the specific pressure range. Important information for experimental research is provided by the C_V computations. We also calculate the Debye temperature, bulk modulus, etc. This gives valuable information about the prospects and theorists, and experimentalists.

5.1.Introduction:

Intermetallic materials are a type of rich diversity that has attracted researchers from all over the world for inorganic chemistry, physicians, and materials scientists [1-4]. Because of their ductility and tensile strength, the majority of binary intermetallic compounds (AB-type, where "A" is metal and "B" is transition/metal or rare earth metal) and alloys are used [5,6]. These metals exhibit mixed metallic, ionic, and covalent behavior. The two intermetallic compounds have typical characteristics, and they have attributes like physical, chemical, electrical, magnetic, and mechanical are much better. CuZn intermetallic crystallized in body-centered (B_2 , $Pm3m$, Space Group, 221) [4,7]. The creation of trustworthy, self-consistent thermodynamic databases depends on experimental understanding of thermodynamic functions. It is

required for any computer-based content and development process. Intermetallics are materials that consist of a combination of different metals they resulting in a crystallographic structure having an ordered arrangement [8]. Nickel-metal hydride batteries use widely used materials, such as alnico and hydrogen storage materials. Nickel and other titanium-based super alloys are also used in turbine blades. In microelectronics, some silicides are used as a potential barrier. Some industries like aerospace, construction, textiles, and automotive are based on the specific heat measurements. A thermodynamic property of intermetallic compounds provides the various techniques and formulation that allow the maximum possible information which extracted from materials. Thermodynamic properties depend on the state of the system, having several variables such as temperature, volume, and pressure [9].

Thus, in the current study, we computed the specific heat capacity based on CuZn compound within GGA [10] and mBJ [11]. We have used the quasi-harmonic Debye model to calculate the thermodynamic variables under temperature (0 K to 1000 K) and pressure (0 GPa to 16 GPa) in order to make CuZn a suitable material for industrial applications [12–14]. For the CuZn compound, thermodynamic variables such as specific heat at constant volume (C_v) were calculated. In addition, measurements were made of the specific heat at constant volume, which provides details on phase transitions, lattice vibration, and molecular motion. As a result, the current investigation's findings offer crucial information for upcoming theoretical and experimental studies [15].

5.2. Structural properties:

The structural property has been calculated using the WIEN2k code. This crystal structure is stable in the B2 cubic phase shown in Figure 5.1.

The location of the Cu atoms in the B2 phase unit cell of a cesium chloride type structure, having space group 221 and Pm-3m structure. In CuZn compound, the positions of the atoms are given for Cu is (0,0,0), having RMT is 2.2, and for Zn is (0.5, 0.5, 0.5), having RMT is 2.1. We find the optimized lattice parameter is 2.95 Angstrom. Using the equation of state for both the ferromagnetic and non-magnetic states, the total energy has been computed. Our compound's stability in the non-magnetic phase has been demonstrated unequivocally. It indicates that the energy of

the non-magnetic states is minimal. The Birch-Murnaghan equation of state has been used to optimize the energy volume. First, the unit cell volume was fitted to this total energy curve.

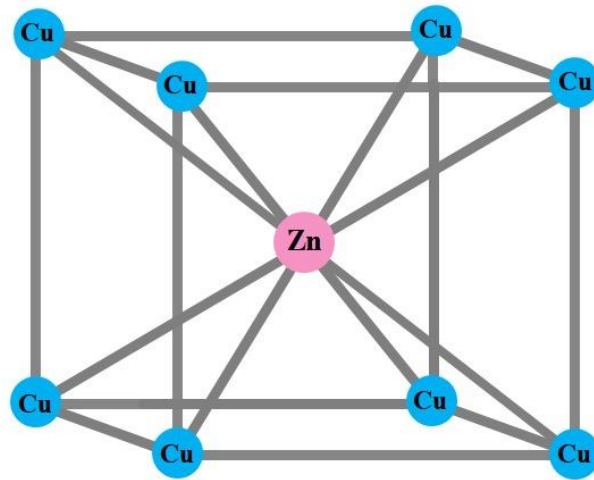


Figure 5.1: Crystal structure of CuZn intermetallic in Pm-3m space group.

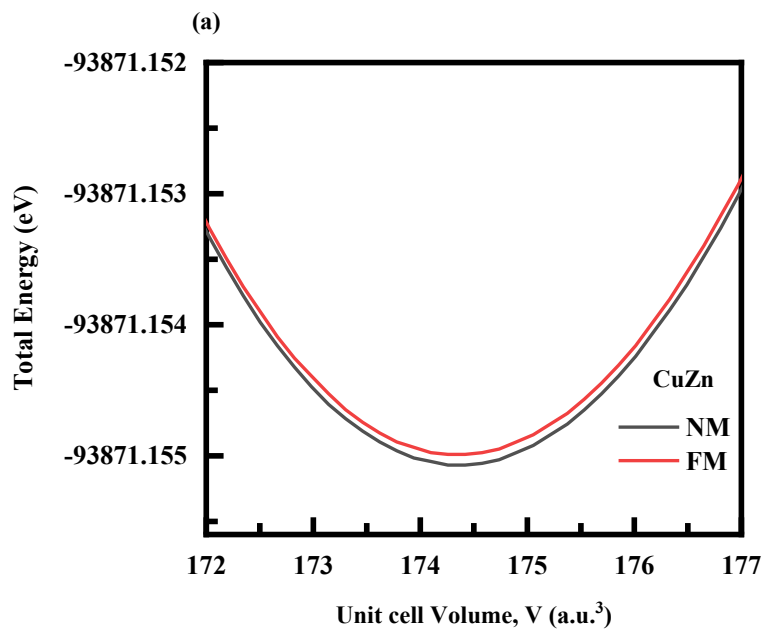


Figure 5.2: Variation of total energy as a function of cell volume of CuZn intermetallic in Pm-3m structure.

5.3. Electronic properties:

Within the spin-polarized calculations, we also calculate the electronic properties of the CuZn compound by treating the localized electrons in the Zn atom's d state. Thus, we use the full potential muffin-tin orbital method to plot an electronic band structure

in Figure 5.3 and the density of states in the calculations for the CuZn compound. the d states' primary contribution to the Fermi Energy crossing. This demonstrates the metallic nature of the CuZn compound.

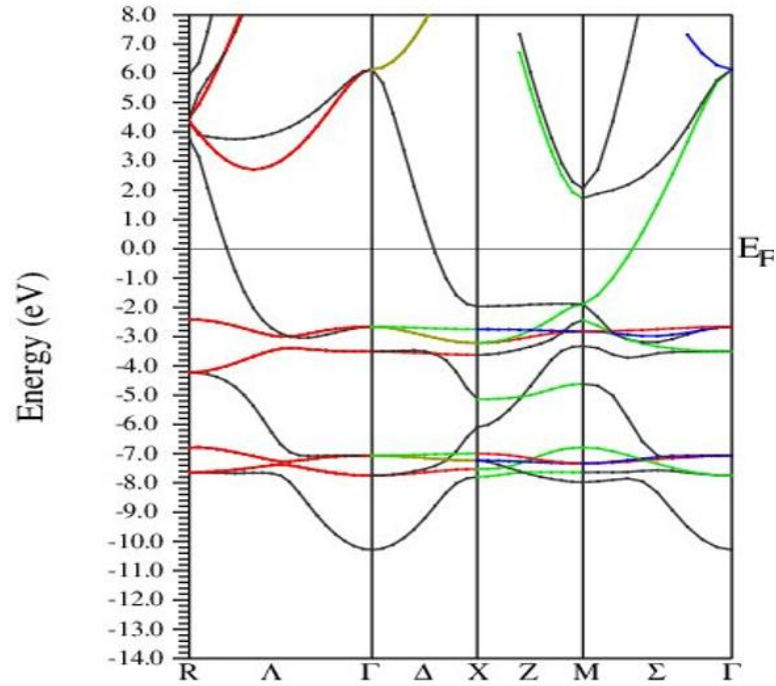


Figure 5.3: Band structure of CuZn intermetallic compound.

In addition, we compute the projected density of states and density of states in the Pm-3m structures, which are shown in Figure 5.4 below. Each of these states provides us with a brief overview of a variety of distinct states and which significantly contribute to the crossover of the Fermi Energy level. The compound's stability within the metallic formation is indicated by the crossover energy level.

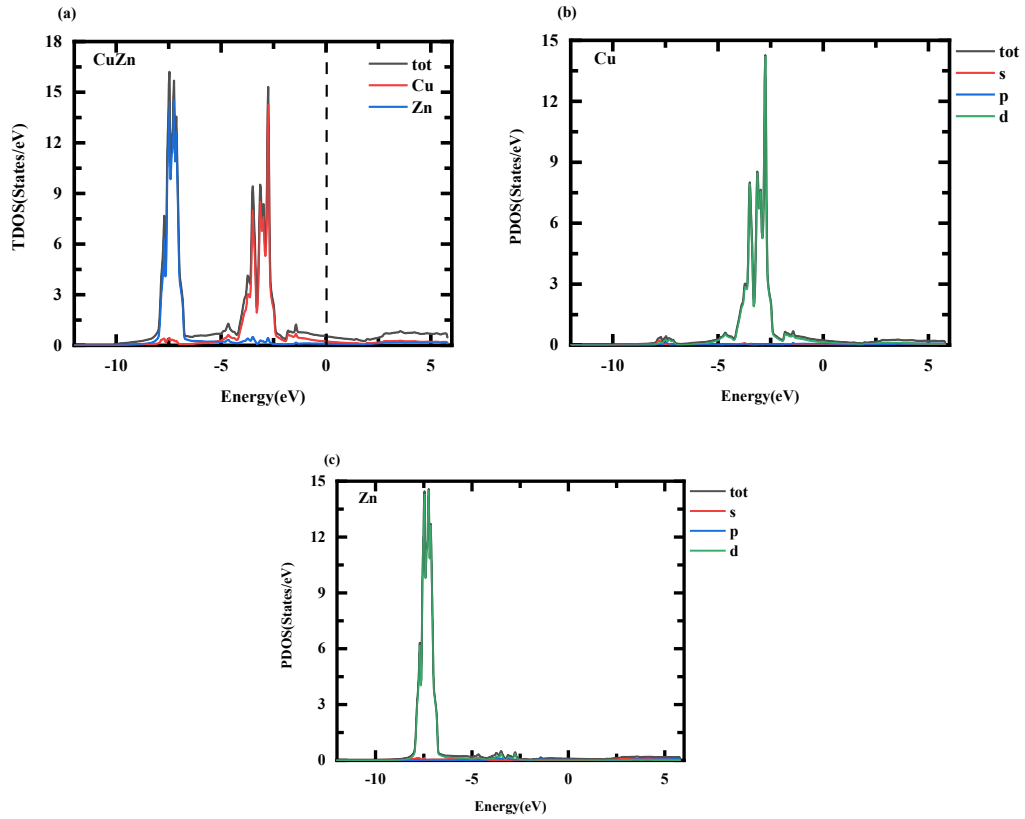


Figure 5.4: Density of states (TDOS) for CuZn intermetallic compound (a) Total density of states for CuZn (b) PDOS for Cu atoms (c) PDOS for Zn atoms

5.4. Thermodynamic properties:

The thermal properties, having renowned materials, and having a very vast applications in device fabrication. Thus, we compute the thermal characteristics in the range of 0 to 1000 K for temperature and 0 to 40 GPa for pressure. Using the quasi-harmonic Debye model, we compute the different thermal properties such as bulk modulus, specific heat, and thermal expansion coefficient. The Debye temperature, an important physical quantity, is one of the key parameters. The information regarding the solids' lattice vibration, which is dependent on the materials' total resistivity, is provided by these temperature-dependent thermal properties. A plot of the unit cell volume for the CuZn compound under various pressure and temperature conditions is shown in Figure 5.5. Figure 5.5 makes it very evident that when temperature rises, the unit cell's volume rises as well, but only to the extent that pressure reaches a certain point. This is carried out when the material expands and contracts. In contrast, a decreasing unit cell volume under increasing pressure indicates a constant temperature.

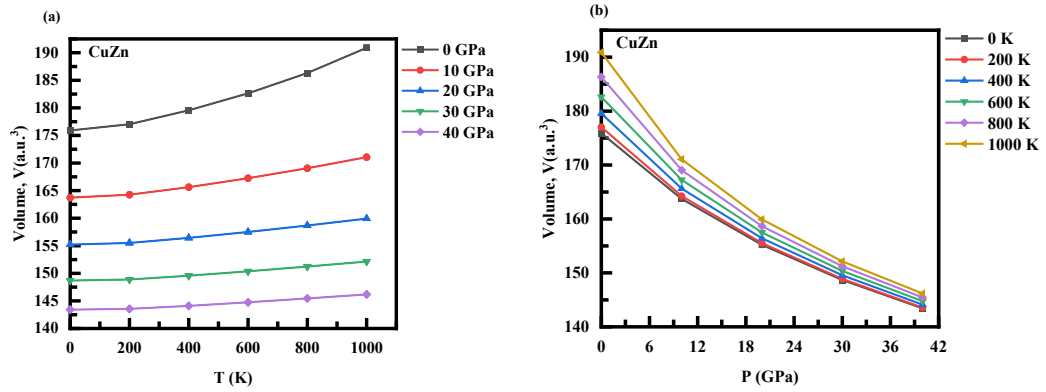


Figure 5.5: Variation of unit cell volume of CuZn intermetallic with temperature and pressure

The bulk modulus's variation with temperature and pressure is shown in Figure 5.6. We can see that it provides information if the bulk modulus drops. If the pressure is found to increase with the bulk modulus, it indicates that the temperature is trending upward. This increase in temperature shows that the material hardness is reduced, and increased pressure increases stress in the compound. The estimated value for bulk modulus is 112.43 GPa at 200 K and 0 GPa.

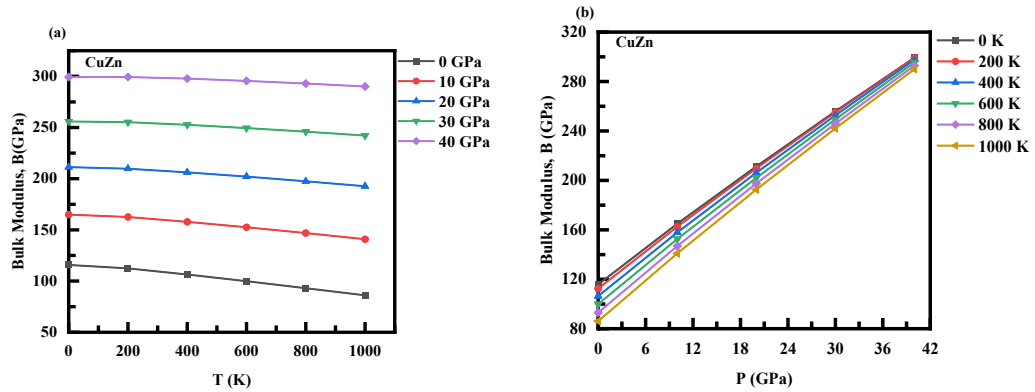


Figure 5.6: Variation of bulk modulus of CuZn intermetallic with temperature and pressure.

The specific heat at constant volume with temperature and pressure is plotted graphically in Figure 5.7. It is clear to us that the molar specific heat fluctuates instantaneously up to 200 Kelvin. This indicates that this is the primary cause of the constant value. The Dulong petit limit is reached by the Debye model at high

temperatures behind this. For CuZn, the computed value of C_v at 1000 K and 0 GPa is $50 \text{ J K}^{-1} \text{ m}^{-1}$.

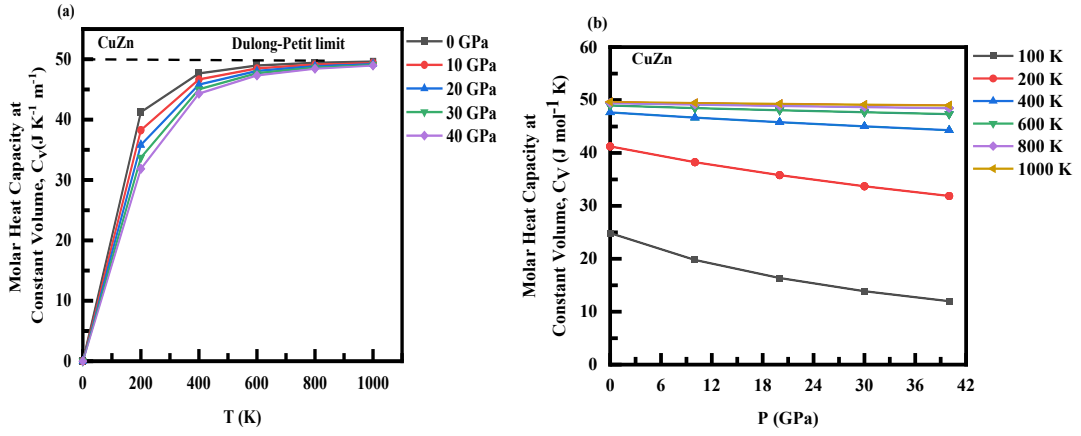


Figure 5.7: Variation of molar heat capacity at a constant volume of CuZn intermetallic with temperature and pressure.

The Grüneisen constant as a function of temperature and pressure is plotted graphically in Figure 5.8. With temperature, the pressure value for that specific temperature increases steadily up to 200 Kelvin. The material gradually increases above this linear temperature, and the opposite phenomenon is seen at a particular temperature when the pressure is raised and the Grüneisen constant value falls. At 0 K and 0 GPa, the Grüneisen constant is estimated to be 2.42.

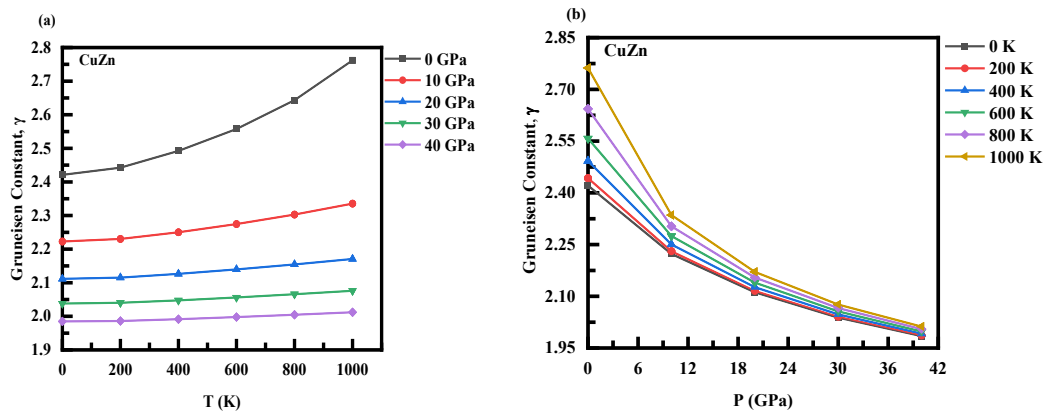


Figure 5.8: Variation of Grüneisen constant of CuZn intermetallic with temperature and pressure.

We plot a graphical representation of the thermal expansion coefficient in Figure 5.9. The figure makes it very evident that if the value of α increases with temperature, then

it becomes very fast at lower temperatures and increases rapidly at high temperatures. In contrast, it is discovered that pressure has very little effect at low temperatures, but that pressure becomes dominant at high temperatures, causing the thermal expansion coefficient to instantly decrease. This indicates that the quasi-harmonic Debye approximation's shortfall at both high and low temperatures has a primary cause. This is crucial because it affects how the atom vibrates when heat is applied from the outside and how much the intratomic distance increases. It is entirely dependent on the pressure and temperature. It indicates that while temperature changes by a constant amount, there is a slight change in dimensions per unit degree. The coefficient of thermal expansion values is computed to be $5.83 \times 10^{-5} \text{ K}^{-1}$ at 200 K and 0 GPa.

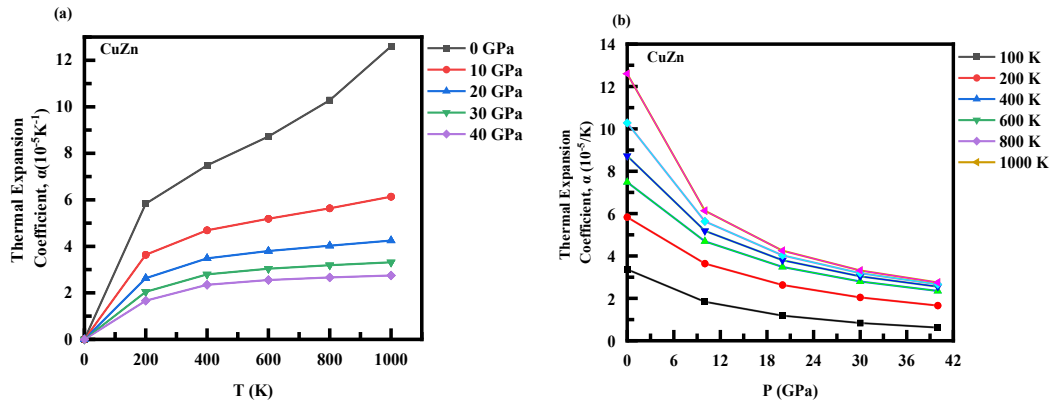


Figure 5.9: Variation of thermal expansion coefficient of CuZn intermetallic with temperature and pressure.

We plot the variation of the Debye temperature with temperature and pressure in Figure 5.10. At 0K and 0 GPa, we estimate the Debye temperature to be 404.49. It depicts what happens when we heat the specified material. It indicates that when heat is applied, the Debye temperature lowers the hardness and changes the behavior. The quasi-harmonic Debye model is used to provide information about the vibrational properties of the lattice.

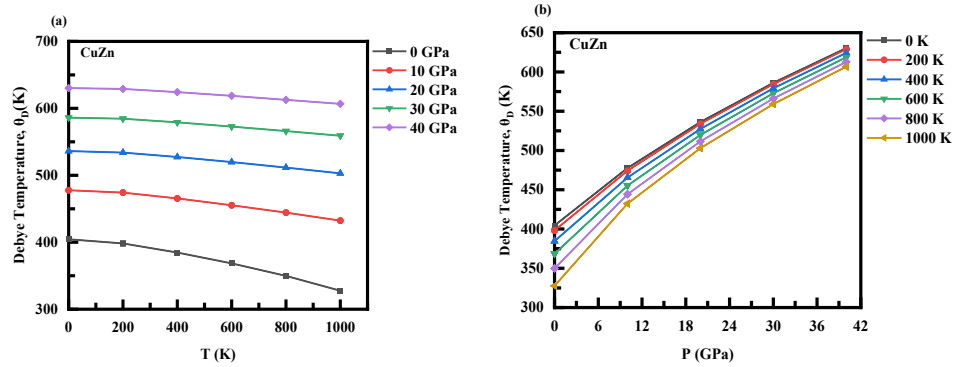


Figure 5.10: Variation of Debye temperature of CuZn intermetallic with temperature and pressure.

In Figure 5.11, Lastly, we have computed the entropy as a function of pressure and temperature outside. Figure 5.10, however, shows how it varies with temperature and pressure changes. Entropy provides us with details about the system's disorder. The figure makes it very evident that entropy is zero at 0 K and 0 GPa and begins to grow exponentially as temperature rises at a certain pressure. The CuZn intermetallic compound's degree of disorder is increasing at higher temperatures, as indicated by the increasing entropy value. According to our computation, the value for CuZn is $69.61 \text{ mol}^{-1} \text{ K}^{-1}$ at 400 K and 0 GPa. It should be noted that there is a slight increase in entropy at higher temperatures. This is because the atoms' vibrations are increasing, which causes the system's internal energy to rise.

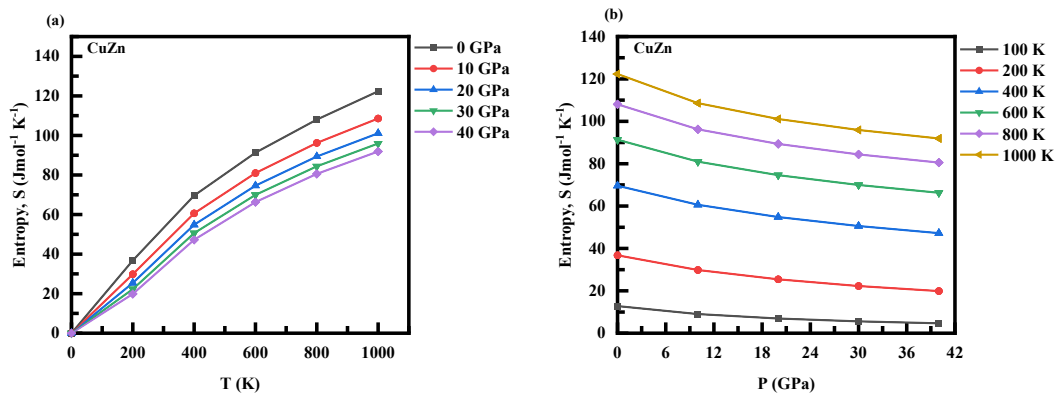


Figure 5.11: Variation of entropy of CuZn intermetallic with temperature and pressure.

5.5.Conclusion:

In summary, we use density functional theory to study the thermodynamic and electronic structural properties. The density functional theory has been used in these computations. First of all, we'll check the structural stability of the compound in the Pm-3m structure. We calculate both states in the ferromagnetic and the non-magnetic after the calculations, and we discover that the outcome demonstrates the stability of our compound in non-magnetic states. We display both the overall and projected state densities, in which we see that the material shows the crossover of the Fermi Energy level, which informs us that the compound has a metallic nature. Lastly, we use the quasi-harmonic Debye model to compute the thermodynamic properties, which provides us with important information. This thermal characteristic provides us with useful information for fabricating devices and generators. Researchers and experimenters have unrestricted access to this as well.

References

1. W. Hume-Rothery (1925). *Journal of the Institute of Metals*, 35, 209.
2. Zintl, E. J. A. C. (1939). Intermetallische verbindungen. *Angewandte Chemie*, 52(1), 1-6.
3. Srivastava, V., Pagare, G., Sanyal, S. P., & Rajagopalan, M. (2009). First principles calculations of Al-rich RE (RE= Ho, Er, Tm and Yb) intermetallic compounds. *physica status solidi (b)*, 246(6), 1206-1214.
4. Paliwal, N., & Srivastava, V. (2012). Band Structure Calculation of AgCd and AgZn Intermetallics.
5. Tao, X., Ouyang, Y., Liu, H., Feng, Y., Du, Y., & Jin, Z. (2008). Elastic constants of B2-MgRE (RE= Sc, Y, La–Lu) calculated with first-principles. *Solid state communications*, 148(7-8), 314-318.
6. X. Tao, Y. Ouyang, H. Liu, F. Zeng, Y. Feng, Z. Jin(2009). *Computational material science*, 40, 226.
7. Keast, V. J., Ewald, J., De Silva, K. S. B., Cortie, M. B., Monnier, B., Cuskelly, D., & Kisi, E. H. (2015). Optical properties and electronic structure of the Cu–Zn brasses. *Journal of Alloys and Compounds*, 647, 129-135.
8. Peng, H. (2013). Brazing of nickel, ferrite and titanium–aluminum intermetallics. In *Advances in Brazing* (pp. 221-248). Woodhead Publishing.
9. Thermodynamic properties and relation, Britannica.
10. Perdew, J. P., Burke, K., & Ernzerhof, M. (1996). Generalized gradient approximation made simple. *Physical review letters*, 77(18), 3865.
11. Tran, F., & Blaha, P. (2009). Accurate band gaps of semiconductors and insulators with a semilocal exchange-correlation potential. *Physical review letters*, 102(22), 226401.
12. Blanco, M. A., Pendás, A. M., Francisco, E., Recio, J. M., & Franco, R. (1996). Thermodynamical properties of solids from microscopic theory: applications to MgF₂ and Al₂O₃. *Journal of Molecular Structure: THEOCHEM*, 368, 245-255.
13. Dar, S. A., Srivastava, V., & Sakalle, U. K. (2017). Ab initio high pressure and temperature investigation on cubic PbMoO₃ perovskite. *Journal of Electronic Materials*, 46, 6870-6877.

14. A. O. Roza, V. Luaea (2011). Physical Review B: Condensed Matter and Materials Physics, 85, 184103.
15. Dar, S. A., Sharma, R., Srivastava, V., & Sakalle, U. K. (2019). Investigation on the electronic structure, optical, elastic, mechanical, thermodynamic and thermoelectric properties of wide band gap semiconductor double perovskite Ba₂InTaO₆. RSC advances, 9(17), 9522-9532.

Conclusion and future perspectives

6.1. Conclusion

The thesis entitled **Theoretical study of Structural, Thermophysical and Mechanical properties of some intermetallic compounds** has described the structural, electronic, elastic, mechanical, and thermodynamic properties of Intermetallic compounds (BeAg, BeAu, BeFe, MgLu, MgHf and CuZn) under a certain temperature and pressure range. To address the aforementioned properties of compounds, we have used a method known as the full potential linearized augmented plane wave method, which depends on the theory that works with the electron density and is named as density functional theory. The used method is unified in the WIEN2k code written in FORTRAN 90. The investigation starts with the structural optimization of the compounds by considering their possible structural phases. BeAg, BeAu, BeFe, MgLu, MgHf, and CuZn are six potential structures for intermetallic compounds, with the former falling under the space group Pm-3m (221). Through the analysis of the E-V curve, it has been discovered that the CsCl structure type is stable for the IMCs and is used for other investigations. As a result of the structural optimization, done through the fitting of E-V data into Birch-Murnaghan EOS as summarized in Table 6.1. Through the fitting of E-V data, magnetic phases for the six compounds are also being optimized by considering the ferromagnetic and non-magnetic phases. The minimum energy for the FM phase over NM for each compound has led to their ferromagnetic nature; otherwise, if the minimum energy is in a non-magnetic phase, it means it leads to their non-magnetic nature. Further, our investigation goes on to find the band structure of each compound, followed by the estimated stable structure and magnetic phase. We used in total potential to find the band structure of the studied compounds. For BeAg, BeAu, BeFe, MgLu, MgHf, and CuZn compounds, GGA approximation in terms of Coulomb repulsion. GGA potential results in the metallic nature of these two compounds.

Fermi level, but the presence of electronic states at E_f preserves the metallic nature of the compounds.

Table 6.1: Calculated ground state properties: unit cell volume V_0 , lattice parameter a_0 , bulk modulus B_0 , first order pressure derivative of bulk modulus B'_0 and equilibrium total energy E_0 of MgX (X=Lu, Hf) intermetallics at 0GPa and 0K

Solid	V_0 (a.u. ³)	a_0 (Å)	B_0 (GPa)	B'_0	E_0 (x10 ² eV)
BeAg	173.39	2.92	119.27	8.66	-1450.32
BeAu	175.88	2.97	150.01	6.87	-5185.05
BeFe	123.30	2.63	177.38	4.33	-350.22
MgLu	344.95	3.71	44.74	4.26	-4020.56
MgHf	285.37	3.48	76.59	3.75	-4161.09
CuZn	174.35	2.96	118.79	5.31	-6902.29

1 a.u. = 0.52917 Å; 1 Å = 10⁻¹⁰ m

Further, the Charpin approach has been used to estimate elastic constants and mechanical properties, as summarized in Table 6.2, to test the capacity of materials under applied stress or their capacity to deform under an applied force. Three elastic constants, namely, C_{11} , C_{12} , and C_{44} , are estimated owing to the cubic symmetry. The estimated elastic constants have led to the calculations of mechanical parameters. An inspection of elastic constants and bulk modulus, these materials are not hard and stiff. B/G values of calculated to 2.15 and 4.02, indicating the ductile nature of BeAg and BeAu, and for BeFe, its value is calculated to 1.71, indicating a brittle nature and 2.089 and 1.167 for MgLu and MgHf reveal ductile and brittle nature, respectively.

Table 6.2: Calculated elastic and mechanical properties for BeX(X=Ag, Au, Fe) intermetallics at 0 GPa and 0 K: elastic constants C_{11} , C_{12} , C_{44} , Bulk Modulus B, Voigt Shear Modulus G_V , Reuss Shear Modulus G_R , Shear Modulus G, Young's Modulus E, Anisotropy Ratio A, Cauchy Pressure $C_{12}-C_{44}$, Bulk modulus to Shear modulus ratio B/G, Poisson Ratio σ , longitudinal velocity V_l , transverse velocity V_t , Average velocity V_m , Debye Temperature θ_D , Melting Temperature T_m .

Properties	BeAg	BeAu	BeFe	MgLu	MgHf
C_{11} (GPa)	165.82	202.06	263.27	57.701	136.460
C_{12} (GPa)	105.76	132.65	135.71	38.179	47.166
C_{44} (GPa)	83.80	39.09	141.87	35.910	85.476
B (GPa)	119.27	150.01	175.69	44.7	76.8
G_V	62.29	37.34	110.63	25.450	69.144
G_R	48.83	37.21	95.23	17.335	77.627
G (GPa)	55.56	37.28	102.93	21.393	65.864
E (GPa)	144.32	103.28	258.35	55.346	153.697
A	2.79	1.13	2.22	3.679	1.914
$C_{12}-C_{44}$ (GPa)	21.96	93.55	-6.16	2.269	-38.310
B/G ratio	2.15	4.02	1.71	2.089	1.167
σ	0.30	0.39	0.25	0.294	0.167
V_l (m s ⁻¹)	5053.92	3485.81	7285.38	3375.896	4547.568
V_t (m s ⁻¹)	2697.73	1679.76	4178.28	1824.841	2875.848
V_m (m s ⁻¹)	3012.83	1888.26	4641.37	2036.660	3163.919
θ_D (K)	384.38	239.45	661.13	205.346	340.685
T_m (K)	1178.17	1337.09	2109.16	894.071	1359.615

1 GPa = 10⁹ Pa

We demonstrate the variations of bulk modulus, Debye temperature, Grüneisen constant, and thermal expansion coefficient within a certain range of temperature and pressure as

summarized in Table 6.3. These variables highlight the thermodynamic stability of materials, which supports the materials to be used in the fabrication of devices. In order to use these materials for high temperature purposes, we have systematically investigated the temperature-induced study of bulk modulus, molar heat capacity at constant volume, thermal expansion coefficient, and Debye temperature. We predict values of Debye temperature as 430 K, 335 K, and 661K for BeX(X=Ag, Au, Fe) at 0 K and 0 GPa, respectively. Both compounds exhibit the Dulong-Petit limit at high temperature with $50 \text{ J K}^{-1} \text{ m}^{-1}$, a value of molar heat capacity at constant volume. To understand the vibrational behavior of the studied materials, Debye temperature, heat capacity, and thermal expansion coefficients are calculated. At calculated Debye temperatures of 226 K and 284 K for MgLu and MgHf, respectively, materials exhibit vibrational energy in the crystal lattice that reaches a maximum to excite all possible vibrational modes in the material. The materials' specific heat capacity, thermal conductivity, and other properties related to lattice vibrations are further explained. The molar heat capacity for these materials is calculated in the range of 45-48 $\text{JK}^{-1}\text{m}^{-1}$

Table 6.3: Calculated thermodynamic properties like Volume V (a.u.³), Bulk Modulus B (GPa), Molar heat capacity at constant volume C_V (J K⁻¹ m⁻¹), Grüneisen constant γ , thermal expansion coefficient α (10⁻⁵ K⁻¹), Debye temperature θ_D (K).

Solid	V (a.u. ³)	B (GPa)	C _V (JK ⁻¹ m ⁻¹)	γ	A	θ_D
	0GPa, 0K/ 0GPa, 300K	0GPa, 0K/ 0GPa, 300K	0GPa, 0K/ 0GPa, 300K	0GPa, 0K/ 0GPa, 300K	0GPa, 0K/ 0GPa, 300K	0GPa, 0K/ 0GPa, 300K
BeAg	173.38/ 175.28	119.27/ 110.60	0/ 45.35	2.33/ 2.35	0/ 6.17	429.34/ 418.54
BeAu	175.88/ 177.51	150.01/ 144.73	0/ 46.51	2.34/ 2.38	0/ 5.00	365.76/ 357.86
BeFe	124.96/ 125.77	172.95/ 166.21	0/ 39.93	1.95/ 1.96	0/ 4.21	656.66/ 648.32
MgL u	349.41/ 354.18	43.93/ 41.36	0/ 48.56	1.61/ 1.63	0/ 6.07	226.12/ 221.21
MgH f	286.63/ 289.44	75.67/ 72.20	0/ 47.78	1.75/ 1.77	0/ 4.54	284.56/ 279.7
CuZn	175.91/ 178.22	115.78/ 104.29	0/ 45.88	2.42/ 2.47	0/ 6.82	404.49/ 391.81

6.2. Future perspectives

The investigated compounds produce fascinating and fruitful results, making them ideal for a variety of applications. Spintronics requires ferromagnetic and non-magnetic materials, and our results procured the same. Such materials are also applicable in spin valve generators. Hence, the future scope of these Intermetallic compounds is promising and spans across various fields of science and technology. The entire study is producing beneficial and useful findings that give significant direction to the experimental study. It is important to note that the future Intermetallic compounds depend on ongoing research and development in material synthesis, characterization techniques, and theoretical

understanding of their properties. As scientists and engineers dig deeper into understanding and manipulating these compounds, new and exciting applications are likely to emerge that further expand their scope and impact in various scientific and technological domains.

List of publications

1. Nitika and Vipul Srivastava, “A Computational Modeling on thermodynamic performances of BeX(X=Ag, Au) intermetallics”, The Journal of Chemical Thermodynamics, Vol. 188, Pg. No. 107175, 2023 (Sci Indexed Journal, Q2, IF 2.6, SJR 0.665).
2. Nitika and Vipul Srivastava, “Specific heat of intermetallic compound CuZn: A first-principles study”, AIP Conference Proceedings, Vol. 2800, Pg. No. 020153, 2022, (Sci Indexed Journal, SJR 0.152).
3. Nitika and Vipul Srivastava, “A Computational Modeling on Thermodynamical Performances of BeFe Intermetallic”, Submitted in Chemistry Africa, 2024 (Sci Indexed Journal, Q3, IF 2.2, SJR 0.372).
4. Nitika, Lakshita Sehgal, V. Revath, and Vipul Srivastava, "A comprehensive insight into the DFT based mechanical and thermodynamic performances of MgX (X=Lu, Hf) intermetallics", Catalysis, 2024, (Q3 category, IF 2.8, SJR 0.296).

List of conferences attended

- 1) Presented a paper in SCOPUS Indexed under the topic “Specific heat of Intermetallic compound CuZn: A first-principles study” in the International conference on Materials for Emerging Technologies (ICMET-21) held on February 18-19, 2022, organized by department of Research Impact and Outcome, Division of Research and Development, Lovely Professional University, Punjab.
- 2) Attended webinar on “Awareness Program to Introduce Giloy in Routine Life for Immunity Development” supported by National Medicinal Plant Board, Ministry of AYUSH held on March 26, 2022.
- 3) Attended 4th international conference on “Interdisciplinary Approaches in Science, Engineering and Technology (ICIASET-2023) organized by Department Applied Science, M.P. Council of Science and Technology, Bhopal held on July 27-28, 2023.
- 4) Presented a paper in 5th international conference on “Recent Advances in Fundamental and Applied Sciences (RAFAS-2024)” held on April 19-20, 2024, Lovely Professional University, Punjab.